# NONLINEAR VIBRATIONS AND REDUCED ORDER MODELING OF BOLTED JOINTS

A THESIS SUBMITTED TO
THE GRADUATE SCHOOL OF NATURAL AND APPLIED SCIENCES
OF
MIDDLE EAST TECHNICAL UNIVERSITY

BY

HÜMEYRA BEYAN

IN PARTIAL FULFILLMENT OF THE REQUIREMENTS
FOR
THE DEGREE OF MASTER OF SCIENCE
IN
MECHANICAL ENGINEERING

NOVEMBER 2022

Approval of the thesis:

**NONLINEAR VIBRATIONS AND REDUCED ORDER MODELING OF BOLTED JOINTS**

submitted by **HÜMEYRA BEYAN** in partial fulfillment of the requirements for the degree of **Master of Science** i**n Mechanical Engineering, Middle East Technical University** by,

Prof. Dr. Halil Kalıpçılar
Dean, Graduate School of **Natural and Applied Sciences** _____

Prof. Dr. Sahir Arıkan
Head of the Department, **Mechanical Engineering** _____

Prof. Dr. Ender Ciğeroğlu
Supervisor, **Mechanical Engineering, METU** _____

**Examining Committee Members:**

Assoc. Prof. Dr. Mehmet Bülent Özer
Mechanical Engineering, METU _____

Prof. Dr. Ender Ciğeroğlu
Mechanical Engineering, METU _____

Assist. Prof. Dr. Gökhan Özgen
Mechanical Engineering, METU _____

Assist. Prof. Dr. Orkun Özşahin
Mechanical Engineering, METU _____

Assist. Prof. Dr. Saeed Lotfan
Mechanical Engineering, Gebze Technical University _____

Date: 29.11.2022

**I hereby declare that all information in this document has been obtained and presented in accordance with academic rules and ethical conduct. I also declare that, as required by these rules and conduct, I have fully cited and referenced all material and results that are not original to this work.**

Name Last name: Beyan, Hümeyra

Signature:

# ABSTRACT

## NONLINEAR VIBRATIONS AND REDUCED ORDER MODELING OF BOLTED JOINTS

Beyan, Hümeyra
Master of Science, Mechanical Engineering
Supervisor: Prof. Dr. Ender Ciğeroğlu

November 2022, 95 pages

Due to ease of mounting, high strength feature and availability, bolted joints are one of the most common and widely used connection method. The contact between connected bodies is ensured by preload force on bolts which affect the stiffness and damping characteristics of the assembled system and introduce nonlinearity. To obtain the dynamic characteristic of systems with bolted joints accurately, the nonlinearity effect should be included.

With high fidelity contact model's accurate response can be obtained whereas the computational cost is drastically increased. The reduced-order modeling of bolted connections is essential to obtain the nonlinear dynamic response with adequate accuracy.

The aim of the work represented in this thesis is to decrease the computational cost of the reduced contact model by utilizing modal superposition method with response-dependent nonlinear modes.

Keywords: Reduced Order Joint Model, Modal Superposition Method, Response Dependent Mode Shapes, Nonlinear Vibrations

# ÖZ

## CİVATALI BAĞLANTILARIN DOĞRUSAL OLMAYAN TİTREŞİMİ VE İNDİRGENMİŞ MODELİ

Beyan, Hümeyra
Yüksek Lisans, Makina Mühendisliği
Tez Yöneticisi: Prof. Dr. Ender Ciğeroğlu

Kasım 2022, 95 sayfa

Cıvatalı bağlantılar montaj kolaylığı, yüksek dayanım özelliği ve bulunabilirlik nedeniyle sıkça kullanılan bir bağlantı yöntemidir. Bağlanan parçalar arasındaki temas önyükleme kuvveti ile sağlanmakta olup sistemin direngenlik ve sönüm karakteristiğini etkilemekte ve doğrusal olmayan davranış göstermektedir. Cıvataları bağlantıların olduğu sistemlerin dinamik davranışını doğru elde edebilmek için doğrusal olmayan davranışın etkisi hesaba katılmalıdır.

Yüksek doğrulukta temas modelleri ile hassas sonuçlar elde edilebilse de hesaplama maliyeti oldukça artmaktadır. İndirgenmiş cıvatalı bağlantı modelleri doğrusal olmayan dinamik davranışın yeterli doğrulukla elde edilmesi için gereklidir.

Bu tezde yer alan çalışmanın hedefi indirgenmiş temas bağlantısının hesaplama maliyetini cevaba bağlı doğrusal olmayan sistem modlarını kullanarak azaltmaktır.

Anahtar Kelimeler: İndirgenmiş Bağlantı Modeli, Modal Süperpozisyon Yöntemi, Cevaba Bağlı Mod Şekli, Doğrusal Olmayan Titreşimler

To My Father Şinasi

## ACKNOWLEDGMENTS

I would like to thank my supervisor Prof. Dr. Ender Ciğeroğlu for his supervision, guidance, criticism and support throughout the research.

I also want to express my gratitude to my dear colleagues, Aykut Çardak and Tahsin Ahi for their technical suggestions and comments.

Another gratitude must go to my colleagues at Roketsan Inc., without their technical suggestions and support, this thesis would not have been completed.

I'm grateful to my friends and family, who supported and encouraged me.

I would like to thank my dear friend Tutku Konuk who has provided me emotional support in my life.

Last but not least, I am grateful to my mischievous cats Bal and Mila for the joy they brought into my life.

## TABLE OF CONTENTS

## LIST OF TABLES

TABLES

## LIST OF FIGURES

FIGURES

# CHAPTER 1

# INTRODUCTION

To obtain the realistic behavior of mechanical systems, the nonlinear characteristics within the structures should be considered. The complexity of the solution process is significantly increased as the nonlinearity effect is imposed within system equations of large nonlinear structures.

The sources of nonlinearities could be divided into three effects: geometric nonlinearities, material nonlinearities, and contact in-between parts. The geometric nonlinearities can be observed in systems such as high-level vibrating beam-like structures which undergo large deformations. The hardening phenomenon also referred to as stress stiffening, is a widely seen example of this nonlinearity type. The overall stiffness of the system increases as displacement values changes. Another source of nonlinearity could be the nonlinear elastic behavior of materials such as elastomeric mounts. The most common source of nonlinearity is the contact status in-between parts, leading to stiffness and/or damping changes. This phenomenon is apparent, especially in a system where bolted joints connect bodies.

## 1.1 Literature Survey

Nonlinear dynamic equations could be solved with time and frequency domain methods. The earliest studies which determined the response of nonlinear dynamical systems were conducted in time domain methods. The method proposed by Cameron and Griffin [1] used both frequency and time domain methods to calculate the steady-state response of the systems under harmonic excitations. In 2017, Rezaiee et al. [2] proposed an explicit higher-order time integration algorithm. In spite of the straightforward solution process and relatively reliable results which can be obtained

by these methods, the significance of the required solution time is the major drawback that restrains their application to small-scale dynamic problems. There are many studies available in the literature which examines a more efficient algorithm for time-domain solution methods [3] and hybrid solution methods [4] [5] [6] .

The frequency domain methods are better alternatives for the calculation of large-scale physical systems due to decreased computational time requirement. The harmonic balance method (HBM) which was proposed by Urabe [7] in 1965 is one of the most efficient solution methods which was applied when strong nonlinearities are present [8] [9] .

As the number of harmonics required to model a nonlinear system is increased, the accuracy of the solution with HBM is increased with increased computational time. To overcome this time limitation many HBM algorithms are studied [10] [11] [12] [13] [14] . The number of harmonics can be fixed or different for each degree of freedom in the system. The harmonics number can be fixed throughout the solution process or increased with a predetermined amount based on a criterion.

Sert and Ciğeroglu [15] proposed a two-step pseudo-response-based adaptive harmonic balance method. The unnecessary harmonics are eliminated by a two-step harmonic selection criterion. The decreased computational time and improved accuracy level of obtained results make this adaptive algorithm state of the art.

In 1985, Menq and Griffin [16] published a new method that examined the response of a frictionally damped beam under harmonic motion where the nonlinear force is calculated by using the first two terms of Fourier series expansion. In 1986, Menq et. al. [17] [18] proposed a new method in which the dynamic response of frictionally damped systems under high normal loads is examined. The most vital outcome of their study is to show the significance of including partial slip phenomena when the contact pressure in between parts is high compared to excitation force.

In 1989, Budak and Ozguven [19] represented a method for the response of systems in which symmetrical nonlinearities are present. In this method, the nonlinearities

are represented as springs and dampers. The extended method [20] shows the application of describing function method for the calculation of nonlinear force in matrix form. Tanrıkulu et al. [21] extended this methodology by generalizing the implementation procedure of describing function at which the harmonic vibration analysis is conducted for multi-degree of freedom (MDOF) nonlinear systems.

Kuran and Ozguven [22] developed a modal superposition method that defined the multi-harmonic nonlinear force utilizing describing function method. The number of equations which is necessary to solve was decreased by the implementation of linear system modes to equations. The calculated response in the resonance region was reliable even though only one mode was used.

In 1998, Yang et al. [23] proposed a new contact model which includes both tangential motions of friction and normal motion. The detailed study on stick-slip characteristics showed that the source of stiffness change is separation motion. Chen and Menq [24] used constrained mode shapes of frictionally constrained blade systems to predict the response at the resonance region. Receptance method was also utilized, which decreased the dimension of the solved equation set, hence the decrease in required computational time.

Cigeroglu et al. [25] proposed a new modal superposition method with a distributed parameter two-dimensional microslip friction model. In the continuation of this work published in 2008 [26] , the three-dimensional relative motion between contact surfaces is expressed by the modal superposition method and decomposed into two one-dimensional in-plane components and an out-of-plane component which decreases the required solution time further.

Petrov [27] proposed a method in which the effect of mode number retained in the calculation of the FRF matrix is examined. The significant advantage of this method, besides its accurate results, is its applicability to finite element models easily. The accurate results of the bladed disk model at which contact is modeled were obtained.

Krack et al. [28] extended the work of Rosenberg [29] at which nonlinear normal modes (NNM) are calculated to find the response of structures with self-excitation and harmonic forcing. The following study by Krack [30] extended this concept even further by considering the systems under periodic motion. The work conducted by Touze [31] pointed out that for the increased response levels, the accuracy of the reduced model decreases.

The calculation of NNMs of large-scale systems is a challenging task that limits the availability of using NNM method while the response of large physical systems is considered. To overcome this difficulty, Karaagacli et al. [32] examined a case study in which response dependent nonlinear modes are used in the calculation of NNMs.

Ferhatoglu et al. [33] proposed a new modal superposition method with the hybrid mode shape (HM) concept. For certain types of nonlinearities, the nonlinearity acts as if it has two limiting conditions. For example, for gap nonlinearity, the limiting stiffness value is equivalent to the stiffness of the nonlinear element. The nonlinear force contribution is defined by describing function method. For each nonlinear element, the ratio of the real part of describing function and the limiting stiffness value is engaged to calculate hybrid modes, which will be used in the modal superposition step. The continuation of this work [34] [35] reorganized the system matrix definitions such that the required solution time for the solution of complex systems is further decreased.

Ferhatoglu et al. [41] proposed a modal superposition method with response-dependent nonlinear modes (RDNM) for the periodic vibration analysis of large MDOF nonlinear systems. In this study, the contribution of the real part of the nonlinearity matrix to overall stiffness is taken into account, and the updated eigenvalue problem at each response level is solved. The resulting RDNMs are used in system equations to decrease the number of nonlinear equations.

The research on the modeling of joint connections is mainly focused on high-fidelity models since the linear joint models available in the literature could not model the energy loss of the system adequately.

In 2005, Segalman [36] proposed a four-parameter Iwan model for lap-type joints. A parallel-series Iwan system is implemented to equations by using trancuated power-law spectra. With this approach, both microslip and macroslip regimes of friction in harmonically loaded lap joints were captured accurately.

In 2016, Brake et. al. [37] tested three different modeling approaches available in the literature on the Brake-Reuss beam [38] . The first method was Sandia's modeling approach using a four-parameter Iwan element at which transient time domain analysis is conducted. In the other two modeling methods, the contact elements were based on Jenkins elements. The investigated methods were able to capture the nonlinear responses similarly. They show that the microslip behavior present in small-amplitude responses can be modeled by implementing multiple Jenkins elements whose computational cost is not feasible. The shortcoming of the whole-joint element was its inability to capture the detailed contact state distribution.

In 2019, Karapıstık and Cigeroglu [39] [40] developed a new reduced-order modeling method for the response determination of bolted joint connections. A two-step reduction methodology is followed. Instead of modeling the contact behavior between parts with macroslip elements, a microslip friction element at which macroslip elements are connected is implemented to decrease the dimension of the equation of motion. These microslip elements are reduced by optimization of the number and parameters of included macroslip elements.

## 1.2 Objective of the Thesis

The bolted joints are one of the most common and widely used connection method. To obtain the dynamic characteristic of systems with bolted joints accurately, the nonlinearity effect should be included. With high-fidelity contact models, an accurate response can be obtained whereas the computational cost is drastically increased. The reduced-order modeling of bolted connections is essential to obtain a nonlinear dynamic response with adequate accuracy.

The aim of the work represented in this thesis is to decrease the computational cost of the reduced contact model by utilizing modal superposition method with response dependent nonlinear modes.

In this thesis, the reduced-order model of bolted joint connections is presented. The contact model is reduced by the two-step reduction methodology proposed by Karapistik [40] . The nonlinear response of bolted joint connection is solved utilizing the response-dependent nonlinear modes.

The first step of contact model reduction is defining a joint region that consists of macroslip elements connected as parallel springs. The response characteristic of the joint region is similar to microslip friction elements. The second step of contact modal reduction is the optimization of the number of elements inside the joint region of interest. With reduced joint definition, the same hysteresis loop is obtained with fewer macroslip elements inside joint regions. The computational time required to calculate the nonlinear force is further decreased with a decrease in the number of macroslip elements.

With the utilization of RDNM, the number of modes included to the response calculation is reduced; hence, the computational time is reduced while preserving the accuracy of the response. The accuracy of the proposed method and the superior performance of RDNM are investigated in two case studies where representative finite element models of lap joint connection models are constructed and the results

are compared with results of the modal superposition method with linear mode shapes.

## 1.3 Outline of the Thesis

In Chapter 2, modeling methods for forced vibrations of nonlinear systems is examined. First, frequency domain solution methods Harmonic Balance Method (HBM), Modal Superposition Method (MSM) and Modal Superposition Method with Response Dependent Mode Shapes (RDNM) are inspected in detail. Second, mathematical modelling of the nonlinear force calculation is explained. The transition angles are given for single harmonic motion. Lastly, the numerical solution procedures: Newton's Method, Arc-Length Continuation Method, and Predictor for Path Following Method are summarized.

In Chapter 3, the validation of the proposed reduction method is demonstrated in two case studies while both 1D dry friction elements with constant normal load and variable normal load are defined separately. The first case study model consists of two beams connected with three bolts, whereas in the second case study four bolts are used for the connection. The two-step contact reduction methodology is explained in detail. At each reduction step, the effect of implementing the response-dependent nonlinear modes is demonstrated.

In Chapter 4, the summary of the study is given along with the possible future studies on the reduction method.

# CHAPTER 2

# MODELLING OF FORCED VIBRATIONS OF NONLINEAR SYSTEMS

## 2.1 The Nonlinear Equation of Motion

The most straightforward notation for the equation of motion of a vibratory system (EOM) at which a nonlinear effect is present can be written as follows

$$M \cdot \ddot{x(t)} + C \cdot \dot{x(t)} + i \cdot H \cdot x(t) + K \cdot x(t) + F_N(t) = F(t) \qquad (2.1)$$

where x(t) is the displacement vector of the system. M, C, H, and K stand for mass, viscous damping, structural damping, and stiffness matrices of the system of interest. $F_N(t)$ and $F(t)$ are the internal nonlinear forcing vector and the excitation force, $t$ is time, respectively.

### 2.1.1 Harmonic Balance Method (HBM)

By representing the excitation force $F(t)$ as a harmonic forcing, the displacement vector $x(t)$ is expected to be in the form of harmonic motion whose mathematical equivalence is defined in Equation ( 2.2) and Equation ( 2.3) by implementing Fourier series expansion.

$$F(t) = F_0 + \sum_{i=1}^{N_h} F_{s_i} \cdot \sin(i \cdot \omega \cdot t) + F_{c_i} \cdot \cos(i \cdot \omega \cdot t) \qquad (2.2)$$

$$x(t) = x_0 + \sum_{i=1}^{N_h} x_{s_i} \cdot \sin(i \cdot \omega \cdot t) + x_{c_i} \cdot \sin(i \cdot \omega \cdot t) \quad (2.3)$$

where $F_0$ and $x_0$ are bias terms of excitation forcing and response vectors, respectively. Subscript within summation operator "$i$" stands for $i^{th}$ harmonic, and $N_h$ is the total number of harmonics. $F_{s_i}$, $F_{c_i}$, $x_{s_i}$, and $x_{c_i}$ are sine and cosine coefficients of corresponding harmonics, and $\omega$ is the frequency.

The integral formulae for the internal nonlinear forcing vector $F_N(t)$ are provided in Equations ( 2.4), ( 2.5), and ( 2.6) where $\theta = \omega \cdot t$.

$$F_{N_0} = \frac{1}{2\pi} \cdot \int_0^{2\pi} f_N(\theta) \cdot d\theta \quad (2.4)$$

$$F_{N_{s_i}} = \frac{1}{\pi} \cdot \int_0^{2\pi} f_N(\theta) \cdot \sin(i \cdot \theta) \cdot d\theta \quad (2.5)$$

$$F_{N_{c_i}} = \frac{1}{\pi} \cdot \int_0^{2\pi} f_N(\theta) \cdot \cos(i \cdot \theta) \cdot d\theta \quad (2.6)$$

After implementing the expanded displacement, nonlinear force, and excitation force vectors to EOM, the coefficients of similar trigonometric terms are balanced to determine the unknown terms.

The single harmonic motion of systems is examined within the scope of this thesis.

### 2.1.2 Modal Superposition Method (MSM)

With the utilization of HBM, although the EOM is represented with real terms, the number of nonlinear equations to be solved can be very large, especially for systems with many degrees of freedom (DOF). Consequently, numerical difficulties such as the decrease in convergence rate and increase in computation time can be encountered. In order to decrease the number of equations to be solved, Modal Superposition Method (MSM) is used in this study.

The response vector is defined in terms of the linear system modes as Equation ( 2.7).

$$x(t) = \sum_{m=1}^{N_m} a_m \cdot \phi_m \cdot e^{i \cdot \omega t} \quad (2.7)$$

where $\phi_m$ is the $m^{th}$ mass normalized mode shape of the linear system, $a_m$ is the complex coefficient of $m^{th}$ mode, and $N_m$ is the number of modes. Substituting the new form of the response Equation ( 2.7) into the EOM Equation ( 2.1) and pre-multiplying with $\phi^T$ , the motion equation can be expressed as follows

$$\phi^T \cdot \left(-\omega^2 \cdot M + i \cdot \omega \cdot C + (K + i \cdot H)\right) \cdot \phi \cdot a + \phi^T \cdot F_N = \phi^T \cdot F \quad (2.8)$$

Since mass normalized mode shapes are considered, Equation ( 2.8) reduces to Equation ( 2.9).

$$(-\omega^2 \cdot I + i \cdot \omega \cdot C_d + \Omega + i \cdot H_d) \cdot a + \phi^T \cdot F_N = \phi^T \cdot F \quad (2.9)$$

where Ω is a diagonal matrix consisting of squares of natural frequencies, $I$ is the identity matrix, $C_d$ is a modal viscous damping matrix and $H_d$ is a modal structural damping matrix.

The nonlinear equation number is reduced to $(3 \cdot N_m)$ when single harmonic motion with bias terms is examined, which is drastically less compared to the number of total DOFs. While deciding on the number of modes included in the solution process of EOM, the nonlinear force vector $F_N$ should be considered.

### 2.1.3 Modal Superposition Method with Response Dependent Mode Shapes (RDNM)

As the nonlinearity effect within the system increases, the number of linear modes required to include MSM formulation is increased to calculate the nonlinear response accurately. Ferhatoğlu et al. [41] proposed a new modal superposition method called Response Dependent Mode Shapes (RDNM). Using Describing Function Method (DFM), the internal nonlinear forcing vector can be defined as follows

$$F_N(x) = (\Delta_{re} + i \cdot \Delta_{im}) \cdot x \quad (2.10)$$

where $\Delta_{re}, \Delta_{im}$ are real and complex parts of the nonlinearity matrix. The EOM Equation ( 2.1) becomes Equation ( 2.11) after implementing Equation ( 2.10) for the nonlinear forcing term.

$$M \cdot \ddot{x(t)} + C \cdot \dot{x(t)} + i \cdot (H + \Delta_{im}) \cdot x(t) + (K + \Delta_{re}) \cdot x(t) = F(t) \quad (2.11)$$

In Equation ( 2.11), the effect of nonlinearity on the overall stiffness of the system is apparent. The system's new eigenvalue problem (EVP) becomes Equation 2.13, where obtained mode shape is response dependent mode $\phi_N$ of corresponding nonlinearity value.

$$(K + \Delta_{re}) \cdot u = \omega_N^2 \cdot M \cdot u \quad (2.12)$$

The size of EVP is $nxn$ for Equation ( 2.12) where n denotes the DOF of the linear system. To decrease the size of EVP, Dual Space Method [41] is implemented. The RDNM takes the form defined in Equation ( 2.13) where $\tilde{\phi}$ is the modal matrix obtained from the updated form of EVP in Equation ( 2.14) whose size is $N_m x N_m$ and Ω is the eigenvalue matrix of linear system.

$$\phi_N = \phi \cdot \tilde{\phi} \quad (2.13)$$

$$(\Omega + \phi^T \cdot \Delta_{re} \cdot \phi) \cdot \tilde{u} = \tilde{\omega}^2 \cdot I \cdot \tilde{u} \quad (2.14)$$

The response dependent nonlinear mode is dependent on the nonlinearity value at corresponding frequency value. With changing energy level of the response, RDNM also changes which is similar to Nonlinear Normal Mode (NNM) concept. The advantage of RDNM compared to NNM is the simplicity of calculation process, especially for realistic large MDOF systems.

It should be noted that the calculation of nonlinear force with DFM is not required to implement RDNM. The calculated nonlinear force value with Fourier coefficients can also be used by calculating the corresponding stiffness value of nonlinearity by the real part of the ratio of force value to displacement value.

## 2.2 Mathematical Modelling of Nonlinear Force

In this thesis, the source of nonlinearity in focus is the friction caused by contact in-between two or more bodies. There are two approaches available in the literature to model friction contact: macroslip and microslip. The normal force resulting from preload of bolted connection is small compared to the excitation force. For higher contact force values, partial slip occurs, which cannot be modeled with macroslip. Ergo, the mathematical formulation of 1D macroslip friction model is implemented and examined in detail.

### 2.2.1 1D Dry Friction Element with Constant Normal Load

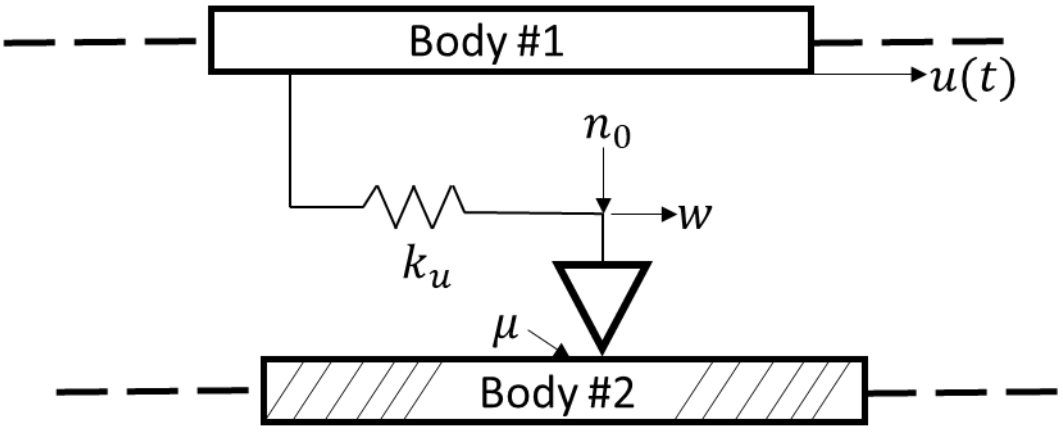


Figure 2.1. Distributed Contact Model of 1D Dry Friction with Constant Normal Load

The tangential motion in-between bodies are considered such that Body #2 is grounded, whereas Body #1 moves with relative input $u(t)$. At the contact node of

these two bodies, the slip motion $w(t)$ occurs. The force equality at spring located in-between bodies at tangential direction is as follows,

$$f = k_u \cdot (u - w) \quad (2.15)$$

If Body #1 slips, the friction force becomes constant, and it is expressed as,

$$f = \pm\mu \cdot n0 \quad (2.16)$$

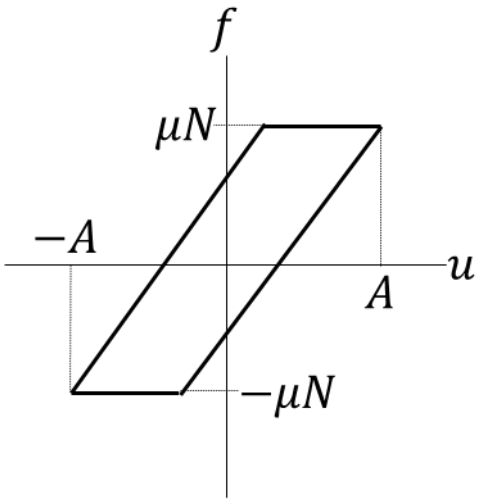


Figure 2.2. Hysteresis Loop of 1D Dry Friction Element with Constant Normal Load

In Equation ( 2.15), $k_u$ stands for the tangential stiffness value, and in Equation ( 2.16), $\mu$ is the friction coefficient, $n_0$ is the normal load value.

By assuming single harmonic motion, obtained the hysteresis loop of constant normal load 1D Dry friction element is given in Figure 2.2. The relative tangential motion is as follows

$$u = A \cdot \sin(\theta) \dots (\theta = \omega \cdot t) \quad (2.17)$$

Slip to stick transition occurs when both Equation ( 2.15) and Equation ( 2.16) is satisfied. Examining the time derivative of Equation ( 2.18) and Equation ( 2.19), it is apparent that this transition occurs at the instant in which relative motion $u$

reverses its direction. The corresponding transition angles are calculated as $\pi/2, 3\pi/2$.

$$\dot{f} = k_u \cdot (\dot{u} - \dot{w}) = 0 \quad (2.18)$$

$$\dot{u} = A \cdot \cos(\theta) \cdot \omega = 0 \quad (2.19)$$

Stick to positive slip transition occurs when

$$f = k_u \cdot (u - u_0) + f_0 = \mu \cdot n_0 \quad (2.20)$$

where $f_0$ and $u_0$ are the friction force and displacement values at the beginning of positive slip state which is $f_0 = -\mu \cdot n_0$ and $u_0 = u(3\pi/2) = -A$. Implementing these formulae into Equation ( 2.20),

$$\theta_{SP} = 2 \cdot \pi - \sin^{-1}(1 - \frac{2 \cdot \mu n_0}{k_u \cdot A}) \quad (2.21)$$

Stick to negative slip transition occurs when

$$f = k_u \cdot (u - u_0) + f_0 = -\mu \cdot n_0 \quad (2.22)$$

where $f_0 = \mu \cdot n_0$ and $u_0 = u(\pi/2) = A$. Implementing these formulae into Equation ( 2.22),

$$\theta_{SN} = \pi - \sin^{-1}(1 - \frac{2 \cdot \mu n_0}{k_u \cdot A}) \quad (2.23)$$

The resultant friction force values are summarized in Equation ( 2.25).

In addition to these conditions, the complete stick case is possible at which stick to slip transition does not occur, and the elements stay in the stick state. The corresponding friction force for complete stick is provided in Equation ( 2.24).

$$f(\theta) = \begin{cases} k_u \cdot (A \cdot \sin(\theta) - A) + \mu \cdot n_0 & \dots \pi/2 < \theta < 3\pi/2 \\ -\mu \cdot n_0 & \dots \theta_{SN} < \theta < 3\pi/2 \\ k_u \cdot (A \cdot \sin(\theta) + A) - \mu \cdot n_0 & \dots 3\pi/2 < \theta < \theta_{SP} \\ \mu \cdot n_0 & \dots \theta_{SP} < \theta < 5\pi/2 \end{cases} \quad (2.25)$$

$$f(\theta) = k_u \cdot u \quad (2.24)$$

### 2.2.2 1D Dry Friction Element with Normal Load Variation

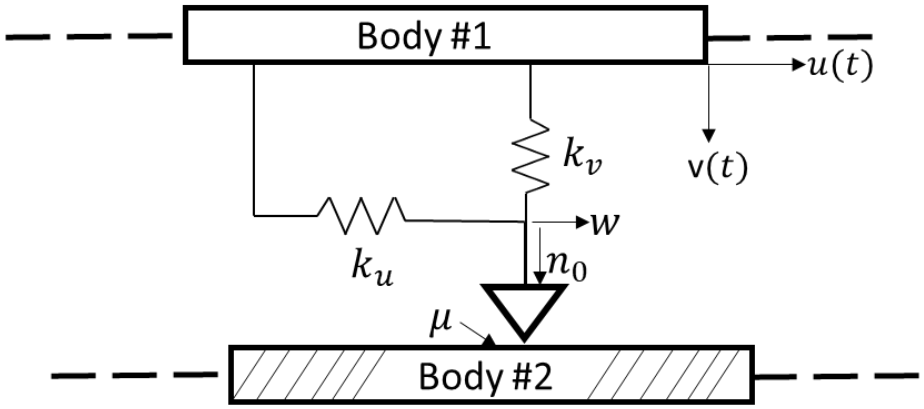


Figure 2.3. Distributed Contact Model of 1D Dry Friction with Variable Normal Load

The constant normal load assumption is valid if only relative motion in-between bodies stay on the contact plane, whereas this may not be the case for all design configurations. The local separation from the contact plane can be analyzed by including the motion in the normal direction. The representation of friction with normal load variation is given in Figure 2.3.

Similar to the constant normal load case, Body #2 is taken as grounded, whereas Body #1 moves with relative input $u(t)$ and $v(t)$. The normal force at contact interface acts as follows

$$n(t) = \begin{cases} n_0 + k_v \cdot v & \dots v(t) \geq \frac{-n_0}{k_v} \\ 0 & Otherwise \end{cases} \quad (2.26)$$

The friction force in tangential spring is equal to Equation ( 2.15). Unlike the constant normal load assumption, the direction of tangential motion may not change at the transition instant from slip to stick. The slip velocity of stick to positive slip and negative slip are stated in Equations ( 2.27) and ( 2.28).

$$\dot{w} = \dot{u} - \frac{\mu \cdot k_v}{k_u} \cdot \dot{v} \quad (2.27)$$

$$\dot{w} = \dot{u} + \frac{\mu \cdot k_v}{k_u} \cdot \dot{v} \quad (2.28)$$

The criteria for positive slip to stick and negative slip to stick is provided in Equations ( 2.29) and ( 2.30).

$$\dot{u} - \frac{\mu \cdot k_v}{k_u} \cdot \dot{v} = 0 \quad \& \quad \ddot{u} - \frac{\mu \cdot k_v}{k_u} \cdot \ddot{v} < 0 \quad (2.29)$$

$$\dot{u} + \frac{\mu \cdot k_v}{k_u} \cdot \dot{v} = 0 \quad \& \quad \ddot{u} + \frac{\mu \cdot k_v}{k_u} \cdot \ddot{v} > 0 \quad (2.30)$$

The transition from stick to positive slip and negative slip is provided in Equations ( 2.31) and ( 2.32).

$$k_u \cdot (u - u_0) + f_0 - \mu \cdot (n_0 + k_v \cdot v) = 0 \quad \& \quad k_u \cdot \dot{u} - \mu \cdot k_v \cdot \dot{v} > 0 \quad (2.31)$$

$$k_u \cdot (u - u_0) + f_0 + \mu \cdot (n_0 + k_v \cdot v) = 0 \quad \& \quad k_u \cdot \dot{u} + \mu \cdot k_v \cdot \dot{v} < 0 \quad (2.32)$$

As friction force in normal direction decreases, separation in tangential direction can occur. The criteria at the beginning of separation and at the end of separation is provided in Equations ( 2.33) and ( 2.34).

$$n_0 + k_\nu \cdot \nu = 0 \ldots \dot{v} < 0 \qquad (2.33)$$

$$n_0 + k_\nu \cdot \nu = 0 \ldots \dot{v} > 0 \qquad (2.34)$$

As a result, four different contact states might occur. The detailed sequences of friction characteristics with corresponding transition angles are taken as stated in Yang et. al.'s study [23] . For brevity of this document, these formulae are not included.

## 2.3 Solution of Nonlinear Algebraic Equations

The EOM given in Equation ( 2.1) is a set of nonlinear ordinary differential equations, whereas the corresponding nonlinear algebraic equation set is given in Equation ( 2.9), and its residual vector is Equation ( 2.35). As mentioned in the previous section, the internal nonlinear for $F_{NL}$ depends on the value of response $x$.

$$R(x, \omega) = (-\omega^2 \cdot I + i \cdot \omega \cdot C_d + (1 + i) \cdot \Omega) \cdot a + \phi^T \cdot F_N - \phi^T \cdot F \qquad (2.35)$$

The algebraic equation set given in Equation ( 2.9) is dependent on both displacement and frequency, frequency $\omega$ is taken as a path following parameter since the system's response throughout a frequency range is desired. As one of the unknowns from Equation ( 2.35) is chosen as the path following parameter, the remaining unknown $x$ can be solved iteratively with Newton's Method. The path following method Arc-Length Continuation Method is utilized to solve for path following parameter $\omega$.

### 2.3.1 Newton's Method

Expanding Equation ( 2.35) in Taylor series around x, the redefined form is as follows,

$$R_i(x + \Delta x, \omega) = R_i(x, \omega) + \sum_{j=1}^{n}(\frac{\partial R_i}{\partial x_j} \cdot \Delta x_j) + O(\Delta x^2) \quad (2.36)$$

where matrix of partial derivatives $\frac{\partial R_i}{\partial x_j}$ is defined as Jacobian matrix J and $i$ is iteration number. The simplified form of displacement x is given in Equation ( 2.37). Iterations of displacement vector $x_i$ is stopped when a predetermined error limit for residual vector is achieved.

$$x_{i+1} = x_i - J(x_i, \omega)^{-1} \cdot R(x_i, \omega) \quad (2.37)$$

Calculating the Jacobian matrix with analytical notation is not always possible, as the nonlinearity effect gets more dominant the expression in Equation ( 2.35) gets more complex. A numerical approximation to the Jacobian matrix can be used in these cases. Two of these approximations are the implementation of forward difference and central difference formula. Since the order of central difference formula is nearly two times more than forward difference formula, forward difference notation in Equation ( 2.38) is implemented in the calculation process for the rest of the study.

$$J_{ij}(x_i, \omega) = \frac{R_i(x + h_j \cdot e_j, \omega) - R_i(x, \omega)}{h_j} \quad (2.38)$$

where $h_j$ is the step size scaled with square root of precision of the function calculation and $e_j$ is the unit vector in $j^{th}$direction. While calculating residual vector for new value of x which is $x + h_j \cdot e_j$, the value of external force does not change. Hence, the difference between the remaining part of residual vector is calculated to

determine Jacobian matrix. To further reduce computational time for Jacobian calculation, one can refer to a new Jacobian calculation method proposed by Kızılay [42] .

### 2.3.2 Arc-Length Continuation Method

Since more than one equilibrium state is possible at same frequency value and there may be cases at which calculated Jacobian matrix is singular, the frequency response function of Equation ( 2.35) can be solved by changing the new path following parameter even around turning points.

Representation of arc-length continuation method around a solution point is given Figure 2.4. The new path following parameter is the radius of a hypothetical sphere ($\Delta s$) in which the next solution is looked for. The new unknown vector in Equation ( 2.39) consists of displacement vector $x$ and frequency $\omega$. The equation of this hypothetical sphere with radius $s$ centered at last solution point defines the relationship between unknowns $x$ and $\omega$ as stated in Equation ( 2.40).

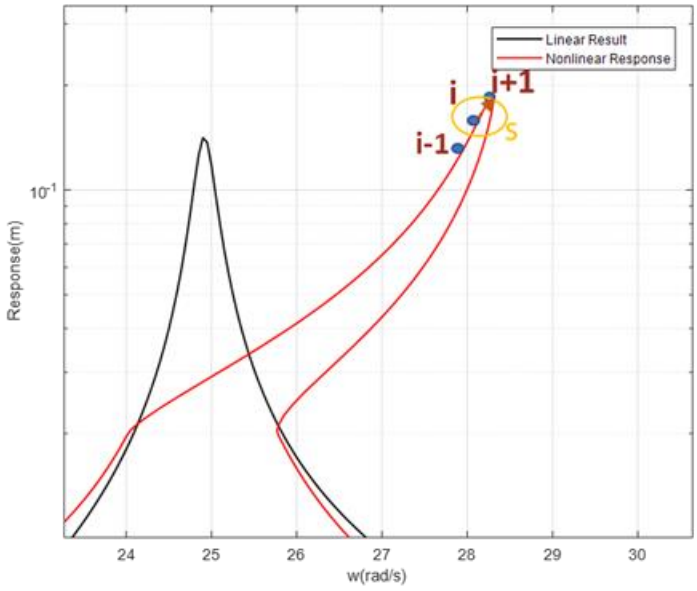


Figure 2.4. Representation of Hypothetical Circle in Arc-Length Continuation Method

$$q = \begin{Bmatrix} x \\ \omega \end{Bmatrix} \quad (2.39)$$

$$h(x_i, \omega_i) = (\Delta q)_i^T \cdot (\Delta q)_i - \Delta s^2 \; where \; \Delta q_i = \begin{Bmatrix} \Delta x_i \\ \Delta \omega_i \end{Bmatrix} \quad (2.40)$$

Equation ( 2.35) and Equation ( 2.40) is solved with Newton's Method whose solution form is stated in Equation ( 2.41).

$$\Delta q_{i+1} = \Delta q_i - \begin{bmatrix} \frac{\partial R(\{x\}_i, \omega_i)}{\partial x} & \frac{\partial R(\{x\}_i, \omega_i)}{\partial \omega} \\ \frac{\partial h(\{x\}_i, \omega_i)}{\partial x} & \frac{\partial h(\{x\}_i, \omega_i)}{\partial \omega} \end{bmatrix}^{-1} \cdot \begin{Bmatrix} R(x_i, \omega_i) \\ h(x_i, \omega_i) \end{Bmatrix} \quad (2.41)$$

The partial derivative of additional equation is shown in Equation ( 2.42).

$$\begin{bmatrix} \frac{\partial h(\{x\}_i, \omega_i)}{\partial x} & \frac{\partial h(\{x\}_i, \omega_i)}{\partial \omega} \end{bmatrix} = 2 \cdot \Delta q_i^T \quad (2.42)$$

### 2.3.3 Predictor for Path Following Method

A good initial guess is required to ensure the convergence of Newton's Method. $1^{st}$ order predictor is included in the solution process. A tangent vector to the solution curve is obtained by taking the derivative of the residual vector Equation ( 2.35) with respect to $\omega$. Rearranging Equation ( 2.43)( 2.44), formula of tangent vector is obtained as Equation ( 2.44).

$$\frac{dR(x,\omega)}{d\omega} = \frac{\partial R(x,\omega)}{\partial x} \cdot \frac{\partial x}{\partial \omega} + \frac{\partial R(x,\omega)}{\partial \omega} \quad (2.43)$$

$$\frac{\partial x}{\partial \omega} = -J(x,\omega)^{-1} \cdot \frac{\partial R(x,\omega)}{\partial \omega} \quad (2.44)$$

The final form of the initial guess for the next iteration is given in Equation ( 2.45) which is calculated by implementing Equation ( 2.44) into $1st$ order Taylor series expansion of the solution point at the next frequency value.

A similar approach is followed to determine the initial guess for arc-length continuation method. The guess vector of $x$ as shown in Equation ( 2.45), implemented into arc-length Equation ( 2.40) whose simplified form is stated in Equation ( 2.46). The sign of $\delta\omega$ is obtained from the sign of determinant of Jacobian as Equation ( 2.47).

$$x(\omega + \delta\omega) = x(\omega) - J(x,\omega)^{-1} \cdot \frac{\partial R(x,\omega)}{\partial \omega} \cdot \delta\omega \quad (2.45)$$

$$\delta\omega = \pm \frac{\Delta s}{\sqrt{\left(J(x,\omega)^{-1} \cdot \frac{\partial R(x,\omega)}{\partial \omega}\right)^2 + 1}} \quad (2.46)$$

$$\delta\omega = sign(|J(x,\omega)|) \cdot \delta\omega \quad (2.47)$$

# CHAPTER 3

# REDUCED ORDER JOINT MODELING UTILIZING RESPONSE DEPENDENT NONLINEAR MODES

In Chapter 3.1, the response of the case study model is examined by utilizing 1D dry friction element with constant normal load whereas in Chapter 3.2, 1D dry friction element with variable normal load is implemented. First, FEA model of the bolted joint assembly is constructed, and the normal load values on the contact surface are calculated with nonlinear static analysis. The node-to-node contact model is constructed using the modes of the linear system. To illustrate the effect of utilizing response dependent mode shapes, high fidelity model and the reduced contact models are solved with both classical MSM at which the linear system modes are used and MSM with RDNM. The obtained FRFs and solution times are compared. The performance of the reduction methodology is demonstrated on two different case studies: a 3-bolted half lap joint and a 4- bolted half lap joint.

## 3.1 Reduced Order Modeling Utilizing 1D Dry Friction Element with Constant Normal Load

### 3.1.1 Case Study Model 1: Three-Bolted Assembly

The 3-bolted lap joint assembly modeled in commercial FEA software Abaqus [43] is given in Figure 3.1. The representative half-lap joint model consists of two beams connected by three M8 bolts and three nuts. Bolt and nuts are taken as a single part due to the threaded connection in-between them. Dimensions of the beam are given in Figure 3.2. The material of all parts is defined as steel, whose material properties are given in Table 3.1.

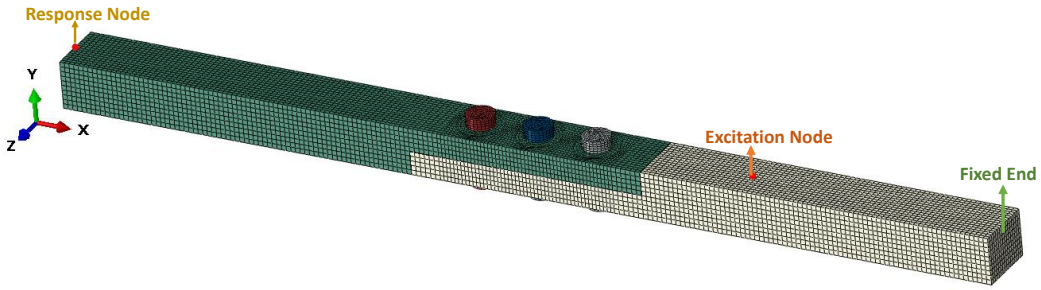


Figure 3.1. Finite Element Model of 3-Bolted Assembly

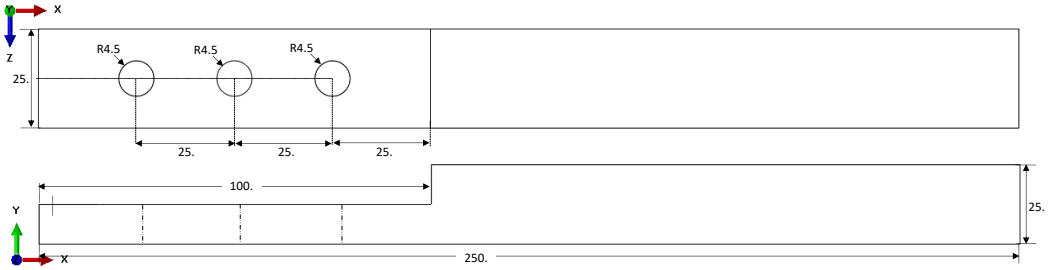


Figure 3.2. Dimensions of Beam Design 1

Table 3.1. Material Properties of Steel

| Density ($kg/m^3$) | Elastic Modulus (GPa) | Poisson's Ratio |
|---|---|---|
| 7900 | 190 | 0.3 |

The tangential behavior of contact between beams is defined with penalty friction formulation available in Abaqus software. The friction coefficient of penalty friction is defined as 0.1. The contact between beams and bolt heads/nuts is assumed to stay in stick since the contact area is small, resulting in high normal load distribution under low/ medium excitation levels. Hence, tie constraint, which restrains the relative motion in-between surfaces, is defined in these contact regions.

Nonlinear static analysis is conducted for fix-free boundary condition to obtain the initial normal load distribution on the contact surface. The preload value of M8 bolts is defined as 10 kN applied from cross section located at the mid-length bolt shank. The obtained result of contact force distribution in the direction of contact surface normal is given in Figure 3.3.

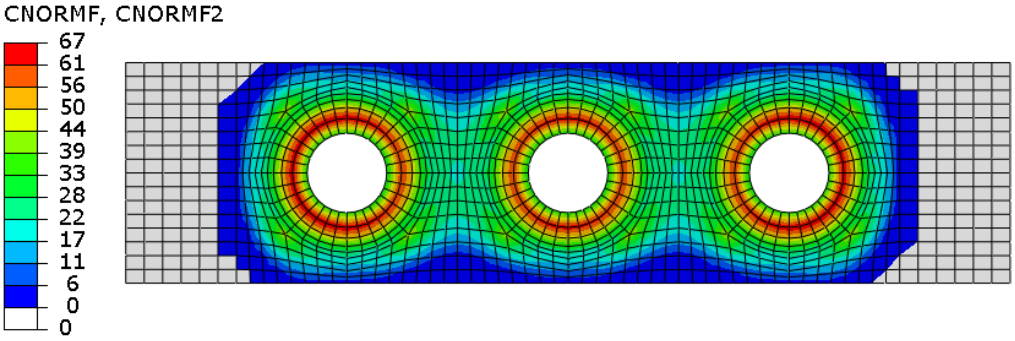


Figure 3.3. Normal Force Distribution on Contact Surface of 3- Bolted Lap Joint

#### 3.1.1.1 Representative High-Fidelity Model

The high-fidelity model consists of nodes in contact, a response node and an excitation node. The linear system model is constructed by using the mass-normalized mode shapes of the node region of interest and the corresponding eigenvalues. In the nonlinear model, 1D dry friction elements with constant normal load are defined in-between coincident nodes in the contact surface. The location of the node region of interest is chosen by examining the normal force distribution given in Figure 3.3.The node region of interest consists of 1183 nodes, as specified in Figure 3.4.

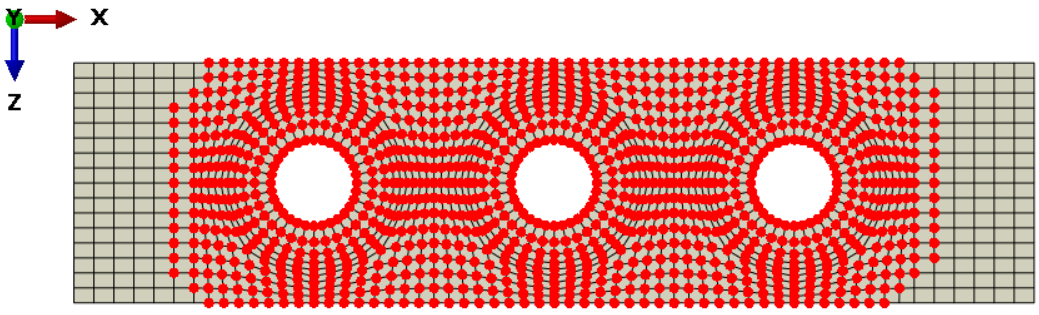


Figure 3.4. Locations of Interested Nodes

Modal analysis is conducted in Abaqus FEA software to calculate the system's natural frequencies and mode shapes of the node region of interest. Contact definition between beams is removed in this analysis since modes and natural

frequencies of the linear system are required. The nonlinear equation set is solved by utilizing Modal Superposition Method. Tangential stiffness and friction coefficients of 1D macroslip element are given in Table 3.2. Normal load values on friction elements are taken from the result of nonlinear static analysis. For this part of the study, normal loads are taken as constant. It should be kept in mind that normal load stays constant for specific design configurations. The motion in the direction of contact surface normal not only results in a change of normal force but might also result in local separation of contact surfaces.

Table 3.2. Tangential Stiffness and Friction Coefficient of 1D Dry Friction Element with Constant Normal Load

| $k_u$ | $\mu$ |
|---|---|
| 100 $^{kN}/_{mm}$ | 0.1 |

The first four bending modes of the system are implemented in mathematical model, which are given in Figure 3.5, Figure 3.6, Figure 3.7, and Figure 3.8. Force is applied perpendicular to the contact surface from node specified in Figure 3.1. The equation set is solved utilizing Arc-Length Continuation Method, which is examined in Chapter 2.

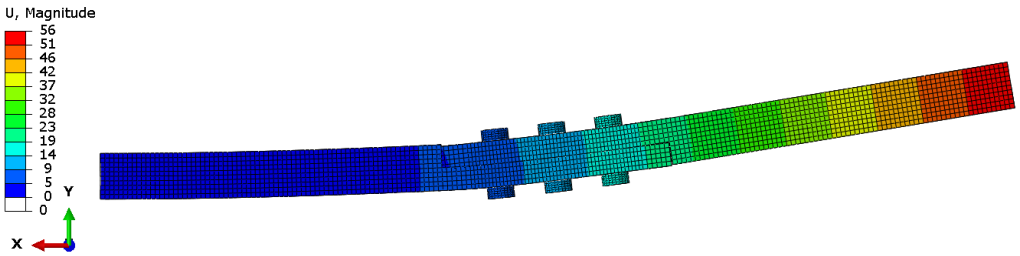


Figure 3.5. First Bending Mode (71 Hz)

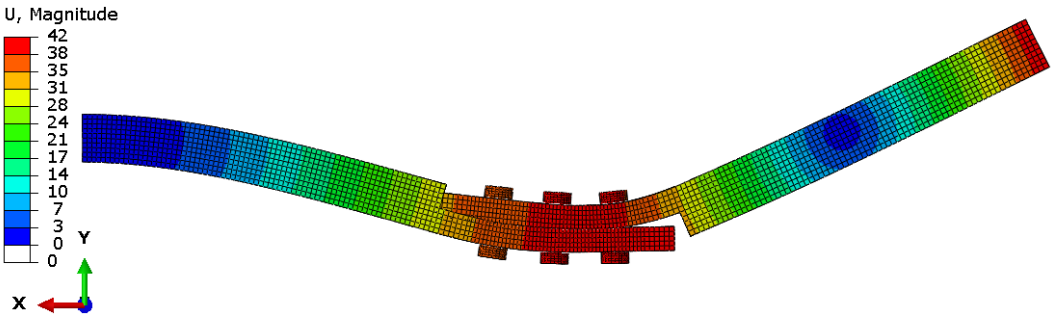


Figure 3.6. Second Bending Mode (362 Hz)

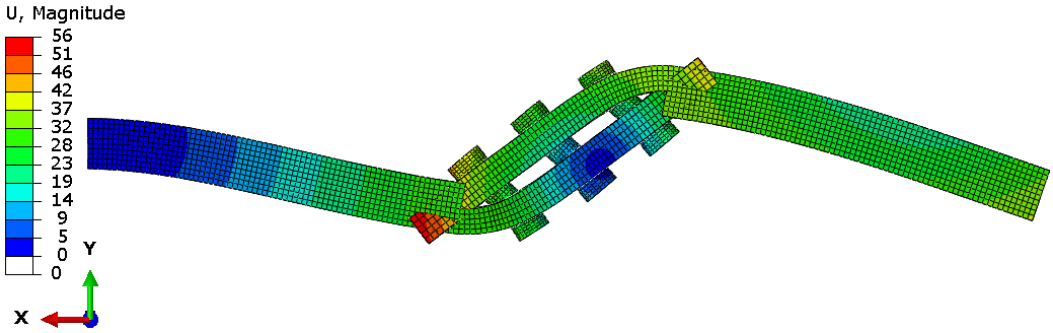


Figure 3.7. Third Bending Mode (946 Hz)

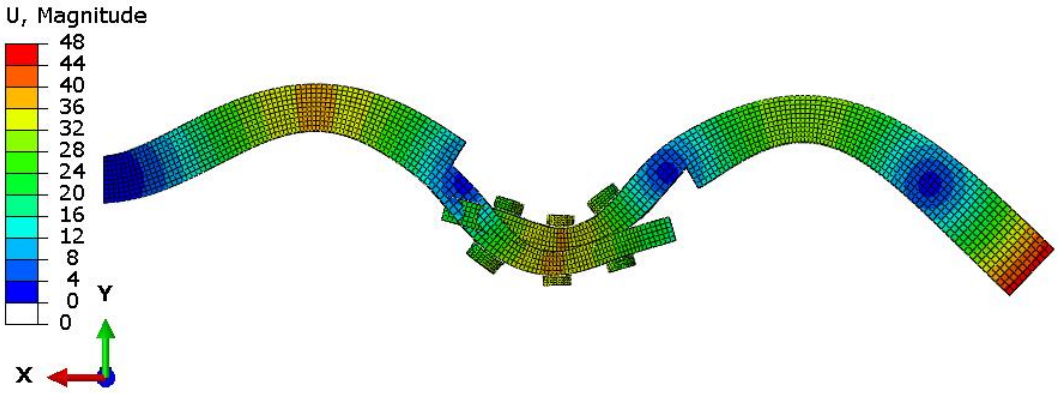


Figure 3.8. Fourth Bending Mode (2571 Hz)

Frequency response functions are calculated for several forcing values, which are given in Figure 3.9. The position of the response node is specified in Figure 3.1. For low excitation force value (0.001 N), dry friction elements stay stuck which is called as completed stick condition; hence energy is not lost as hysteric motion is not present. As excitation force increases, the response amplitude level decreases because the slip-stick motion transition starts to dominate the motion, resulting in energy loss. The presence of slip motion limits the stiffness value, which also results in the decrease of resonance frequency in addition to the response level.

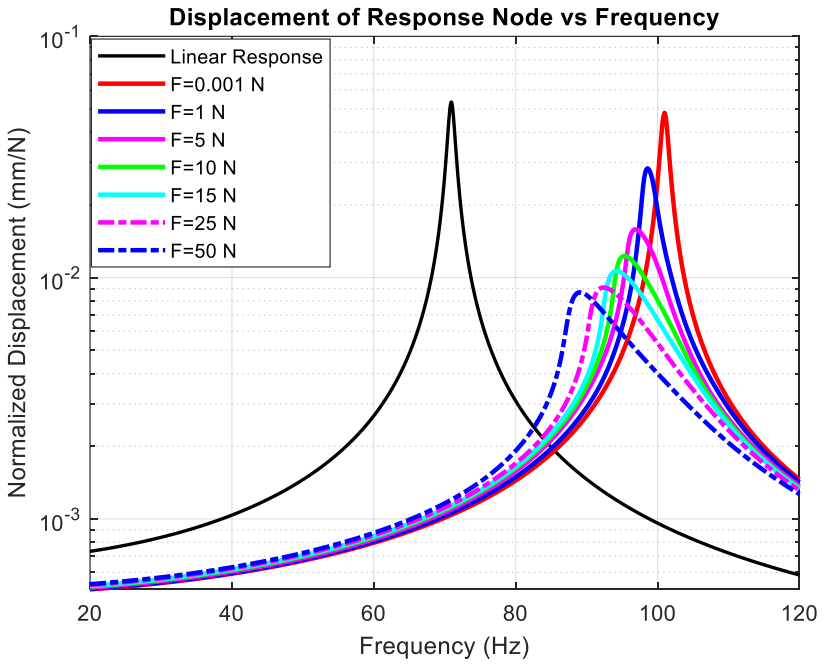


Figure 3.9. Normalized Response (mm/N) vs. Frequency (Hz) Graph

### 3.1.1.2 Calculation of Response Utilizing Modal Superposition Method with Response Dependent Nonlinear Modes

As stated in Chapter 2, in the classical Modal Superposition Method, the number of nonlinear equations equals the number of modes included in the solution process. For strong nonlinearities, the linear mode shapes of the system do not form an adequate basis to calculate the nonlinear response of the system. As a result, the

number of modes included in the solution should be increased to capture the accurate response level and characteristic. With the utilization of response dependent nonlinear modes, the required number of modes to obtain accurate response decreases since the calculated nonlinear mode shapes depend on the level of nonlinear force value.

At each solution point, the stiffness contribution of nonlinear force is calculated for each 1D dry friction element. As stated in Chapter 2, the real value of ratio of the nonlinear force value at last solution point to the relative displacement value gives the corresponding stiffness value. The nonlinearity matrix is constructed with these stiffness values. The calculated response dependent mode is used throughout iterations of the corresponding solution point. Since the calculated mode shape is dependent on the last solution point's response level, it changes during the frequency range of interest as the total energy level of the system changes.

High fidelity model is employed using one response dependent nonlinear mode, and corresponding results along with classical Modal Superposition Method’s results is given in Figure 3.10.

The nonlinear mode shapes of three bolted joint assembly are well separated for low to medium excitation levels. Hence, the obtained FRFs with one dependent nonlinear mode are compatible with the results of classical modal superposition method in which four linear system modes is used.

For medium to high excitation levels, as the system's total energy is decreased, the difference between calculated FRFs becomes more apparent. Increasing the number of RDNMs included in solution equations can decrease this difference for higher forcing levels.

It should also be noted that although the utilization of Dual Space Method to EVP decreases the dimension of EVP problem, it might also decrease the accuracy of the calculated mode shapes. This phenomenon is due to excluding some of the terms in Equation ( 2.9). The effect of this phenomenon can be found in [41] . Since the

performance advantage of RDNMs, when constant number of modes are used in classical MSM, is the focus of this work, the effect of using different linear modes to EVP Equation is not examined further. Hence, only the first four bending modes of the linear system are implemented to calculate the RDNM throughout case studies.

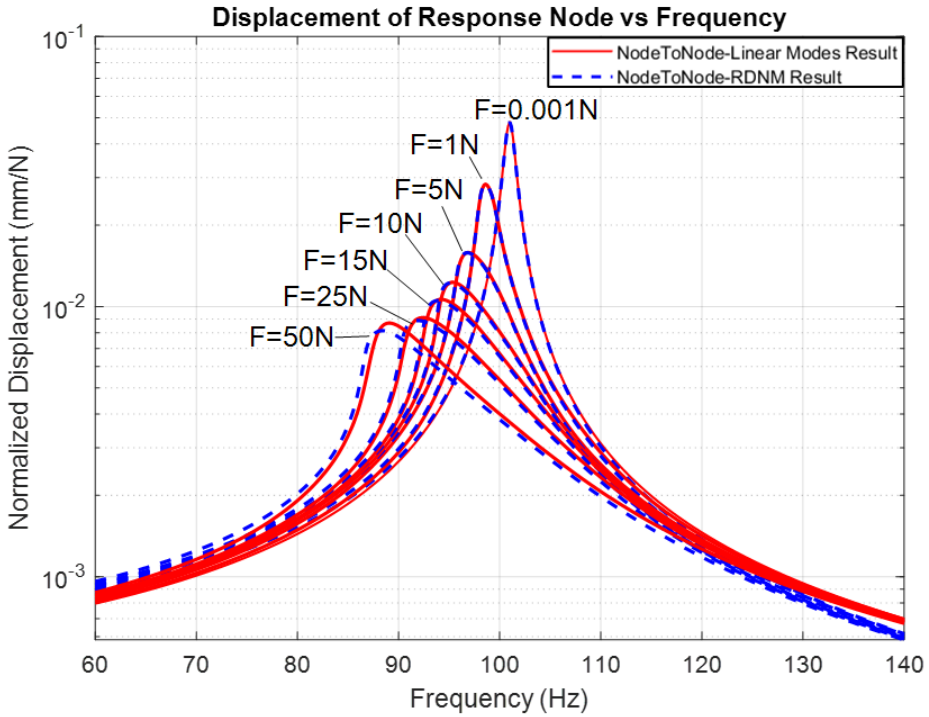


Figure 3.10. Normalized Response (mm/N) vs. Frequency (Hz) Utilizing Response Dependent Nonlinear Modes Graph 1

The solution times of high-fidelity model with linear system modes and RDNM are given in Table 3.3. The analyses are performed on a computer with AMD Ryzen7 4800H, a Radeon Graphics 2.90 GHz processor, 8 GB RAM, and a 64-bit operating system. For all excitation levels, the computational time with RDNM is nearly half the computational time of MSM with linear system modes. The reduced computational time also emphasizes that the computational time spent to solve the redefined form of EVP is insignificant compared to the time spent to calculate the nonlinear force value.

Since the FRFs throughout the interested frequency range are coherent with the FRFs calculated with classical MSM for different excitation levels and the computational time is reduced to nearly half, it is apparent that RDNMs form a solid basis for nonlinear response space.

Table 3.3. Computational Times with Linear Modes and RDNM

| Excitation Force Value (N) | Computational Time with Classical MSM(s) | Computational Time MSM with RDNM (s) | Reduction Percentage in Time (%) |
|---|---|---|---|
| **0.001** | 685.3 | 295.8 | 56.84 |
| **1** | 695.3 | 312.1 | 55.11 |
| **5** | 727.1 | 318.9 | 56.14 |
| **10** | 699.3 | 321.9 | 53.98 |
| **15** | 677.1 | 316.2 | 53.30 |
| **25** | 745.1 | 328.8 | 55.88 |
| **50** | 638.6 | 343.7 | 46.18 |

#### 3.1.1.3 First Reduction Step for Contact Model

The contact forces around bolt holes are higher than the force values around the edges. The variability of contact force results in partial slip on the surface, which can be modeled by the microslip friction model. The reduced contact model in this part of the study is proposed by Karapistik [40] . The approximated microslip element is constructed by connecting macroslip elements as parallel spring elements. The contact surfaces are divided into regions of joint at which the overall force is assumed to be transmitted in-between coincident regions.

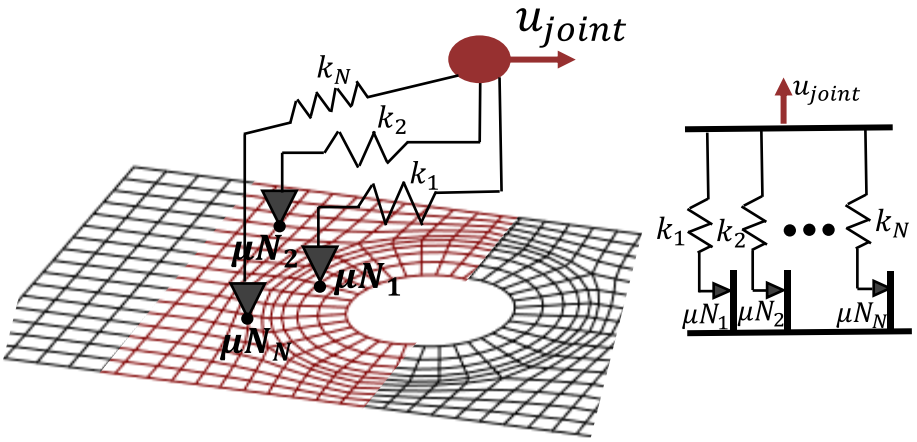


Figure 3.11. Schematic Representation of Reduced Order Joint Model

The representation of the reduced order joint model is given in Figure 3.11. The artificial node locations of joint regions are assumed to be located in the middle of the contact regions. The relative displacement of the joint is given in Equation (3.1) where A and B stand for contact surfaces, and *N* is the number of macroslip elements inside the joint region. The resultant total force value at artificial nodes is defined in Equation ( 3.2).

$$u_{joint} = \left( \frac{1}{N} \cdot \sum_{i=1}^{N} \phi_{A_i} - \frac{1}{N} \cdot \sum_{i=1}^{N} \phi_{B_i} \right) \cdot a \tag{3.1}$$

$$F_{NL_{joint}} = \sum_{i=1}^{N} (F_{s_i} \cdot \sin(i \cdot \omega \cdot t) + F_{c_i} \cdot \cos(i \cdot \omega \cdot t)) \tag{3.2}$$

Two different joint regions, as four joint regions and six joint regions are selected to examine the effect of the joint region's size. The joint regions are selected such that the normal load distribution on each joint region is similar to each other. The selected

joint regions and the corresponding element numbers in each region are given in Figure 3.12 and Figure 3.13.

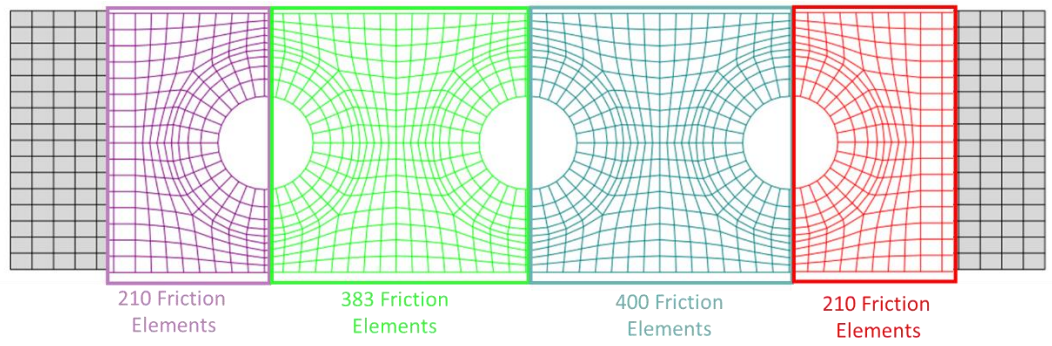


Figure 3.12. Location of 4 Joint Region on Contact Surface

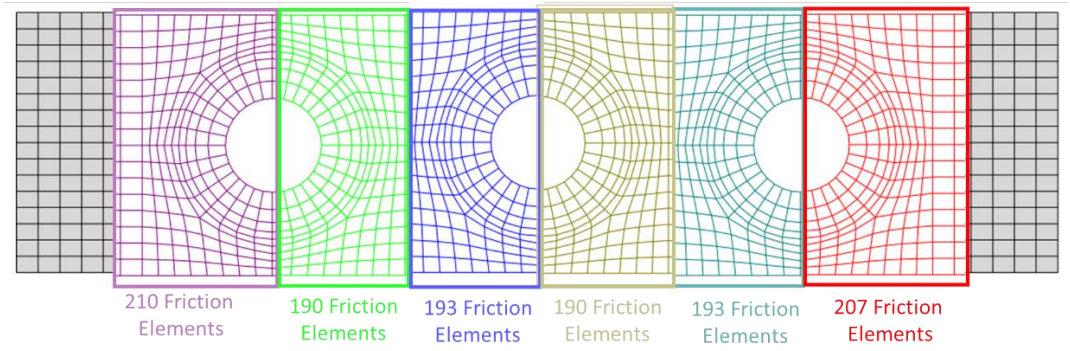


Figure 3.13. Location of 6 Joint Region on Contact Surface

For each joint region, an artificial node located between contact surfaces is defined as Equation (3.1 to calculate the corresponding displacement value. The FRF plots are given separately for different excitation levels from Figure 3.14 to Figure 3.17. The results of the node-to-node contact model calculated with linear system modes are also specified in these plots.

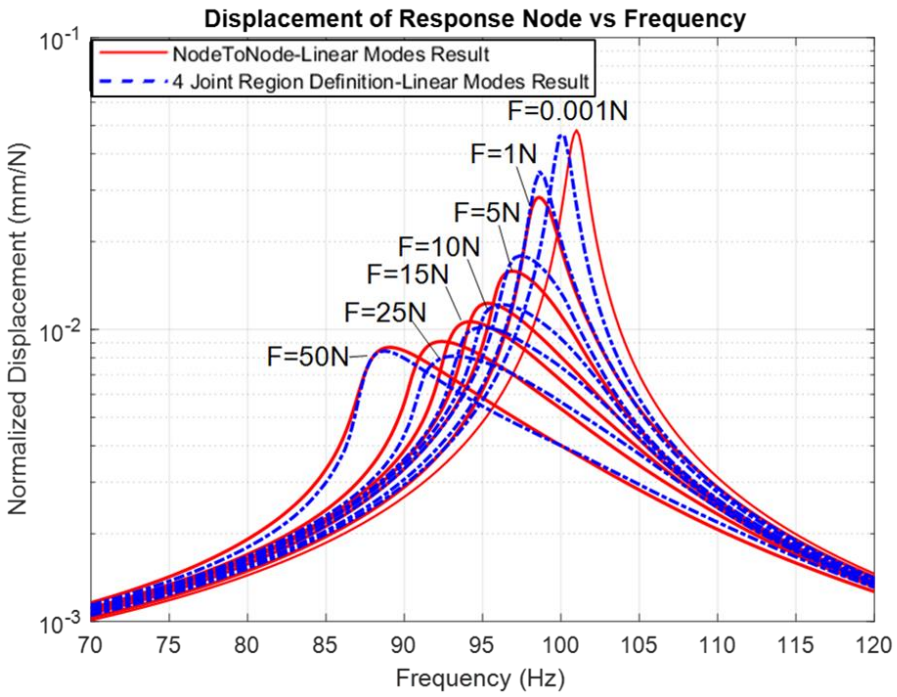


Figure 3.14. Normalized Response (mm/N) vs. Frequency (Hz) Graph for 4 Joint Region Utilizing 4 Linear System Modes

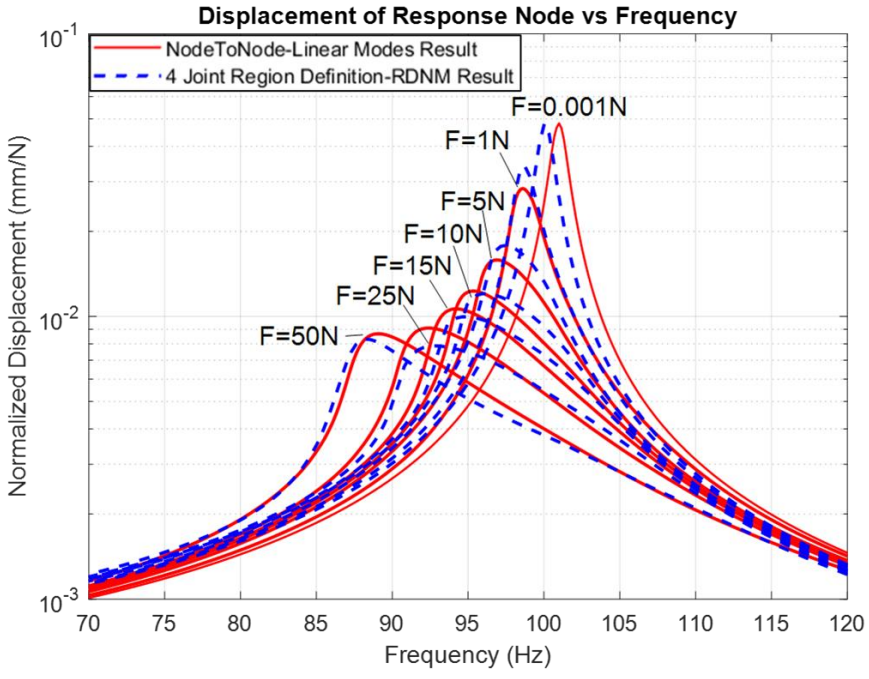


Figure 3.15. Normalized Response (mm/N) vs. Frequency (Hz) Graph for 4 Joint Region Utilizing 1 RDNM

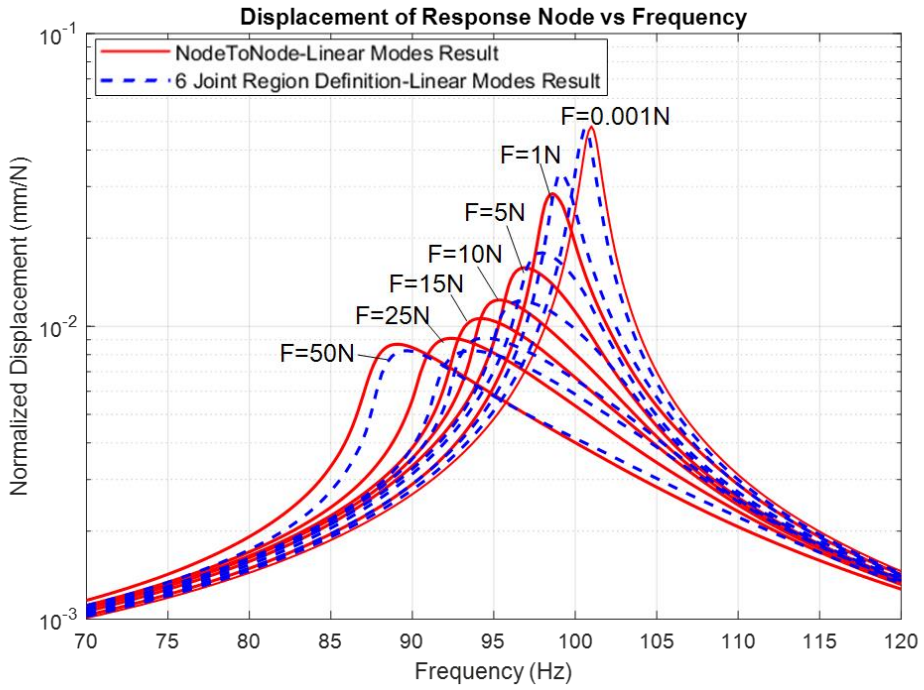


Figure 3.16. Normalized Response (mm/N) vs. Frequency (Hz) Graph for 6 Joint Region Utilizing 4 Linear System Modes

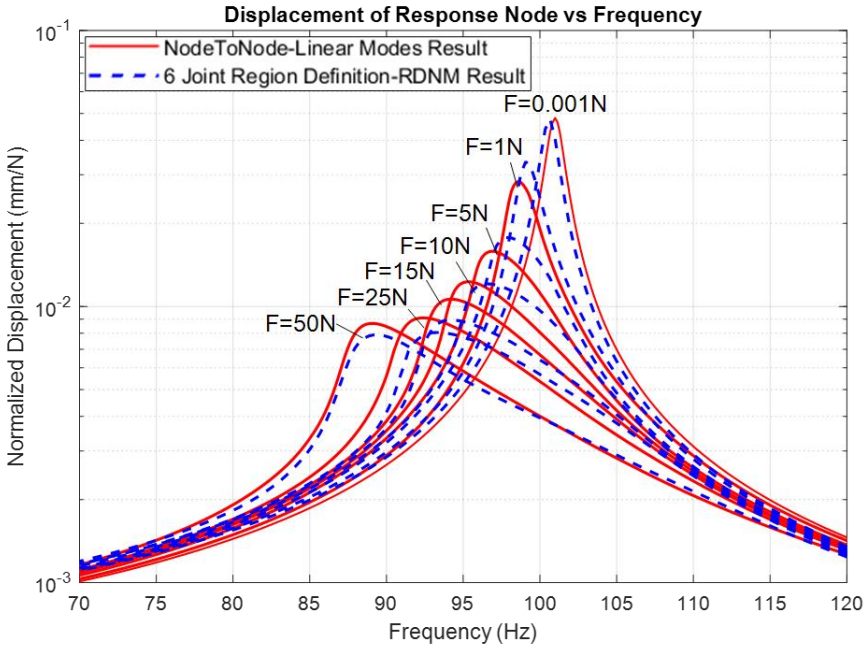


Figure 3.17. Normalized Response (mm/N) vs. Frequency (Hz) Graph for 6 Joint Region Utilizing 1 RDNM

Table 3.4. The Reduction in Computational Times of 6 Joint Region with Linear Modes and RDNM

| **Excitation Force Value (N)** | **Reduction Percentage in Time (%) of 6 Joint Region Utilizing 4 Linear Modes** | **Reduction Percentage in Time (%) of 6 Joint Region Utilizing 1 RDNM** |
|---|---|---|
| *0.001* | 99.74 | 99.92 |
| *1* | 99.72 | 99.91 |
| *5* | 99.77 | 99.91 |
| *10* | 99.72 | 99.90 |
| *15* | 99.71 | 99.90 |
| *25* | 99.72 | 99.90 |
| *50* | 99.74 | 99.90 |

For all excitation levels, the accuracy of obtained results utilizing joint regions improves as the joint region number increases; in other words, the size of the joint region decreases. For low to medium excitation levels ($F = [0.001 \rightarrow 10]N$), the results calculated using RDNM modes are compatible with those obtained with linear system modes. For medium to high excitation levels ($F = [15 \rightarrow 50]N$), the superior performance of RDNM is evident since the accuracy of RDNM results obtained with the same joint region definition is better than results of linear system modes even though only 1 RDNM is implemented in the calculation process.

Since the most accurate solutions are obtained with six joint regions reduction, the corresponding normalized solution times are given in Table 3.4. The solution times are normalized with the computational time of the high-fidelity model with classical MSM. Even for the highest excitation value of 50 N, the computational time is decreased to nearly 0.3% for classical MSM. When RDNMs are utilized in the solution process, this value further reduces to 0.1%, which strongly emphasizes the advantage of using RDNMs.

#### 3.1.1.4 Second Reduction Step for Contact Model

By decreasing the number of macroslip elements inside the joint regions, the required time to calculate the nonlinear force is further decreased. The reduced joint elements' parameters ($k_u, \mu N$) are selected such that the hysteresis loop of the reduced joint element is the same as the hysteresis loop of the joint element of interest.

The cost function defined by Karapistik [40] is used as the optimization problem. In Equation (3.3), $N$ stands for the number of macroslip elements inside the interested joint region, and $n$ is the number of macroslip elements inside the reduced joint element. $A, B, C$ are the magnitude of relative displacement.

$$Cost = \left( \begin{bmatrix} {F_{hyst}}_N^A \\ {F_{hyst}}_N^B \\ {F_{hyst}}_N^C \end{bmatrix} - \begin{bmatrix} {F_{hyst}}_n^A \\ {F_{hyst}}_n^B \\ {F_{hyst}}_n^C \end{bmatrix} \right) \cdot \left( \begin{bmatrix} {F_{hyst}}_N^A \\ {F_{hyst}}_N^B \\ {F_{hyst}}_N^C \end{bmatrix} - \begin{bmatrix} {F_{hyst}}_n^A \\ {F_{hyst}}_n^B \\ {F_{hyst}}_n^C \end{bmatrix} \right)^T \tag{3.3}$$

To minimize the difference between the obtained hysteresis loop and the hysteresis loop of the joint region of interest, nonlinear force values at three different relative displacement magnitudes are used. The relative displacement magnitudes are selected to achieve the same hysteresis loop even at high relative displacement magnitudes. The cost function is solved with "fmincon" a built-in MATLAB function [44] . The total stiffness and normal load values are defined as the limiting values of the parameters for reduced joint elements. With this definition, the unfitted regions at high displacement amplitudes are minimized. Hence, the deviation of the resonance frequency is omitted. The hysteresis loops of the six joint regions are reduced in this step.

Three different element number at the reduced joint region is represented in this document. For brevity of the thesis, only the hysteresis loop of the first joint region which contains 210 macroslip elements, is given along the hysteresis loop of the

reduced joint elements with 4 and 7 elements in Figure 3.18 and Figure 3.19. The normal load values at the nodes positioned at the same diameter are close to each other, hence the relative displacement values at which change of contact state occurs are also similar. As nonlinear force value in the hysteresis loop of joint region definition is the summation of nonlinear force values at each macroslip element, the resultant hysteresis consists of multiple lines with different slopes.

The tangential stiffness and normal load values of the reduced joint elements are given in Table 3.5 and Table 3.6.

Table 3.5. Parameters of Reduced Joint Element with 5 Elements

| | $k_1(kN/mm)$ | $k_2(kN/mm)$ | $k_3(kN/mm)$ | $k_4(kN/mm)$ |
|---|---|---|---|---|
| 1st Joint | 4132.6 | 4801.0 | 3969.5 | 4909.3 |
| 2nd Joint | 5222.5 | 4801.0 | 4813.2 | 4909.3 |
| 3rd Joint | 5222.5 | 4117.3 | 4813.2 | 3687.4 |
| 4th Joint | 5222.5 | 4930.2 | 4813.2 | 5265.3 |
| 5th Joint | 4007.3 | 4930.2 | 4172.0 | 5265.3 |
| 6th Joint | 4801.0 | 4930.2 | 4909.3 | 5265.3 |
| | $\mu N_1(N)$ | $\mu N_2(N)$ | $\mu N_3(N)$ | $\mu N_4(N)$ |
| 1st Joint | 939.2 | 859.7 | 435.7 | 377.1 |
| 2nd Joint | 204.8 | 360.6 | 842.9 | 479.9 |
| 3rd Joint | 331.9 | 367.2 | 221.8 | 299.8 |
| 4th Joint | 467.2 | 470.0 | 355.3 | 185.0 |
| 5th Joint | 228.0 | 223.8 | 917.2 | 418.5 |
| 6th Joint | 444.0 | 895.5 | 230.7 | 837.0 |

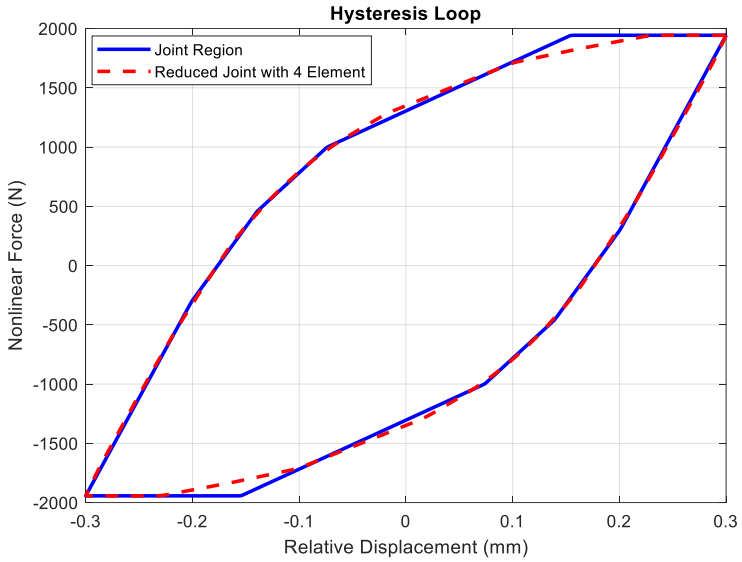


Figure 3.18. Hysteresis Loop of 1st Joint Region with 210 Elements and 4 Elements

Table 3.6. Parameters of Reduced Joint Element with 7 Elements

| | $k_1(\frac{kN}{mm})$ | $k_2(\frac{kN}{mm})$ | $k_3(\frac{kN}{mm})$ | $k_4(\frac{kN}{mm})$ | $k_5(\frac{kN}{mm})$ | $k_6(\frac{kN}{mm})$ | $k_7(\frac{kN}{mm})$ |
|---|---|---|---|---|---|---|---|
| 1st Joint | 2673.1 | 3315.4 | 2727.9 | 2800.5 | 2772.1 | 2813.5 | 3029.6 |
| 2nd Joint | 3315.4 | 2607.4 | 2727.9 | 2800.5 | 2772.1 | 2813.5 | 3029.6 |
| 3rd Joint | 3315.4 | 2727.9 | 2416.8 | 2800.5 | 2772.1 | 2813.5 | 3029.6 |
| 4th Joint | 3315.4 | 2727.9 | 2800.5 | 2260.5 | 2772.1 | 2813.5 | 3029.6 |
| 5th Joint | 3315.4 | 2727.9 | 2800.5 | 2772.1 | 2314.4 | 2813.5 | 3029.6 |
| 6th Joint | 3315.4 | 2727.9 | 2800.5 | 2772.1 | 2813.5 | 2387.9 | 3029.6 |
| | $\mu N_1(N)$ | $\mu N_2(N)$ | $\mu N_3(N)$ | $\mu N_4(N)$ | $\mu N_5(N)$ | $\mu N_6(N)$ | $\mu N_7(N)$ |
| 1st Joint | 187.9 | 416.3 | 629.5 | 88.3 | 193.2 | 434.0 | 371.7 |
| 2nd Joint | 123.0 | 306.0 | 184.3 | 151.4 | 107.6 | 145.3 | 169.2 |
| 3rd Joint | 22.4 | 306.0 | 243.7 | 586.4 | 193.2 | 198.8 | 261.5 |
| 4th Joint | 672.0 | 305.9 | 243.7 | 461.7 | 245.2 | 162.0 | 19.6 |
| 5th Joint | 229.7 | 19.0 | 399.2 | 461.7 | 434.0 | 196.8 | 110.7 |
| 6th Joint | 291.9 | 141.8 | 243.7 | 193.2 | 434.0 | 599.1 | 208.2 |

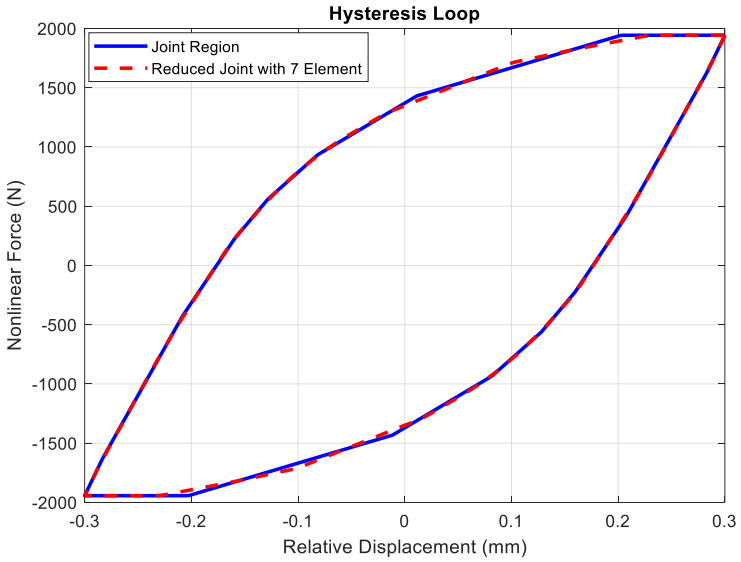


Figure 3.19. Hysteresis Loop of 1st Joint Region with 210 Elements and 7 Elements

The obtained FRF plots at different forcing levels are given in Figure 3.20 to Figure 3.23, along with the results of the node-to-node model with classical MSM. For all excitation levels, the closest result to the results of the node-to-node model is the reduced joint element with 7 elements.

Since the most accurate solutions are obtained with the reduced joint region with seven elements, the corresponding normalized solution times are given in Table 3.7. Similar to first reduction step of contact model, the solution times are normalized with the computational time of high-fidelity model with classical MSM. For the highest applied excitation value of 50 N, the computational time is decreased to 0.05% from %3 for classical MSM. When RDNMs are utilized in the solution process, this value further reduces to 0.03% from 0.1%. Since both the accuracy of the results and the decrease in computational time are better for results obtained with one RDNM, the superior performance of MSM utilizing RDNM is evident.

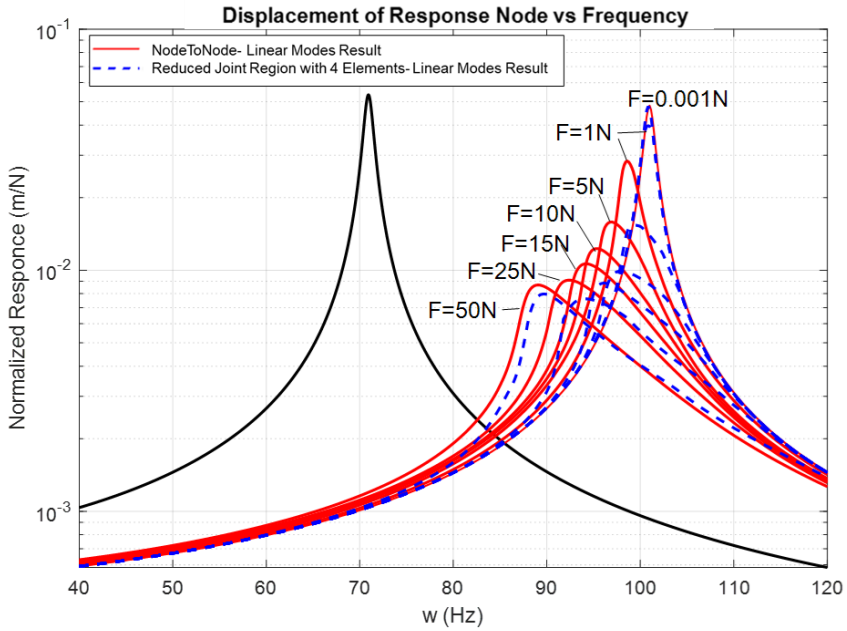


Figure 3.20. The Comparison of Normalized Response (mm/N) vs. Frequency (Hz) Graph for Reduced Joint Definition with 4 Elements Utilizing 4 Linear System Modes

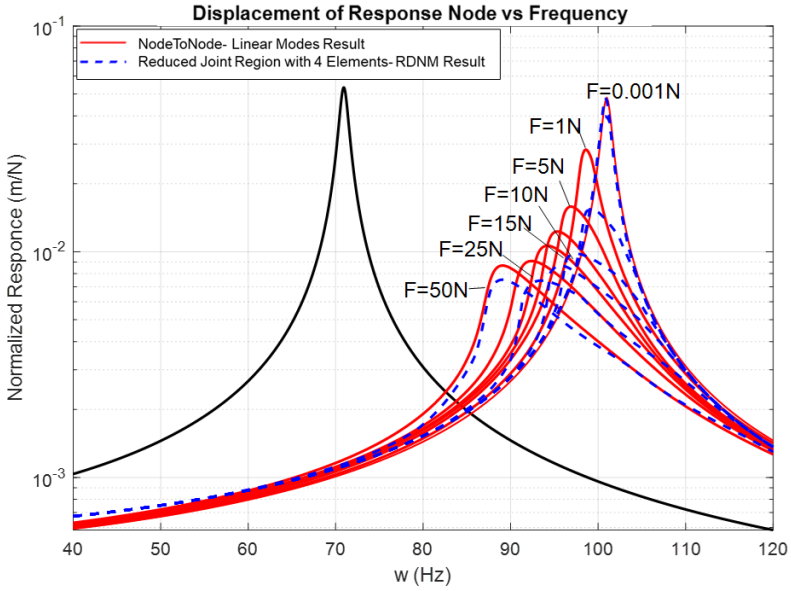


Figure 3.21. The Comparison of Normalized Response (mm/N) vs. Frequency (Hz) Graph for Reduced Joint Definition with 4 Elements Utilizing 1 RDNM

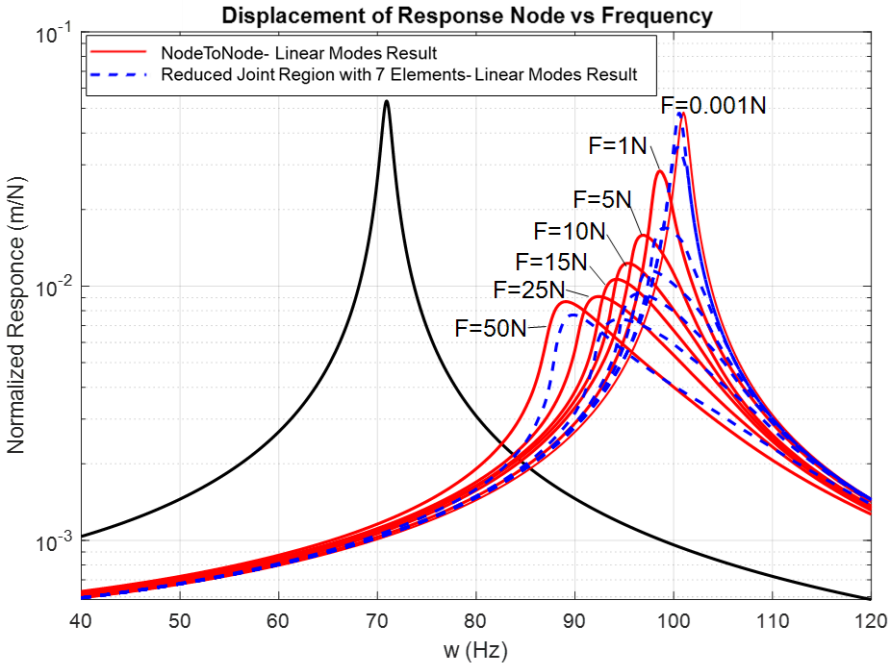


Figure 3.22. The Comparison of Normalized Response (mm/N) vs. Frequency (Hz) Graph for Reduced Joint Definition with 7 Elements Utilizing 4 Linear System Modes

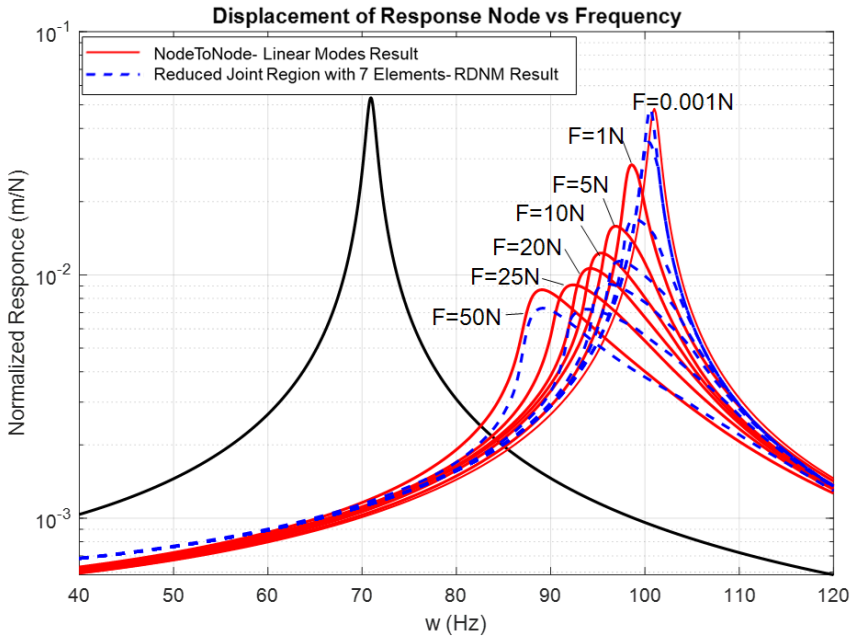


Figure 3.23. The Comparison of Normalized Response (mm/N) vs. Frequency (Hz) Graph for Reduced Joint Definition with 7 Elements Utilizing 1 RDNM

Table 3.7. The Reduction in Computational Times of Reduced Joint Region with 7 Elements for Linear Modes and RDNM

| Excitation Force Value (N) | Reduction Percentage in Time (%) of 7 Element Reduced Joint Region Utilizing Linear System Modes | Reduction Percentage in Time (%) of 7 Element Reduced Joint Region Utilizing 1 RDNM |
|---|---|---|
| 0.001 | 99.955 | 99.978 |
| 1 | 99.956 | 99.979 |
| 5 | 99.958 | 99.978 |
| 10 | 99.956 | 99.977 |
| 15 | 99.954 | 99.976 |
| 25 | 99.957 | 99.978 |
| 50 | 99.950 | 99.972 |

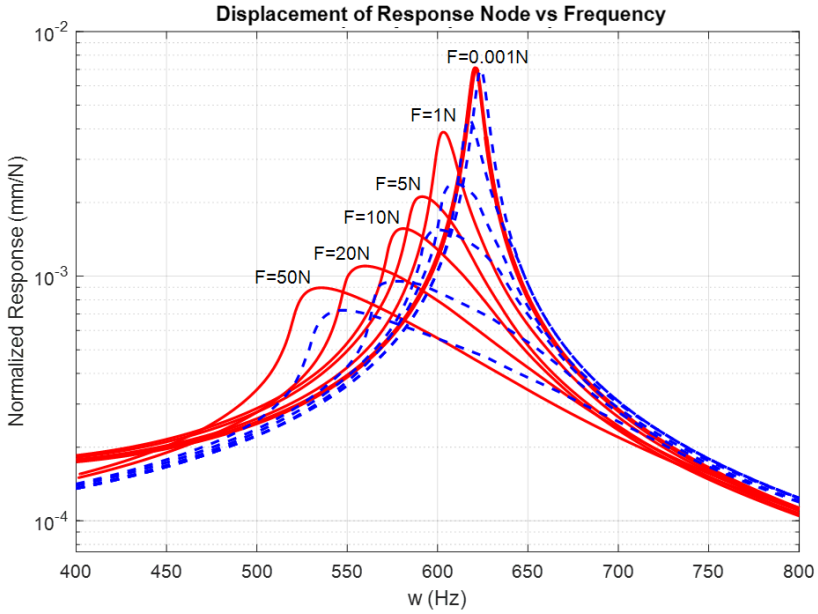


Figure 3.24. Normalized Response (mm/N) vs. Frequency (Hz) Utilizing Response Dependent Nonlinear Modes Around Second Resonance Region

The results around the second resonance region with seven elements reduced joint model are given in Figure 3.24. The results utilizing RDNM are compatible with the high-fidelity model results as in the first resonance region case.

To summarize, the three bolted joint assembly at which 1183 nodes are in contact is examined by utilizing 1D dry friction element with constant normal load. First, the displacement at response node is calculated using classical MSM at which the first four bending mode shapes of the linear system are used. Then, the same node-node model is solved utilizing MSM with RDNMs, at which the nonlinear modes are calculated with the response at the last solution point. The contact model is reduced in two steps. In the first reduction step, the interested contact surface is divided into joint regions at which macroslip elements within each joint region are taken as parallel connected. With this definition, the number of modal coefficients is required to calculate nonlinear force; hence the dimension of the solved equation set is reduced. In the second reduction step, the approximated microslip element is further reduced such that the hysteresis loops of the reduced joint element are the same as the joint elements of interest. For both reduction steps, results of MSM with RDNMs and MSM with linear system modes are given to examine the performance of utilizing RDNM.

At contact reduction steps, the results utilizing RDNM are more accurate than those with linear modes. In the meantime, the required computational time is decreased when RDNMs are used.

### 3.1.2 Case Study Model 2: Four-Bolted Assembly

To examine the performance of the reduction method further, the number of connecting elements is increased and a 4-bolted joint assembly is constructed. The 4-bolted lap joint assembly modeled in commercial FEA software Abaqus [43] is given in Figure 3.25. The representative half-lap joint model consists of two beams connected by four M8 bolts and four nuts. Like 3-bolted lap joint, bolt and nuts are taken as a single part and material of all parts is defined as steel, whose material properties is given in Table 3.1. Dimensions of the beam is given in Figure 3.26.

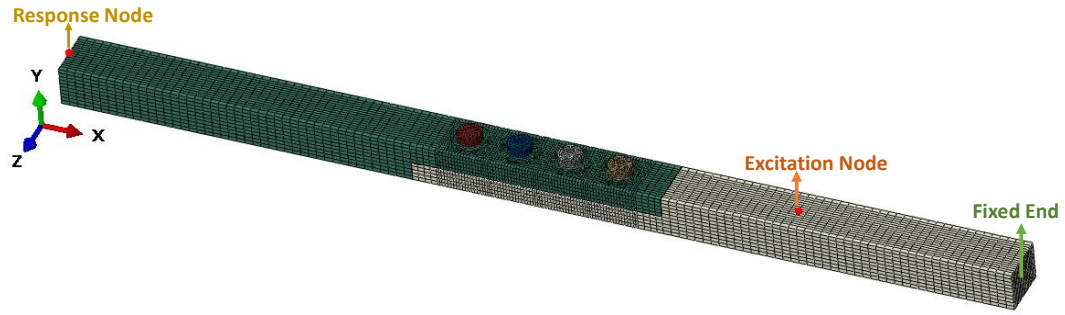


Figure 3.25. Finite Element Model of 4-Bolted Assembly

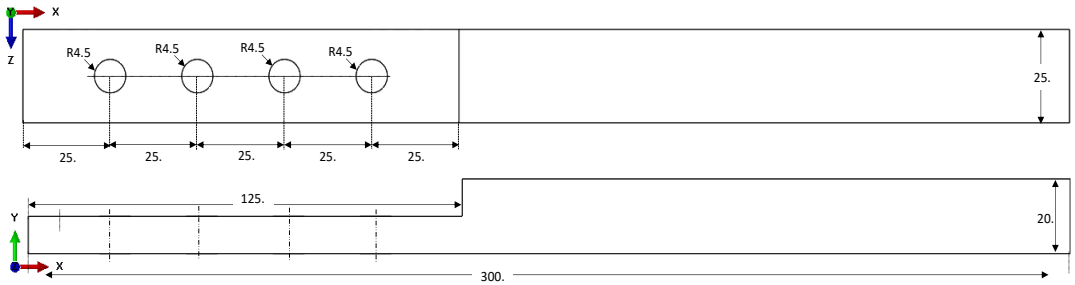


Figure 3.26. Dimensions of Beam Design 2

The contact definitions and connection in-between beams and not heads are defined as in the case of 3 -bolted assembly. The preload value of M8 bolts is defined as 10 kN applied from cross section located at mid-length bolt shank. Nonlinear static analysis is conducted for fix-free boundary condition to obtain the initial normal load distribution on contact surface. The obtained result of contact force distribution in

the direction of contact surface normal is given in Figure 3.27. The region of interest, which contains 1603 nodes, is given in Figure 3.28.

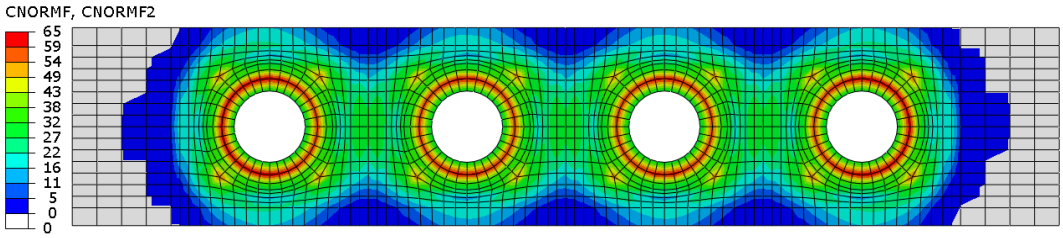


Figure 3.27. Normal Force Distribution on Contact Surface of 4- Bolted Lap Joint

Modal analysis is conducted in Abaqus FEA software to calculate the system's natural frequencies and mode shapes with same model modifications as in the case of 3-bolted half lap joint. The first four bending modes of system is included in the solution set which is given in Figure 3.29, Figure 3.30, Figure 3.31 and Figure 3.32. Tangential stiffness and friction coefficients of 1D macroslip element are given in Table 3.2.

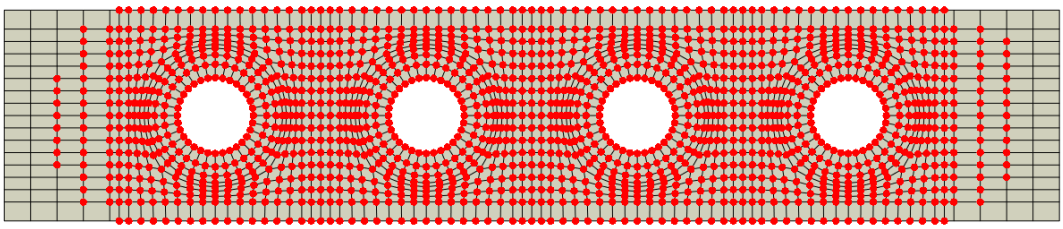

Figure 3.28. Normal Force Distribution on Contact Surface of 4-Bolted Assembly

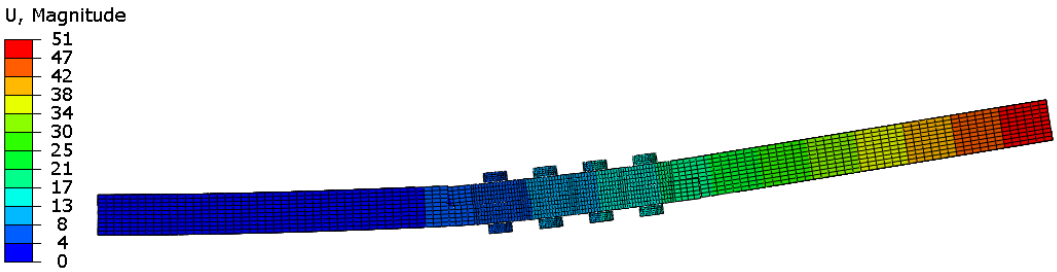


Figure 3.29. First Bending Mode (51 Hz)

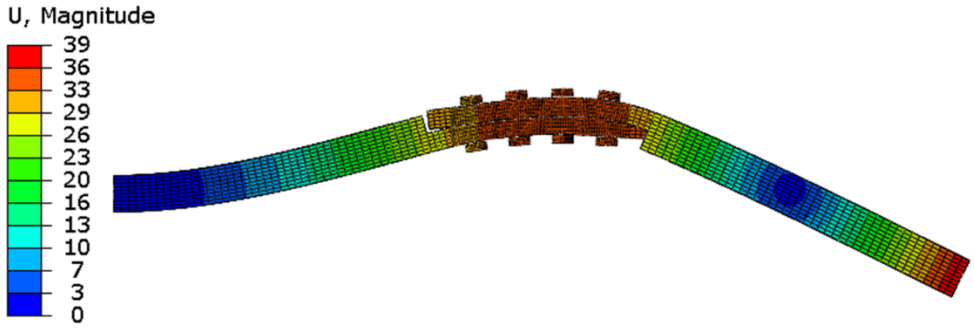


Figure 3.30. Second Bending Mode (263 Hz)

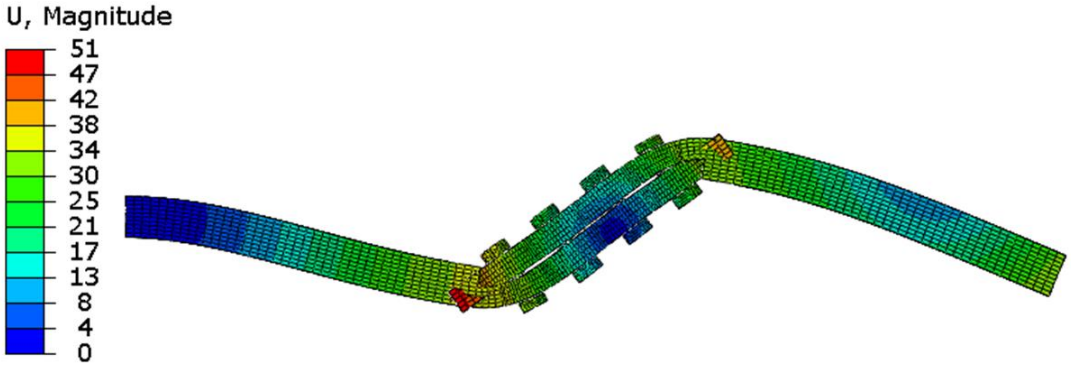


Figure 3.31. Third Bending Mode (731 Hz)

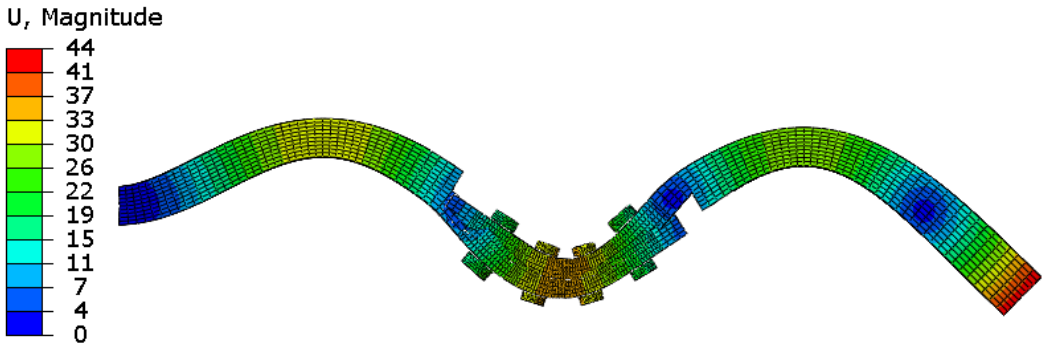


Figure 3.32. Fourth Bending Mode (1899Hz)

#### 3.1.2.1 Results of 4-Bolted Joint: Node-to-Node Model Utilizing RDNM

The displacements of response node represented in Figure 3.25 are given in Figure 3.33. The corresponding FRFs are obtained with four linear system modes and one

RDNM mode separately. The solution times of high-fidelity model with linear system modes and RDNM are given in Table 3.8.

For lower excitation levels such as $0.001\ N, 1\ N, 5\ N, 10\ N$, the results obtained utilizing RDNM is same as the four linear modes. For those force levels, the stick motion dominates the response. As a result of this phenomenon, the nonlinear mode shapes of four bolted joint assembly are well separated for these forcing levels. Therefore, the implementation of one RDNM is sufficient.

For higher excitation levels, as the slip to stick motion is present on the contact surface, total energy is decreased. This decrease of energy level changes the proximity of mode shapes which makes the difference between calculated FRFs more apparent. This difference could be reduced by increasing the number of RDNMs included in solution equations.

For all excitation levels, the computational time with RDNM is nearly half the computational time of MSM with linear system modes. Since the FRFs throughout the interested frequency range are compatible with the FRFs calculated with classical MSM for different excitation levels and the computational time is reduced to nearly half, the superior performance of RDNM is evident.

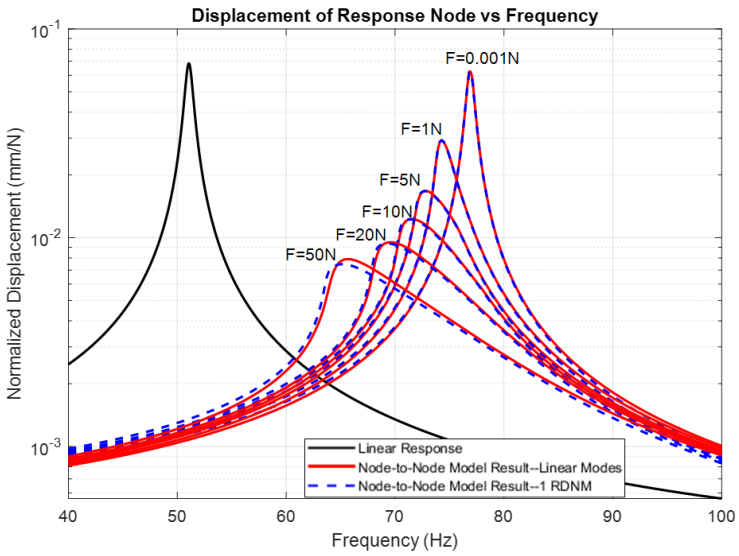


Figure 3.33. Normalized Response (mm/N) vs. Frequency (Hz) Graph

Table 3.8. Computational Times with Linear Modes and RDNM

| Excitation Force Value (N) | Computational Time with Classical MSM (s) | Computational Time MSM with RDNM (s) | Normalized Time of MSM with RDNM % |
|---|---|---|---|
| 0.001 | 561 | 260 | 53.6 |
| 1 | 612 | 276 | 55.0 |
| 5 | 753 | 284 | 62.3 |
| 10 | 784 | 287 | 63.5 |
| 20 | 670 | 293 | 56.2 |
| 30 | 758 | 295 | 61.1 |
| 50 | 689 | 305 | 55.7 |

### 3.1.2.2 Results of 4-Bolted Joint: First Reduction Step of Contact Model

In the first reduction step of contact model, contact region of interest is divided into joint regions whose relative displacement is defined as Equation (3.1) and the resultant total force value at these artificial nodes is Equation ( 3.2).

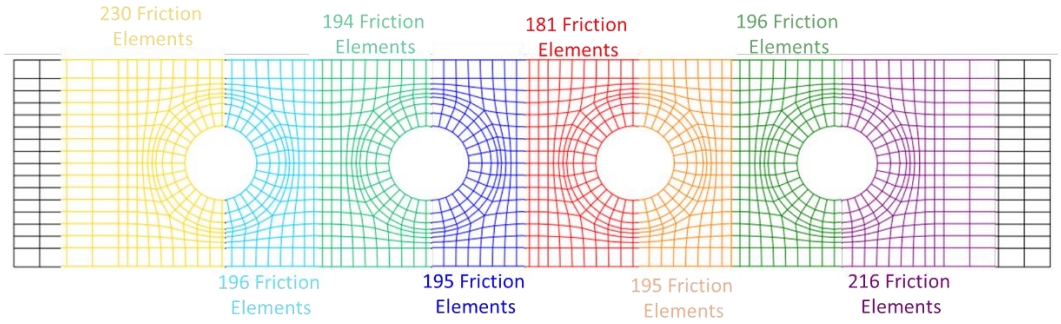


Figure 3.34. Location of 8 Joint Region on Contact Surface

The contact surface of four-bolted joint is eight joint regions. The selected joint regions and the corresponding element numbers in each region are given in Figure 3.34.

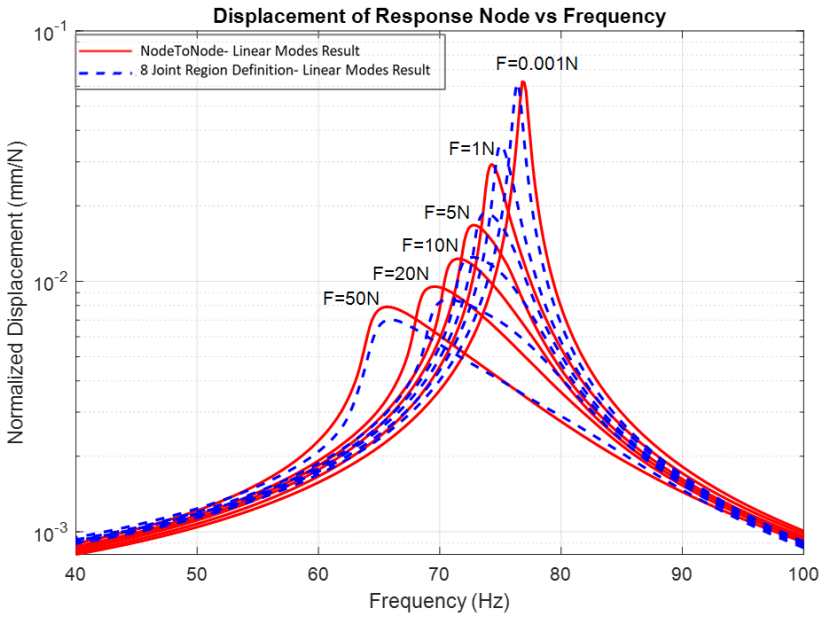


Figure 3.35. Normalized Response (mm/N) vs. Frequency (Hz) Graph of 8 Joint Region Utilizing Linear System Modes

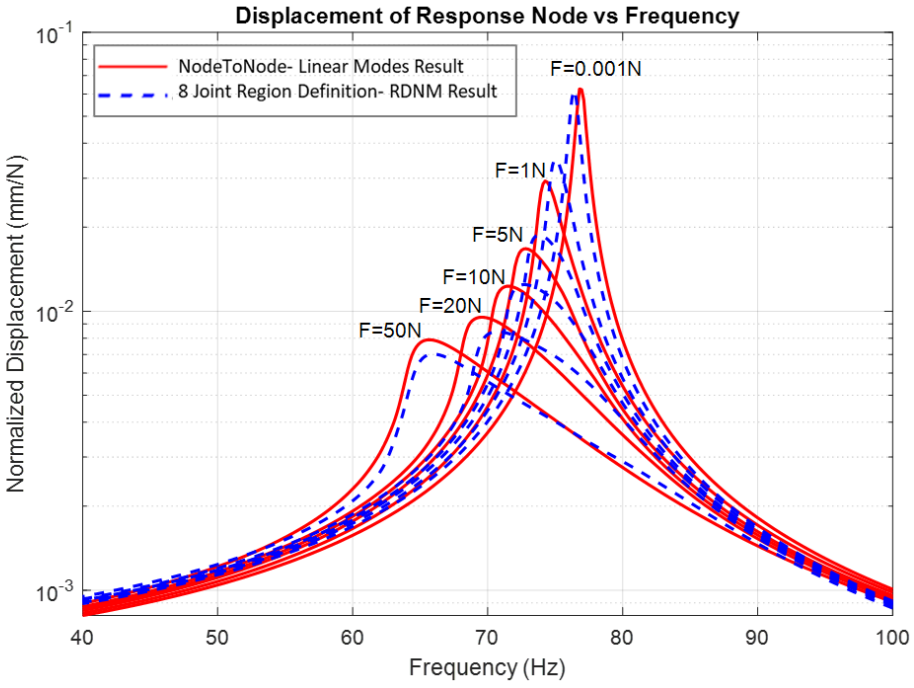


Figure 3.36. Normalized Response (mm/N) vs. Frequency (Hz) Graph of 8 Joint Region Utilizing RDNM

Table 3.9. The Reduction in Computational Times of 8 Joint Region with Linear Modes and RDNM

| Excitation Force Value (N) | Reduction Percentage in Time (%) of 8 Joint Region Utilizing 4 Linear Modes | Reduction Percentage in Time (%) of 8 Joint Region Utilizing 1 RDNM |
|---|---|---|
| 0.001 | 99.578 | 99.875 |
| 1 | 99.538 | 99.872 |
| 5 | 99.677 | 99.889 |
| 10 | 99.662 | 99.870 |
| 20 | 99.631 | 99.849 |
| 30 | 99.662 | 99.875 |
| 50 | 99.624 | 99.853 |

The results of 8 joint definition are represented in Figure 3.35and Figure 3.36 along the results of the node-to-node contact model calculated with linear system modes.

The solution times in Table 3.9 are normalized with the computational time of the high-fidelity model with classical MSM. Even for the highest excitation value of 50 N, the computational time is decreased to nearly 0.4% for classical MSM. When one RDNM is utilized in the solution process, this value further reduces to 0.1%, which strongly emphasizes the advantage of using RDNMs.

#### 3.1.2.3 Results of 4-Bolted Joint: Second Reduction Step of Contact Model

The number of macroslip elements inside joint regions are decreased such that the hysteresis loops of reduced joint is the same as the hysteresis loop of the joint region of interest. The tangential stiffness and normal load values of the macroslip elements

inside the reduced order joints are taken from the results of cost function in Equation (3.3). Similar to 3-bolted joint case, the cost function is solved with “fmincon”[44] .

The joint region definition of 8 regions is examined in this step. The reduced joint regions consist of three and seven macroslip elements whose tangential stiffness and normal load values are given in Table 3.10, and Table 3.11. The hysteresis loops of first reduced joint region are represented along the joint region which contains 230 elements in Figure 3.37 and Figure 3.38.

The obtained FRF plots at different forcing levels are given in Figure 3.39 to Figure 3.42, along with the results of the node-to-node model with classical MSM. For all excitation levels, the closest result to the results of the node-to-node model is the reduced joint element with 7 elements.

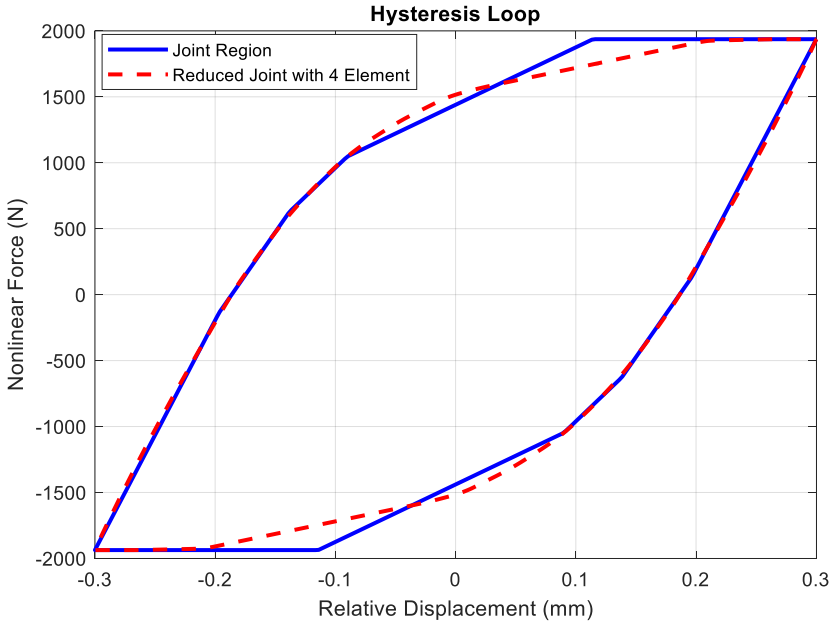


Figure 3.37. Hysteresis Loop of 1st Joint Region with 230 Elements and 4 Elements

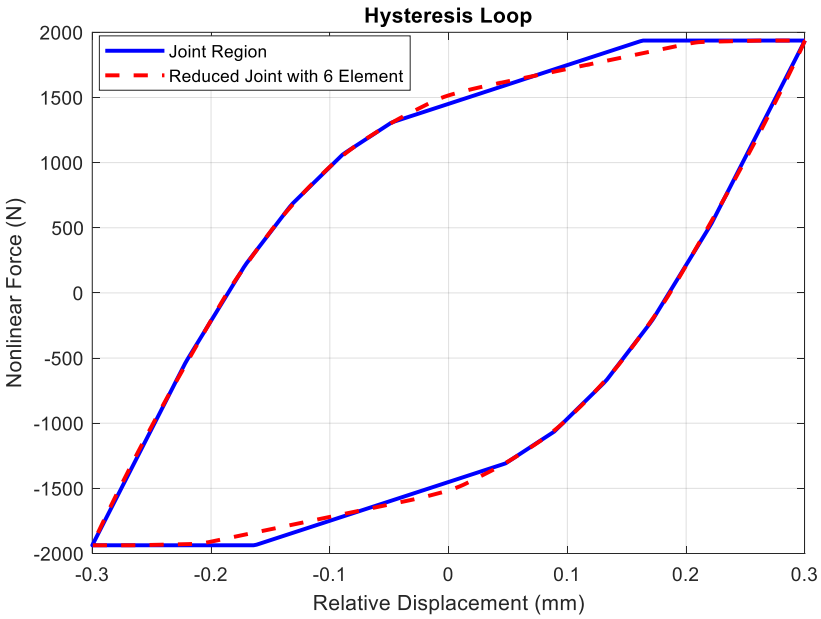


Figure 3.38. Hysteresis Loop of 1st Joint Region with 230 Elements and 7 Elements

Table 3.10. Parameters of Reduced Joint Element with 4 Elements

| | $k_1(^{kN}/_{mm})$ | $k_2(^{kN}/_{mm})$ | $k_3(^{kN}/_{mm})$ | $k_4(^{kN}/_{mm})$ |
|---|---|---|---|---|
| 1st Joint | 3484.7 | 3114.9 | 3228.5 | 3524.5 |
| 2nd Joint | 4948.1 | 4108.4 | 4070.5 | 3971.8 |
| 3rd Joint | 4948.1 | 4108.4 | 4070.5 | 3971.8 |
| 4th Joint | 4948.1 | 4108.4 | 4070.5 | 3971.8 |
| 5th Joint | 3644.1 | 3382.8 | 3282.1 | 3140.4 |
| 6th Joint | 3905.3 | 3986.4 | 4026.0 | 4246.4 |
| 7th Joint | 3905.3 | 3986.4 | 4026.0 | 4246.4 |
| 8th Joint | 3905.3 | 3986.4 | 4026.0 | 4246.4 |
| | $\mu N_1(N)$ | $\mu N_2(N)$ | $\mu N_3(N)$ | $\mu N_4(N)$ |
| 1st Joint | 225.2 | 354.4 | 759.1 | 898.4 |
| 2nd Joint | 902.1 | 465.2 | 515.6 | 494.1 |
| 3rd Joint | 352.5 | 820.6 | 332.1 | 237.5 |
| 4th Joint | 457.1 | 303.1 | 333.8 | 354.3 |
| 5th Joint | 400.4 | 456.3 | 279.5 | 320.1 |
| 6th Joint | 209.0 | 369.0 | 451.5 | 202.1 |
| 7th Joint | 399.4 | 221.5 | 794.8 | 418.2 |
| 8th Joint | 893.2 | 818.8 | 343.1 | 812.6 |

Table 3.11. Parameters of Reduced Joint Element with 7 Elements

| | $k_1(\frac{kN}{mm})$ | $k_2(\frac{kN}{mm})$ | $k_3(\frac{kN}{mm})$ | $k_4(\frac{kN}{mm})$ | $k_5(\frac{kN}{mm})$ | $k_6(\frac{kN}{mm})$ | $k_7(\frac{kN}{mm})$ |
|---|---|---|---|---|---|---|---|
| 1st Joint | 3490.5 | 3264.0 | 3066.2 | 3638.1 | 3170.3 | 2904.1 | 3490.5 |
| 2nd Joint | 4004.7 | 3264.0 | 3250.1 | 3005.9 | 3170.3 | 3324.4 | 4004.7 |
| 3rd Joint | 4004.7 | 3101.6 | 3044.1 | 3005.9 | 3427.4 | 3105.5 | 4004.7 |
| 4th Joint | 4004.7 | 3268.1 | 3228.1 | 3005.9 | 3146.7 | 3525.8 | 4004.7 |
| 5th Joint | 3442.3 | 3105.7 | 3228.1 | 3177.3 | 3403.8 | 3525.8 | 3442.3 |
| 6th Joint | 3634.4 | 3272.2 | 3228.1 | 3088.1 | 3123.1 | 3525.8 | 3634.4 |
| 7th Joint | 1439.9 | 1636.1 | 1614.1 | 1674.3 | 1561.5 | 1762.9 | 1439.9 |
| 8th Joint | 1632.2 | 1636.4 | 1614.2 | 1585.1 | 1561.9 | 1763.3 | 1632.2 |
| | $\mu N_1(N)$ | $\mu N_2(N)$ | $\mu N_3(N)$ | $\mu N_4(N)$ | $\mu N_5(N)$ | $\mu N_6(N)$ | $\mu N_7(N)$ |
| 1st Joint | 314.0 | 630.5 | 270.3 | 10.0 | 678.7 | 767.3 | 314.0 |
| 2nd Joint | 117.3 | 198.7 | 327.6 | 224.7 | 400.5 | 10.1 | 117.3 |
| 3rd Joint | 375.2 | 124.1 | 319.4 | 850.6 | 12.8 | 339.5 | 375.2 |
| 4th Joint | 249.4 | 269.5 | 263.3 | 375.2 | 267.4 | 103.4 | 249.4 |
| 5th Joint | 689.3 | 650.8 | 194.0 | 10.01 | 338.3 | 225.6 | 689.3 |
| 6th Joint | 191.6 | 130.8 | 347.1 | 470.2 | 440.2 | 289.1 | 191.6 |
| 7th Joint | 324.7 | 199.1 | 618.7 | 159.9 | 337.9 | 621.0 | 324.7 |
| 8th Joint | 354.5 | 364.5 | 123.2 | 349.8 | 90.5 | 174.4 | 354.5 |

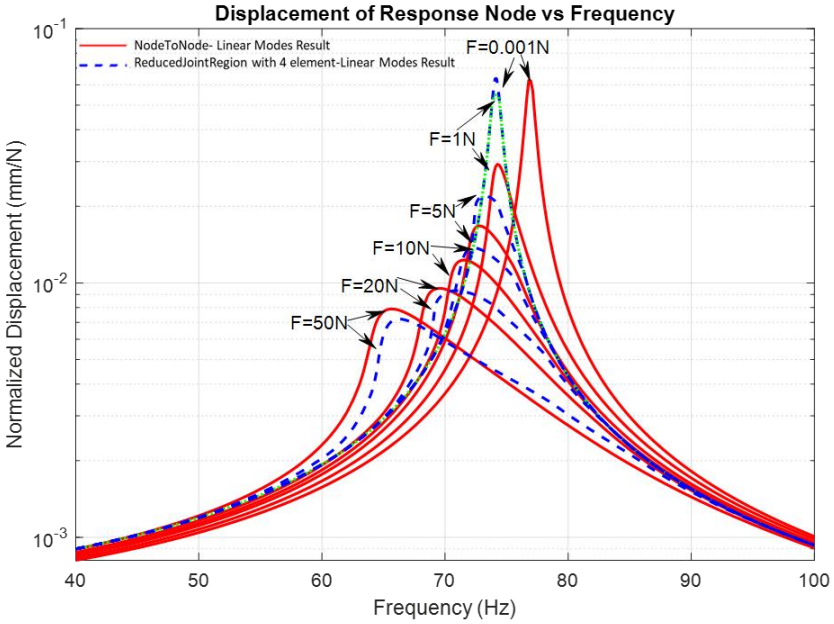


Figure 3.39. Normalized Response (mm/N) vs. Frequency (Hz) Graph of Reduced Joint of 4 Elements Utilizing Linear System Modes

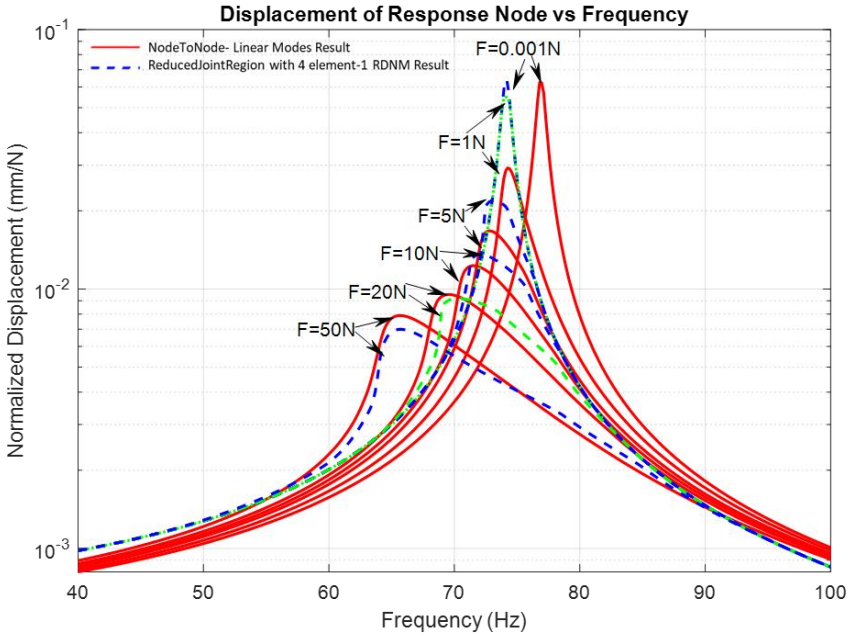


Figure 3.40. Normalized Response (mm/N) vs. Frequency (Hz) Graph of Reduced Joint of 4 Elements Utilizing RDNM

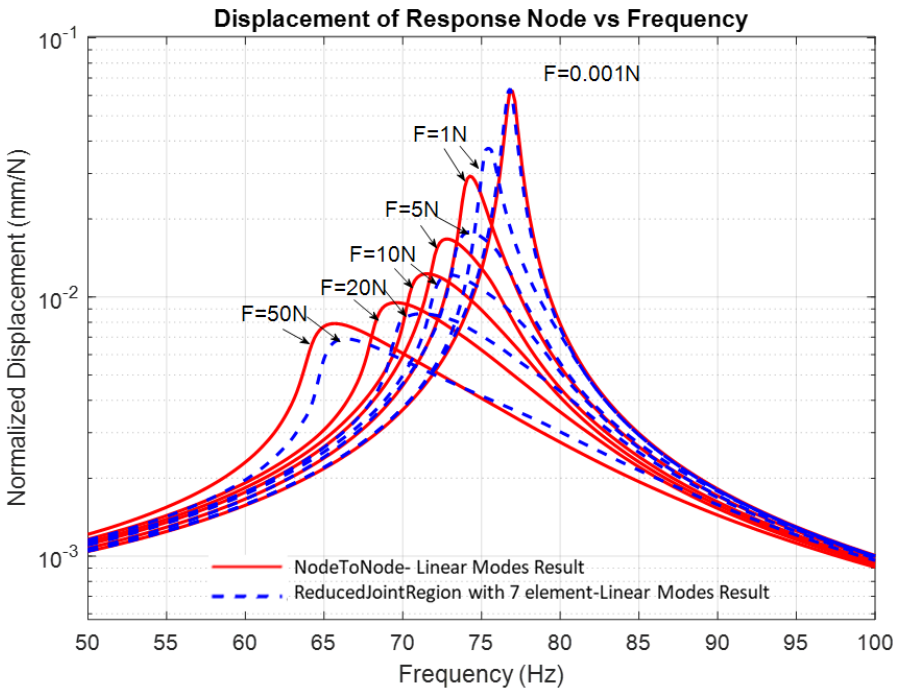


Figure 3.41. Normalized Response (mm/N) vs. Frequency (Hz) Graph of Reduced Joint of 6 Elements Utilizing Linear System Modes

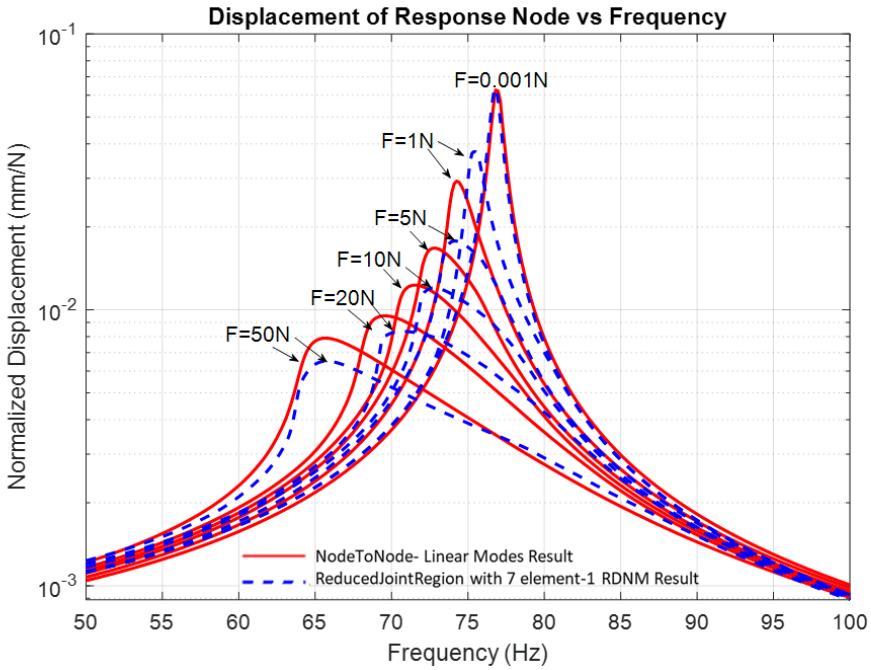


Figure 3.42. Normalized Response (mm/N) vs. Frequency (Hz) Graph of Reduced Joint of 6 Elements Utilizing RDNM

Table 3.12. The Normalized Computational Times of Reduced Joint Region of 6 Elements with Linear Modes and RDNM

| Excitation Force Value (N) | Reduction Percentage in Time (%) of 7 Element Reduced Joint Region with Linear Modes | Reduction Percentage in Time (%) of 7 Element Reduced Joint Region - with RDNM |
|---|---|---|
| 0.001 | 99.9302 | 99.9645 |
| 1 | 99.9331 | 99.9663 |
| 5 | 99.9453 | 99.9712 |
| 10 | 99.9473 | 99.9737 |
| 20 | 99.9376 | 99.9680 |
| 30 | 99.9443 | 99.9706 |
| 50 | 99.9379 | 99.9668 |

Since the most accurate solutions are obtained with the reduced joint region with seven elements, the corresponding normalized solution times are given in Table 3.12. Similar to the first reduction step of contact model, the solution times are normalized with the computational time of node-to-node contact model with linear system modes. For the highest applied excitation value of 50 N, the computational time is decreased to 0.06% from %0.4 for classical MSM. When RDNM is utilized in the solution process, this value further reduces to 0.03% from 0.1%. Since both the accuracy of the results and the decrease in computational time are better for results obtained with one RDNM, the advantage of utilizing RDNM is evident.

To sum up, node-to-node contact model consisting of 1603 nodes at the contact surface is examined in this step. First, 1603 nodes are divided into 8 joint regions which behave as approximated microslip elements. At the second reduction step, the 8 joint regions are reduced such that each reduced joint region consists of 6 macroslip elements whose hysteresis loop is the same as joint region of interest.

## 3.2 Reduced Order Modeling Utilizing 1D Dry Friction Element with Variable Normal Load

### 3.2.1 Case Study Model 1: Three-Bolted Assembly

The case study model is the same as the three-lap joint represented in Chapter 3.1.1. In this part of the study, 1D dry friction element with variable normal load is implemented in the mathematical model. Since variation of normal load across the contact surface is included into formulae, the gap distribution in-between surfaces resultant from preload should be included. The exaggerated deformation of three-bolted lap joint is given in Figure 3.43. The corresponding gap distribution resultant at the end of preload is given in Figure 3.44. The normal load distribution taken from static analysis is redefined such that the gap in-between surfaces is taken as negative normal loads. The resultant gap formula is given in Equation ( 3.4).

$$n0V = n0_{static} - kv \cdot v_{gap} \qquad (3.4)$$

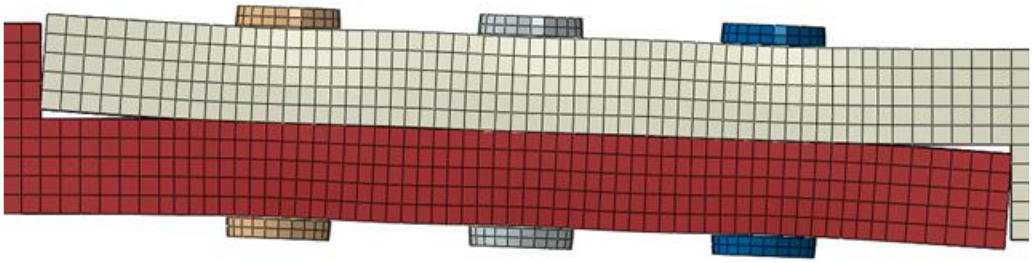

Figure 3.43.Exaggerageted Deformation of Three-Bolted Lap Joint

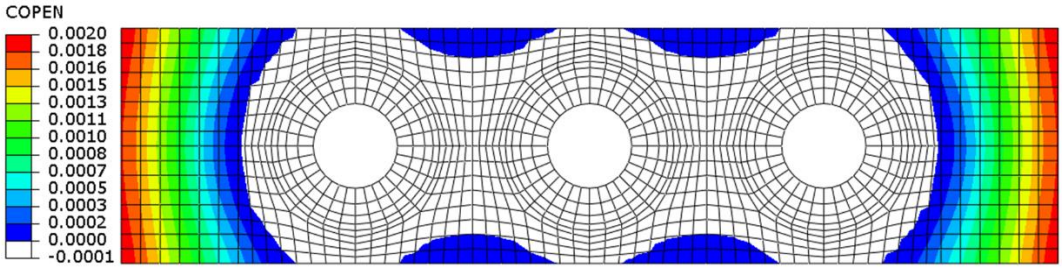


Figure 3.44. Gap Distribution on Contact Surface

The stiffness value in tangential direction and normal direction are given in Table 3.13.The algebraic model of 1D dry friction element with variable normal load is explained in 2.2.2. Since the gap distribution is included in this model, friction elements are connected in-between all of the coincident nodes on contact surface. The resultant friction element number is 1370. The results of high-fidelity model are given in Figure 3.45.

Table 3.13. Tangential-Normal Stiffness and Friction Coefficient of 1D Dry Friction Element with Constant Normal Load

| $k_u$ | $k_v$ | $\mu$ |
|---|---|---|
| 100 $^{kN}/_{mm}$ | 100 $^{kN}/_{mm}$ | 0.1 |

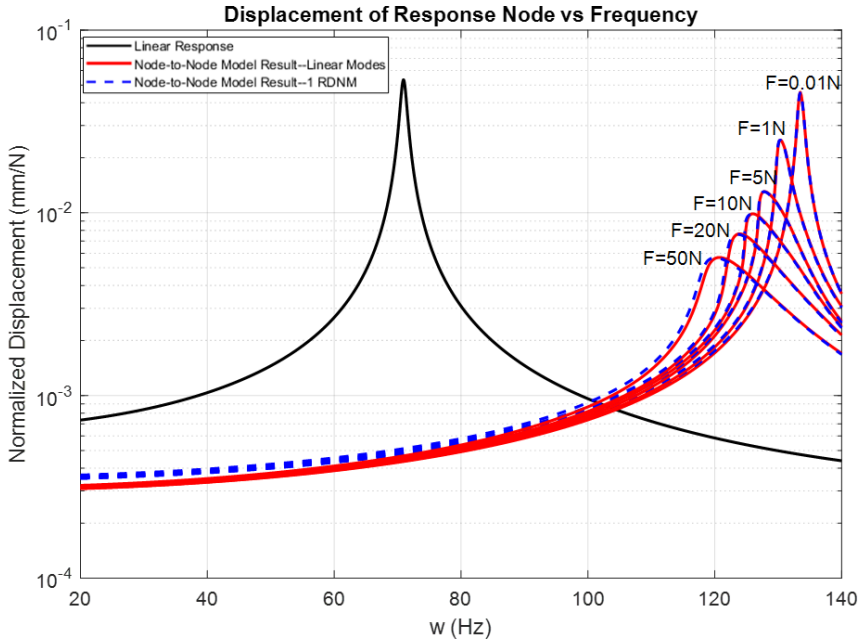


Figure 3.45. Normalized Response (mm/N) vs. Frequency (Hz) Graph

For all excitation levels the result obtained with utilizing RDNM are consistent with the results of linear system modes. The contact states of each excitation level's peak point are given in from Figure 3.46 to Figure 3.51. At lowest excitation level $F = 0.01\ N$, the nodes around bolt hole are in complete stick state whereas node near the

edges are in full separation state. As the excitation level increases, stick-slip motion is seen at some of the nodes which were initially at stick condition. The resultant energy dissipation is apparent by examining the decreasing response level from Figure 3.45.As the excitation level increases the stick-slip motion with separation is seen at nodes located around edges whose normal load level is low. The asymmetry of contact states along x direction is due to fixed-free boundary condition. The relative displacement of right end is higher than the left end for $1^{st}$,$2^{nd}$ and $4^{th}$ bending mode.

The solution times of high-fidelity model with linear system modes and RDNM are given in Table 3.14. For all excitation levels, the computational time with RDNM is nearly %30 of the computational time of MSM with linear system modes.

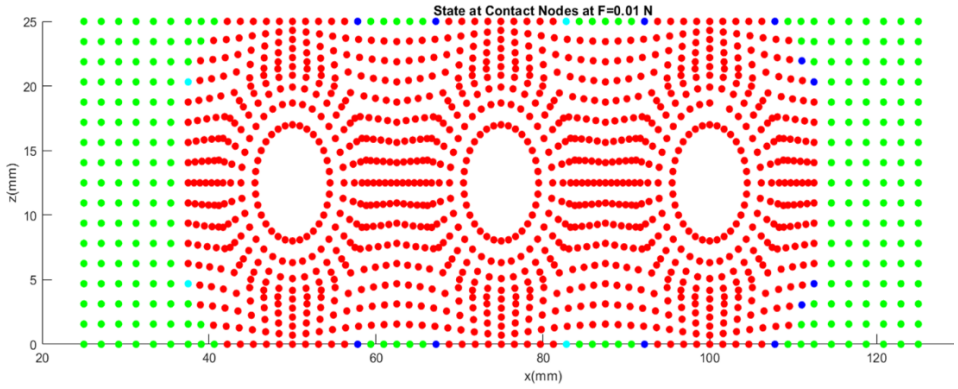


Figure 3.46. Contact state at the peak point of F=0.01 N (Red: Full stick motion; Blue: Stick-slip motion without separation; Cyan: Stick-slip motion with separation Green: Full separation)

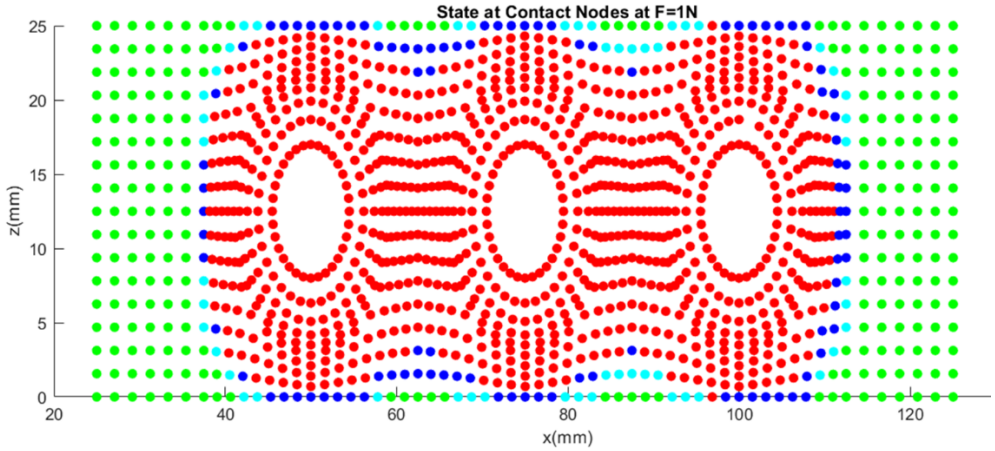


Figure 3.47. Contact state at the peak point of F=1 N (Red: Full stick motion; Blue: Stick-slip motion without separation; Cyan: Stick-slip motion with separation Green: Full separation)

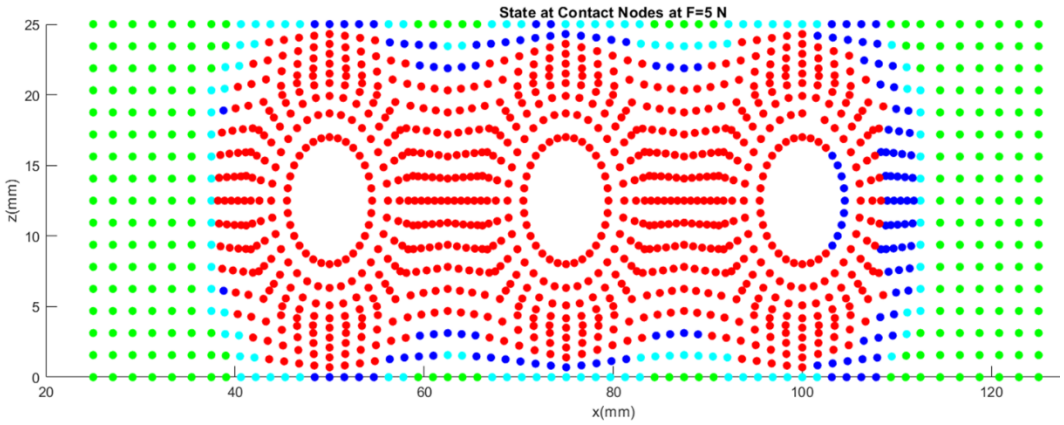


Figure 3.48. Contact state at the peak point of F=5 N (Red: Full stick motion; Blue: Stick-slip motion without separation; Cyan: Stick-slip motion with separation Green: Full separation)

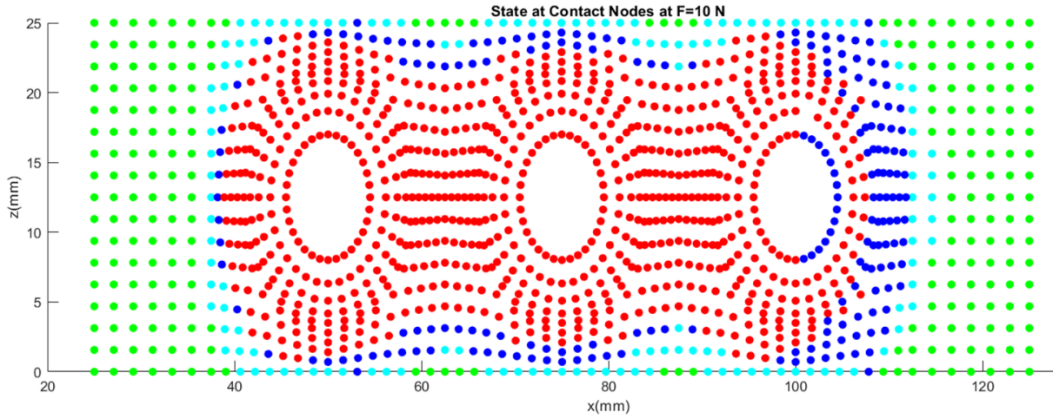


Figure 3.49. Contact state at the peak point of F=10 N (Red: Full stick motion; Blue: Stick-slip motion without separation; Cyan: Stick-slip motion with separation Green: Full separation)

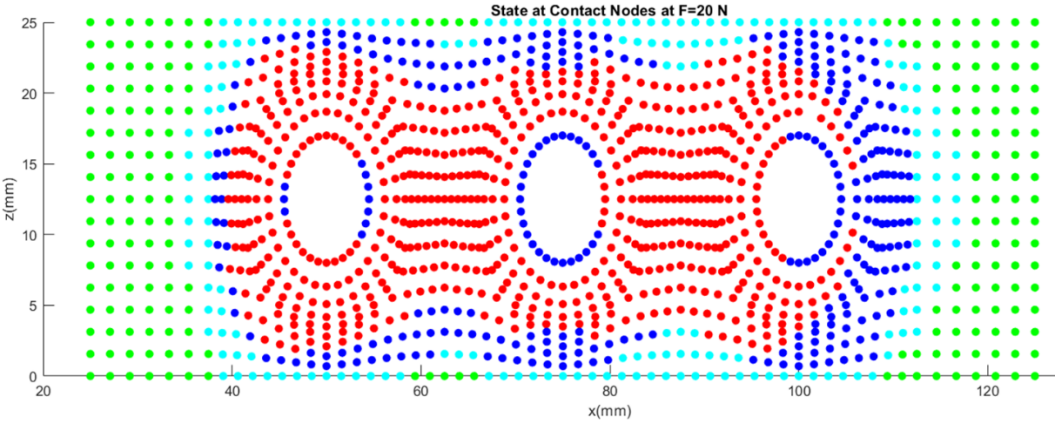


Figure 3.50. Contact state at the peak point of F=20 N (Red: Full stick motion; Blue: Stick-slip motion without separation; Cyan: Stick-slip motion with separation Green: Full separation)

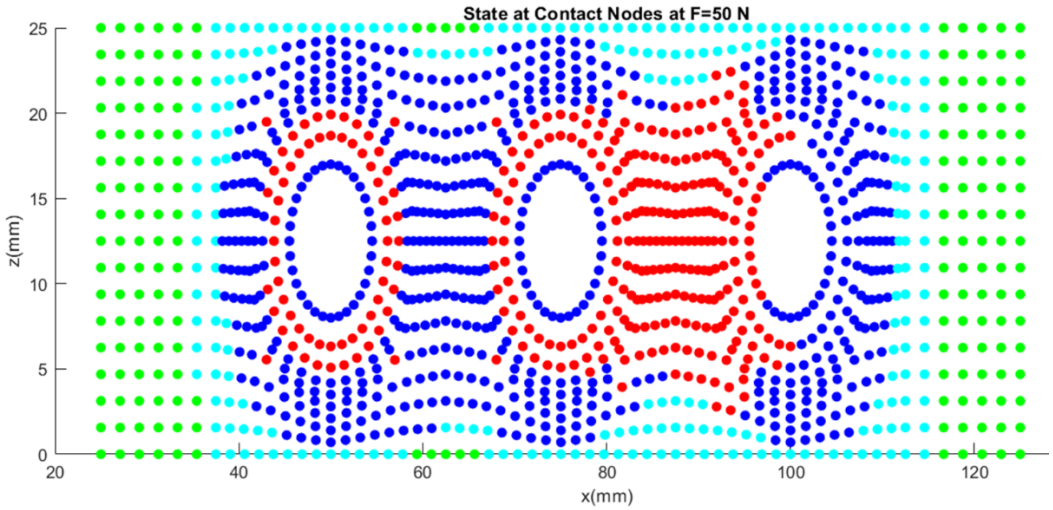


Figure 3.51. Contact state at the peak point of F=50 N (Red: Full stick motion; Blue: Stick-slip motion without separation; Cyan: Stick-slip motion with separation Green: Full separation)

Table 3.14. Computational Times with Linear Modes and RDNM

| **Excitation Force Value (N)** | **Computational Time with Classical MSM (s)** | **Computational Time MSM with RDNM (s)** | **Reduction % in Computational Time with RDNM** |
|---|---|---|---|
| 0.001 | 1025 | 304 | 70.4 |
| 1 | 1178 | 315 | 73.2 |
| 5 | 1197 | 331 | 72.3 |
| 10 | 1149 | 336 | 70.8 |
| 20 | 1216 | 338 | 72.2 |
| 50 | 1239 | 382 | 69.2 |

#### 3.2.1.1 First Reduction Step for Contact Model

The same reduction method explained in Chapter 3.1.1.3 is applied in this step. The joint regions are selected by examining the normal load level along the nodes located at the mid-length of the contact surface. The normal load value along this path is given in Figure 3.53. The 12 joint regions and the corresponding element numbers are in given in Figure 3.53.

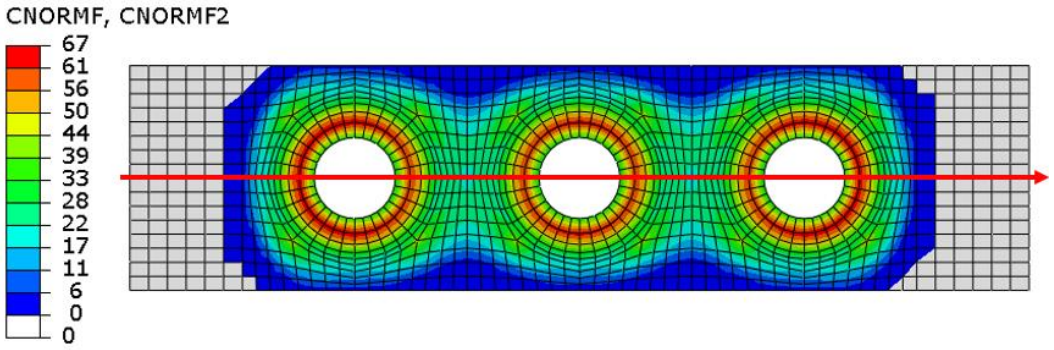


Figure 3.52. Middle Section of Contact Surface

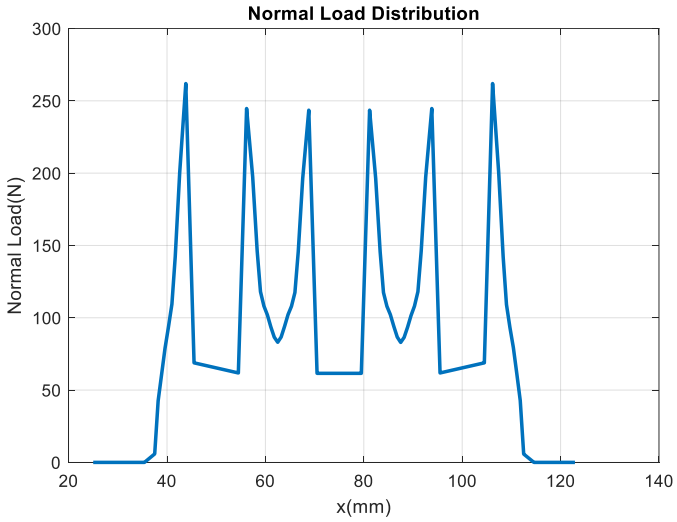


Figure 3.53. Normal Load Values Along the Middle Section Path

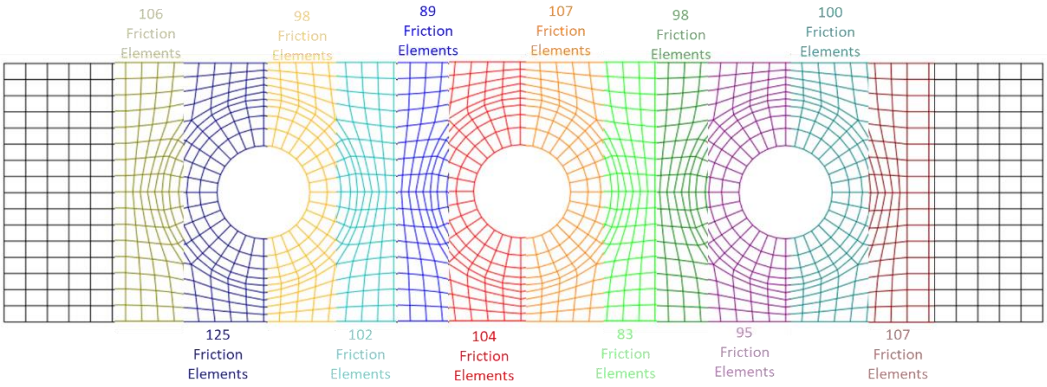


Figure 3.54. Location of 12 Joint Region on Contact Surface

The response obtained with linear system modes and 1 RDNM are given in Figure 3.55 and Figure 3.56. Although there is slight shift of resonance frequencies at lower excitation levels, the peak response values at higher excitation levels are captured with 12 joint region definition. The results of RDNM are coherent with the results of obtained with linear system modes. Examining the reduction of computational time given in Table 3.15, it is apparent that utilization of 1 RDNM is more feasible.

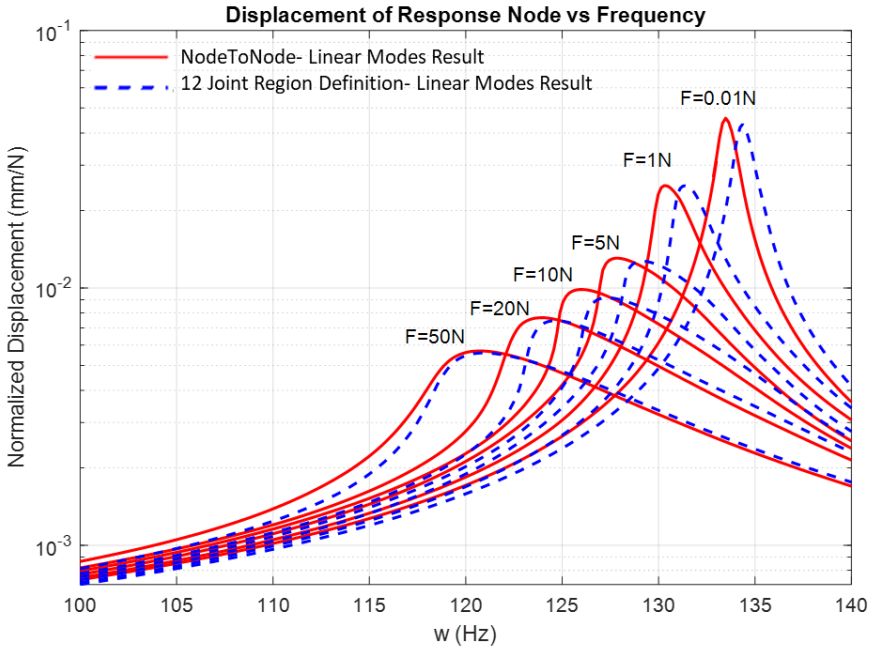


Figure 3.55.Normalized Response (mm/N) vs. Frequency (Hz) Graph for 12 Joint Region Utilizing 4 Linear System Modes

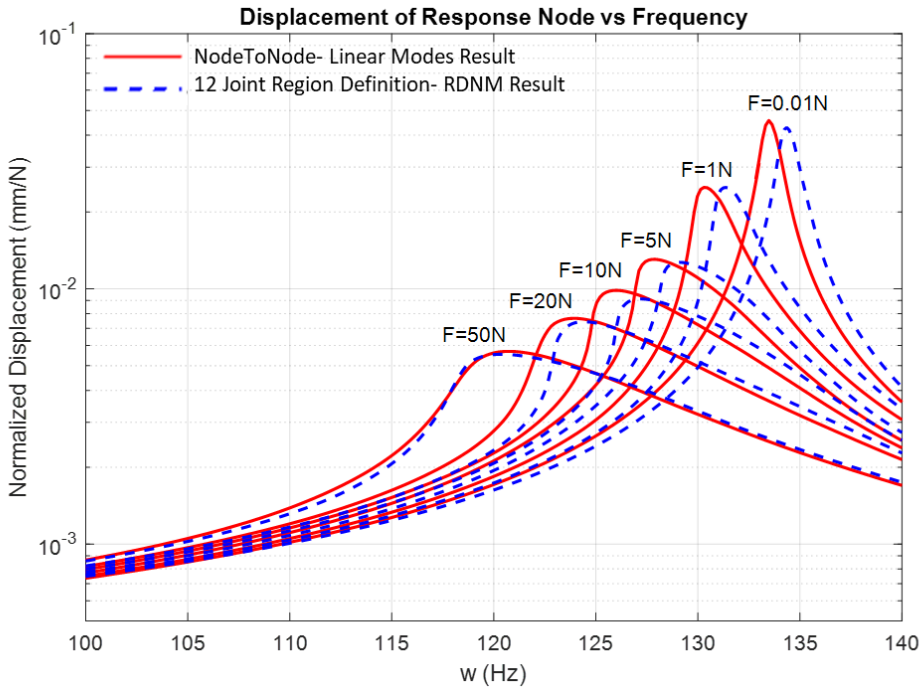


Figure 3.56.Normalized Response (mm/N) vs. Frequency (Hz) Graph for 12 Joint Region Utilizing 1 RDNM

Table 3.15.The Reduction in Computational Times of 12 Joint Region with Linear Modes and RDNM

| **Excitation Force Value (N)** | **Reduction Percentage in Time (%) of 12 Joint Region Utilizing 4 Linear Modes** | **Reduction Percentage in Time (%) of 12 Joint Region Utilizing 1 RDNM** |
|---|---|---|
| 0.001 | 17.0 | 78.1 |
| 1 | 38.3 | 80.4 |
| 5 | 26.4 | 79.7 |
| 10 | 33.2 | 78.7 |
| 20 | 29.6 | 78.9 |
| 50 | 25.4 | 77.3 |

### 3.2.1.2 Second Reduction Step for Contact Model

Unlike 1D dry friction element with constant normal load, the hysteresis behavior of the friction element also depends on the normal motion. There are individual hysteresis loops for different normal motion characteristics. For the simplicity of calculations, the contribution of normal motion to hysteresis is neglected while determining the reduced joint region parameters. The optimized normal stiffness values are taken as the same as the calculated tangential stiffness values.

The optimization procedure explained in Chapter 3.1.1.4 is followed for the calculation process only considering the tangential stiffness ($k_u$) and normal load values ($\mu N$). The reduced joint regions are constructed with 4 macroslip elements. The optimized stiffness and normal load values are given in Table 3.16. The hysteresis loop of 2nd joint region is given in Figure 3.57.

The results of reduced joint region definition are given in Figure 3.58 and Figure 3.59. The results at all excitation levels except $1N$ is consistent with the results of node-to-node model.

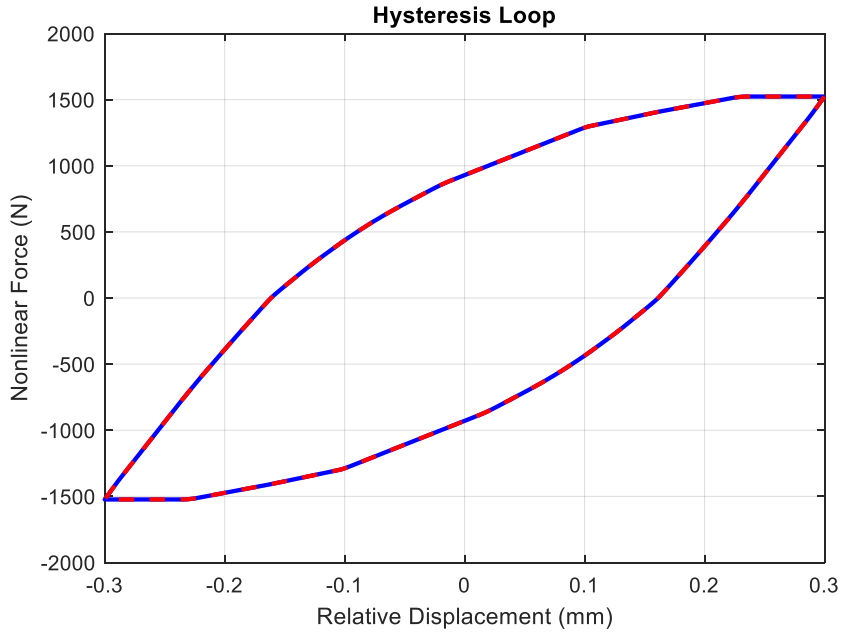


Figure 3.57. Hysteresis Loop of 2nd Joint Region with 125 Elements and 4 Elements

Table 3.16. Parameters of Reduced Joint Element with 4 Elements

| | $k_1(kN/mn$ | $k_2(kN/mm)$ | $k_3(kN/mm)$ | $k_4(kN/mm)$ |
|---|---|---|---|---|
| 1st Joint | 1730.8 | 2286.8 | 2288.3 | 2045.3 |
| 2nd Joint | 1734.8 | 2278.0 | 2625.6 | 2326.6 |
| 3rd Joint | 1734.8 | 2278.0 | 2625.6 | 2326.6 |
| 4th Joint | 1734.8 | 2278.0 | 2625.6 | 2326.6 |
| 5th Joint | 2733.4 | 2067.0 | 1825.9 | 2187.9 |
| 6th Joint | 3047.2 | 2002.7 | 2019.6 | 2437.4 |
| 7th Joint | 3047.2 | 2002.7 | 2019.6 | 2437.4 |
| 8th Joint | 3047.2 | 2002.7 | 2019.6 | 2437.4 |
| 9th Joint | 2103.2 | 2109.9 | 1882.0 | 1970.5 |
| 10th Joint | 2402.3 | 2590.0 | 2453.1 | 1936.5 |
| 11th Joint | 2402.3 | 2590.0 | 2453.1 | 1936.5 |
| 12th Joint | 2402.3 | 2590.0 | 2453.1 | 1936.5 |
| | $\mu N_1(N)$ | $\mu N_2(N)$ | $\mu N_3(N)$ | $\mu N_4(N)$ |
| 1st Joint | 35.5 | 195.3 | 352.9 | 243.7 |
| 2nd Joint | 213.1 | 20.1 | 205.9 | 505.9 |
| 3rd Joint | 35.5 | 238.8 | 575.1 | 156.5 |
| 4th Joint | 35.5 | 362.3 | 124.8 | 111.3 |
| 5th Joint | 244.2 | 190.4 | 232.8 | 334.0 |
| 6th Joint | 714.8 | 223.3 | 152.9 | 580.6 |
| 7th Joint | 410.3 | 349.5 | 188.4 | 127.0 |
| 8th Joint | 154.1 | 17.7 | 14.2 | 195.7 |
| 9th Joint | 305.6 | 203.0 | 143.0 | 37.1 |
| 10th Joint | 116.1 | 203.0 | 402.4 | 41.5 |
| 11th Joint | 177.7 | 203.0 | 208.7 | 281.7 |
| 12th Joint | 534.3 | 561.0 | 228.3 | 42.2 |

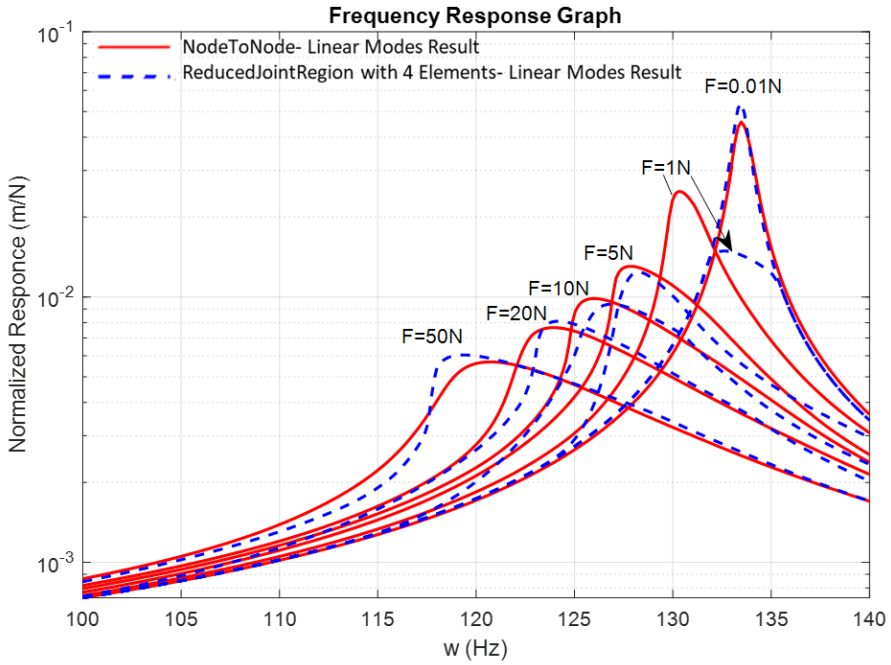


Figure 3.58. Normalized Response (mm/N) vs. Frequency (Hz) Graph of Reduced Joint of 4 Elements Utilizing Linear System Modes

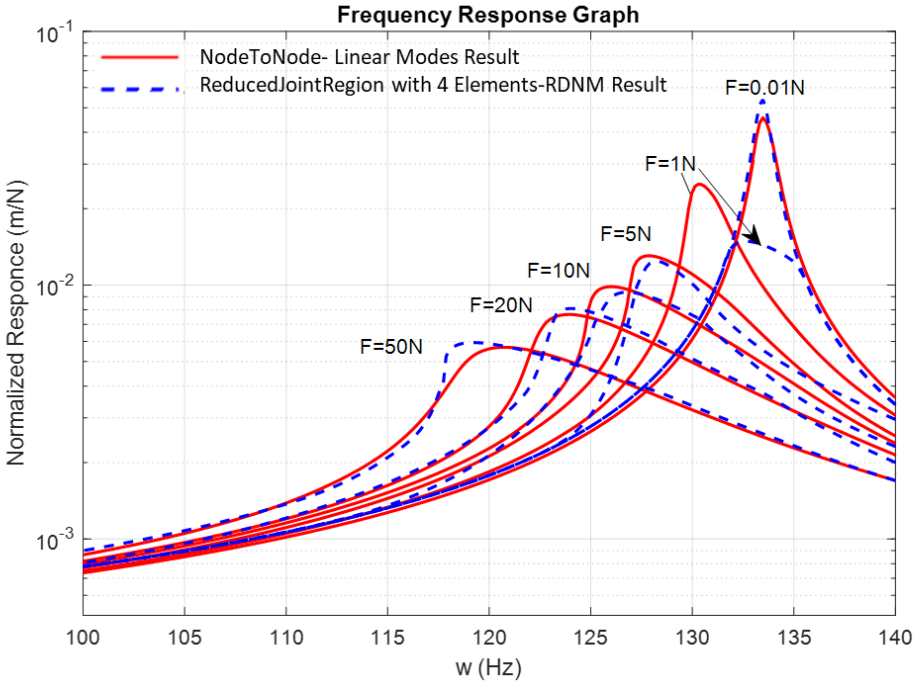


Figure 3.59. Normalized Response (mm/N) vs. Frequency (Hz) Graph of Reduced Joint of 4 Elements Utilizing RDNM

The solution times normalized with the computational time of node-to-node contact model with linear system modes are given in Table 3.17. For the highest applied excitation value of 50 N, the computational time is decreased to 3% from 75% for classical MSM. When RDNM is utilized in the solution process, this value further reduces to 2% from 77%. Since both the accuracy of the results and the decrease in computational time are better for results obtained with one RDNM, the advantage of utilizing RDNM is evident.

Table 3.17. The Reduction in Computational Times of Reduced Joint Region of 4 Elements with Linear Modes and RDNM

| **Excitation Force Value (N)** | **Reduction Percentage in Time (%) of Reduced Joint Region with 4 Elements Utilizing 4 Linear Modes** | **Reduction Percentage in Time (%) of Reduced Joint Region with 4 Elements Utilizing 1 RDNM** |
|---|---|---|
| 0.001 | 96.38 | 98.72 |
| 1 | 96.85 | 98.88 |
| 5 | 96.90 | 98.85 |
| 10 | 96.75 | 98.74 |
| 20 | 96.87 | 98.66 |
| 50 | 96.81 | 98.47 |

To examine the performance of the reduction methodology, the response of three-lap joint is calculated for the stiffness values given in Table 3.18. The result of high-fidelity models is given in Figure 3.60. For all excitation levels, the response calculated with 1 RDNM is the same as the response calculated with linear system modes. The contact states represent in Figure 3.61 to Figure 3.66 are similar to states of 100 $kN/mm$ stiffness value.

Table 3.18. Tangential-Normal Stiffness and Friction Coefficient of 1D Dry Friction Element with Constant Normal Load

| $k_u$ | $k_v$ | $\mu$ |
|---|---|---|
| 50 $kN/mm$ | 50 $kN/mm$ | 0.1 |

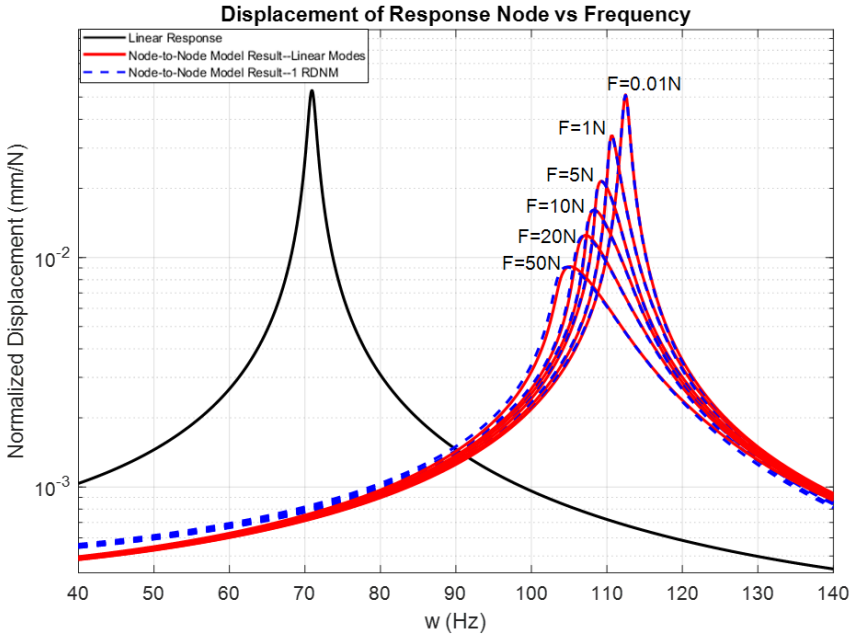


Figure 3.60. Normalized Response (mm/N) vs. Frequency (Hz) Graph

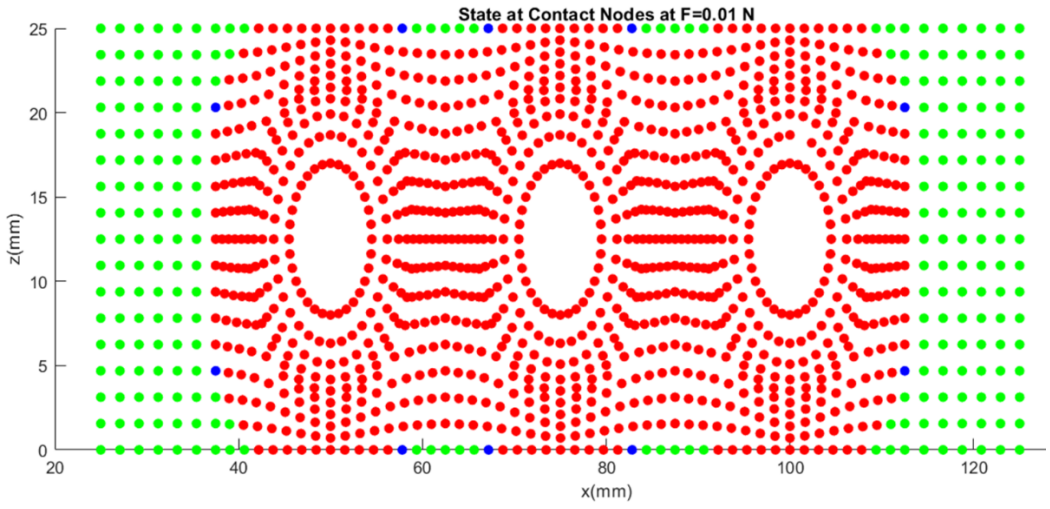


Figure 3.61. Contact state at the peak point of F=0.01 N (Red: Full stick motion; Blue: Stick-slip motion without separation; Cyan: Stick-slip motion with separation Green: Full separation)

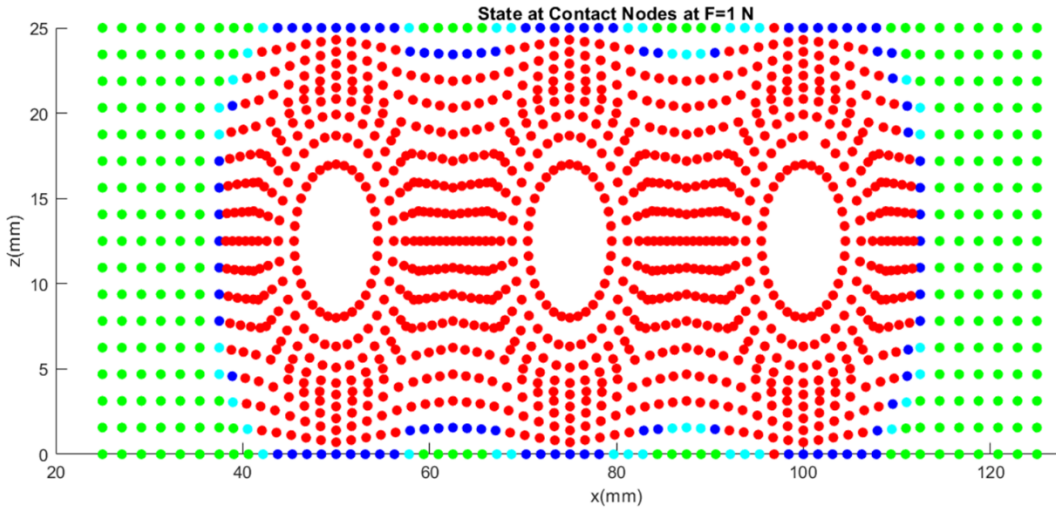


Figure 3.62. Contact state at the peak point of F=1 N (Red: Full stick motion; Blue: Stick-slip motion without separation; Cyan: Stick-slip motion with separation Green: Full separation)

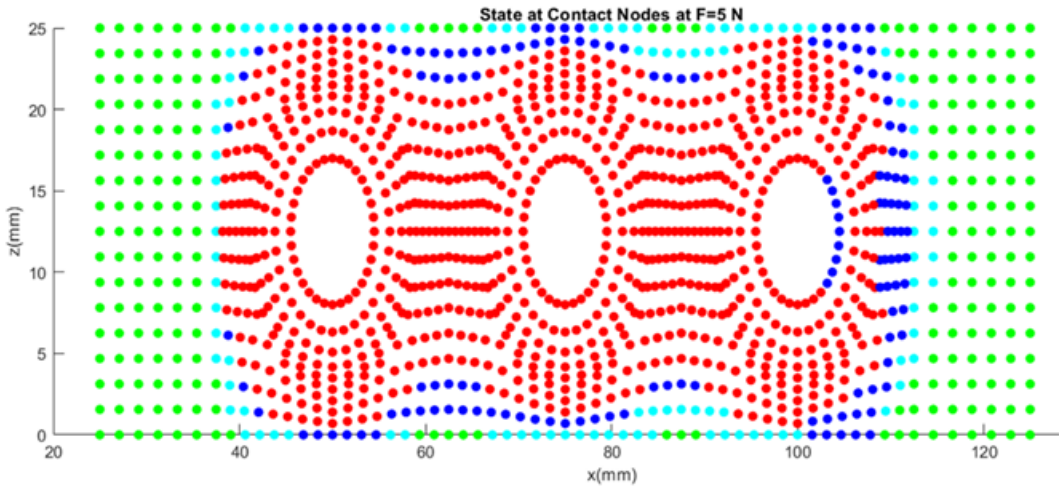


Figure 3.63. Contact state at the peak point of F=5 N (Red: Full stick motion; Blue: Stick-slip motion without separation; Cyan: Stick-slip motion with separation Green: Full separation)

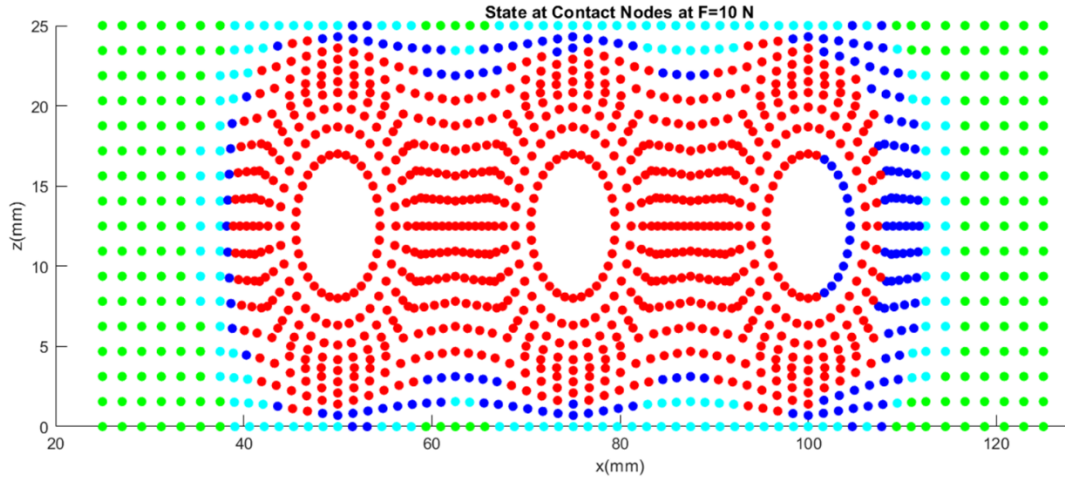


Figure 3.64. Contact state at the peak point of F=10 N (Red: Full stick motion; Blue: Stick-slip motion without separation; Cyan: Stick-slip motion with separation Green: Full separation)

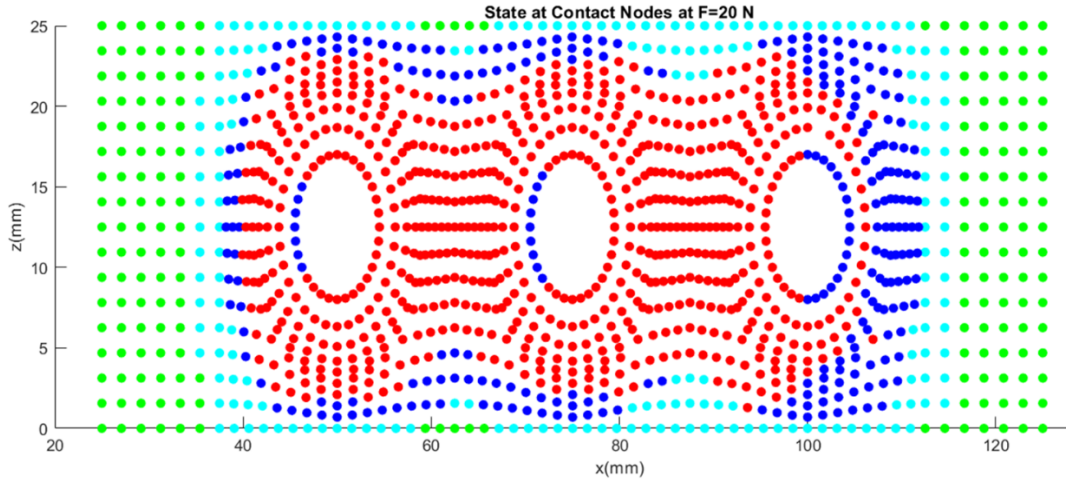


Figure 3.65. Contact state at the peak point of F=20 N (Red: Full stick motion; Blue: Stick-slip motion without separation; Cyan: Stick-slip motion with separation Green: Full separation)

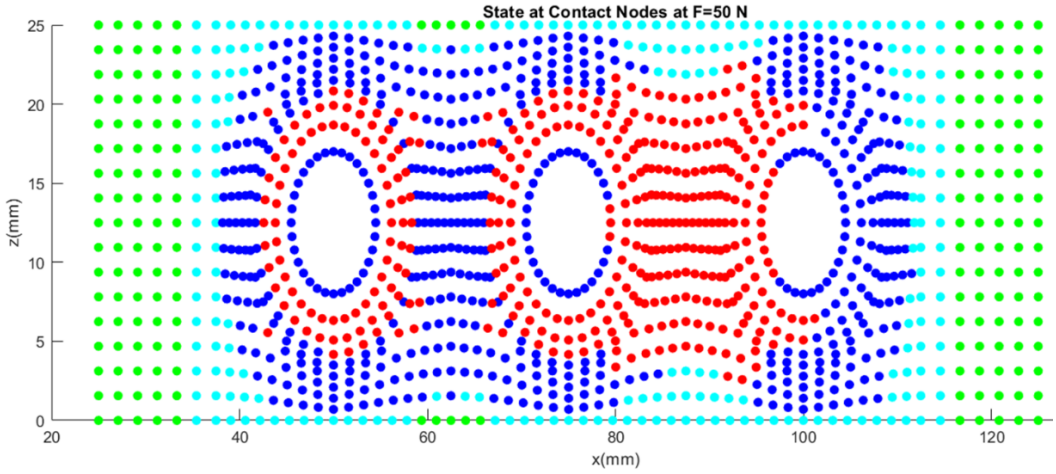


Figure 3.66. Contact state at the peak point of F=50 N (Red: Full stick motion; Blue: Stick-slip motion without separation; Cyan: Stick-slip motion with separation Green: Full separation)

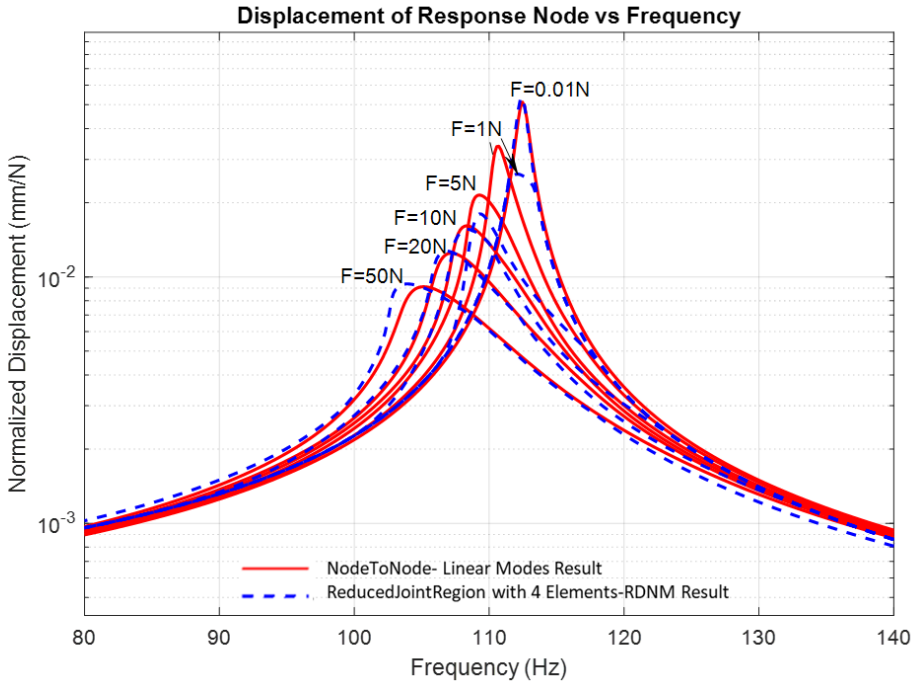


Figure 3.67.The Comparison of Normalized Response (mm/N) vs. Frequency (Hz) Graph for Reduced Joint Definition with 4 Elements Utilizing 1 RDNM

The responses of reduced joint definition for new stiffness value are given in Figure 3.67. The response level calculated with 1 RDNM is similar to results of node-to-node model's results except excitation level of 1 $N$.

To summarize, the three bolted joint assembly at which 1370 nodes are in contact is examined by utilizing 1D dry friction element with variable normal load. Similar to previous case studies, the contact model is reduced in two steps. In the first reduction step, the interested contact surface is divided into joint regions at which macroslip elements within each joint region are taken as parallel connected. In the second reduction step, the approximated microslip element is further reduced such that the hysteresis loops of the reduced joint element are the same as the joint elements of interest. In this step contribution of normal load variation to hysteresis loop is neglected. For both reduction steps, results of MSM with RDNMs and MSM with linear system modes are given to examine the performance of utilizing RDNM.

### 3.2.2 Case Study Model 2: Four-Bolted Assembly

The case study model is the same as the four-lap joint represented in Chapter 3.1.2. In this part of the study, 1D dry friction element with variable normal load is implemented in the mathematical model. The exaggerated deformation of four-bolted lap joint is given in Figure 3.68. The corresponding gap distribution resultant at the end of preload is given in Figure 3.69. The redefined gap formula which includes the effect of clearance in-between surfaces is given in Equation ( 3.4). The responses at different excitation levels obtained with both linear system modes and 1 RDNM is given in Figure 3.70.

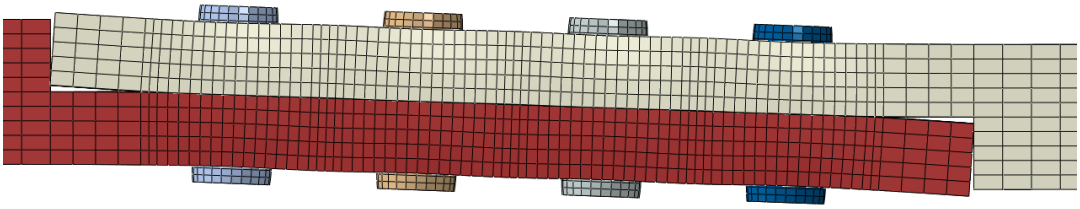

Figure 3.68. Exaggerated Deformation of Four-Bolted Lap Joint

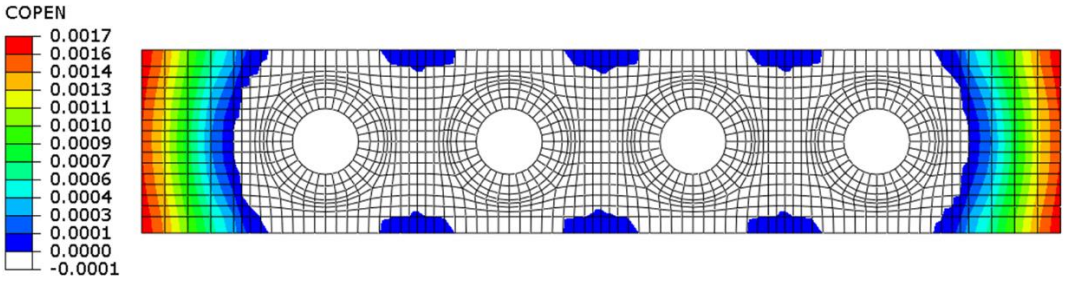


Figure 3.69. Gap Distribution on Contact Surface

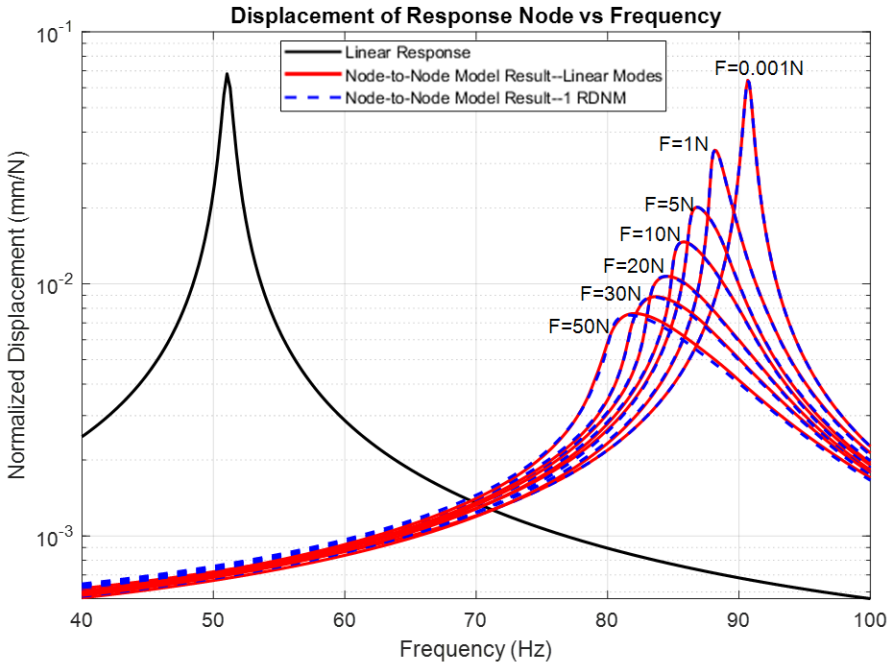


Figure 3.70. Normalized Response (mm/N) vs. Frequency (Hz) Graph

The contact states of peak points at each excitation level is given in from Figure 3.71 to Figure 3.77. For lowest excitation level of $F = 0.001\ N$, the nodes around bolt hole are in complete stick state. As the forcing level increases, nodes located near the outer edges start to slip. With increasing excitation level, the asymmetry of contact states along x direction becomes more apparent. This is due to fixed-free boundary condition and order of relative displacement along contact surface. The reduction in computational time resultant from the utilization of RDNM is given in Table 3.19. For highest excitation level, the computational time is reduced to 70%.

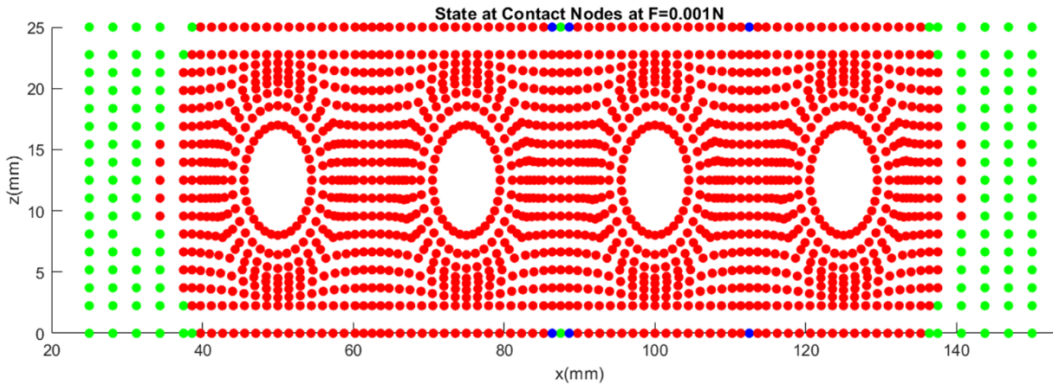


Figure 3.71. Contact state at the peak point of F=0.001 N (Red: Full stick motion; Blue: Stick-slip motion without separation; Cyan: Stick-slip motion with separation Green: Full separation)

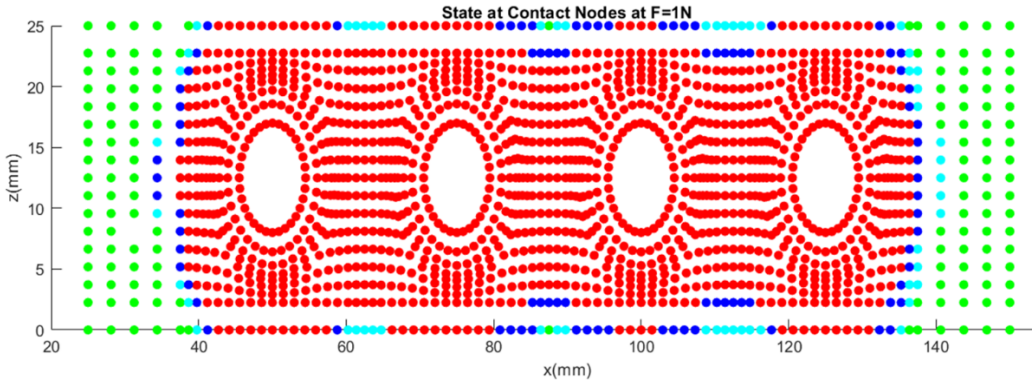


Figure 3.72. Contact state at the peak point of F=1 N (Red: Full stick motion; Blue: Stick-slip motion without separation; Cyan: Stick-slip motion with separation Green: Full separation)

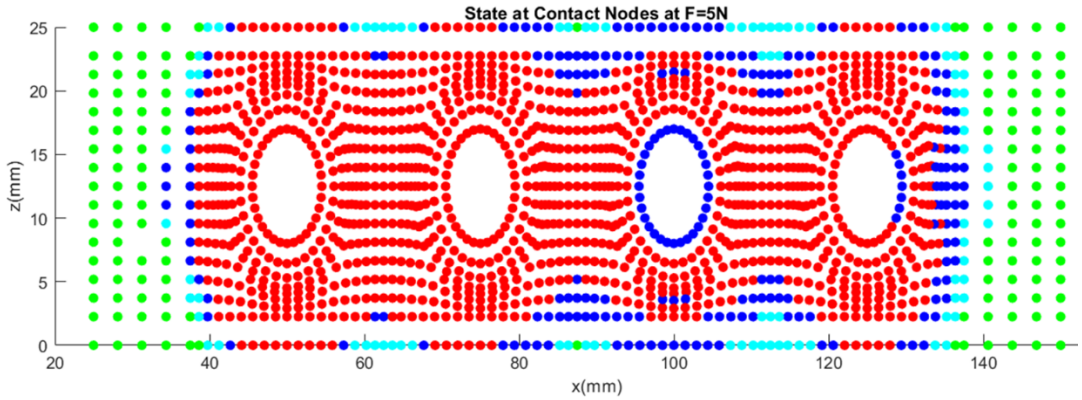


Figure 3.73. Contact state at the peak point of F=5 N (Red: Full stick motion; Blue: Stick-slip motion without separation; Cyan: Stick-slip motion with separation Green: Full separation)

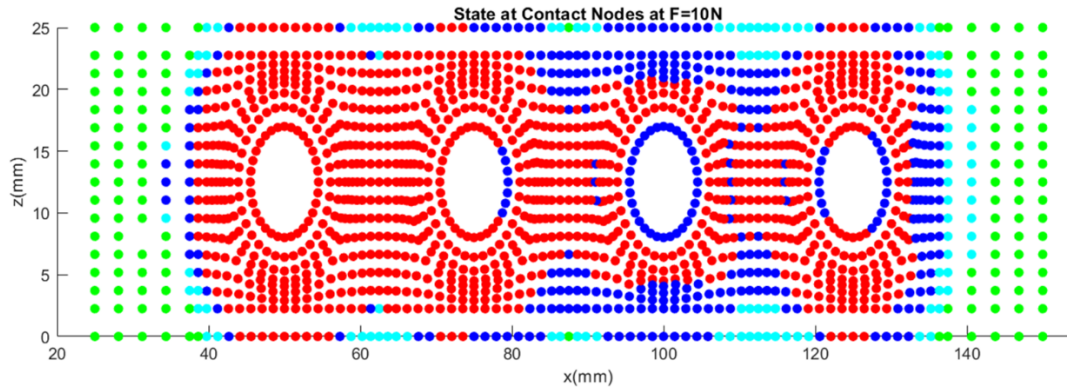


Figure 3.74. Contact state at the peak point of F=10 N (Red: Full stick motion; Blue: Stick-slip motion without separation; Cyan: Stick-slip motion with separation Green: Full separation)

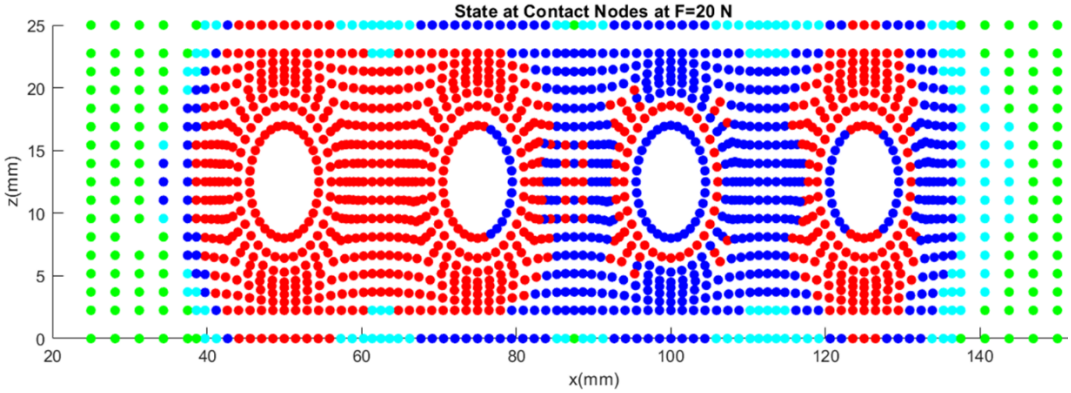


Figure 3.75. Contact state at the peak point of F=20 N (Red: Full stick motion; Blue: Stick-slip motion without separation; Cyan: Stick-slip motion with separation Green: Full separation)

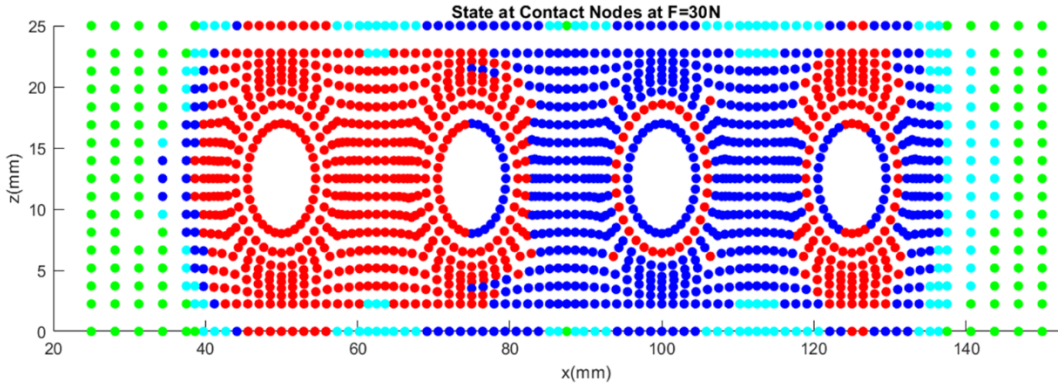


Figure 3.76. Contact state at the peak point of F=30 N (Red: Full stick motion; Blue: Stick-slip motion without separation; Cyan: Stick-slip motion with separation Green: Full separation)

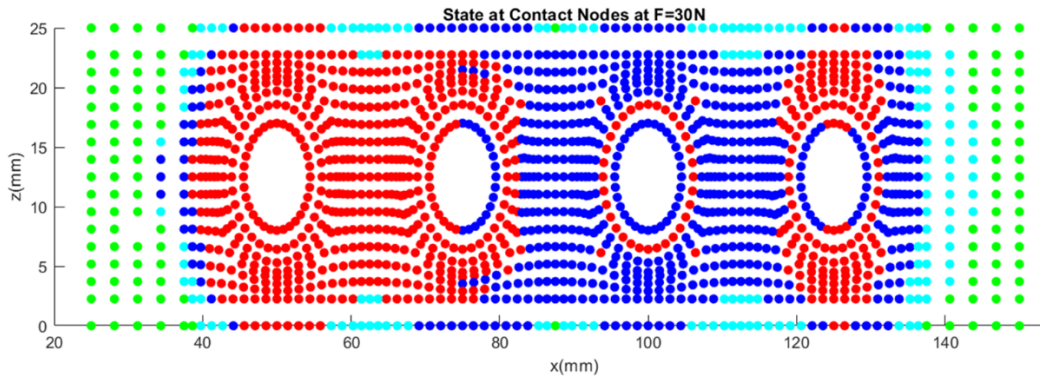


Figure 3.77. Contact state at the peak point of F=50 N (Red: Full stick motion; Blue: Stick-slip motion without separation; Cyan: Stick-slip motion with separation Green: Full separation)

Table 3.19. Computational Times with Linear Modes and RDNM

| **Excitation Force Value (N)** | **Computational Time with Classical MSM (s)** | **Computational Time MSM with RDNM (s)** | **Reduction Time of MSM with RDNM %** |
|---|---|---|---|
| 0.001 | 1518 | 377 | 75.1 |
| 1 | 1529 | 406 | 73.4 |
| 5 | 1562 | 436 | 72.1 |
| 10 | 1641 | 440 | 73.2 |
| 20 | 1633 | 460 | 71.8 |
| *30* | 1690 | 467 | 72.4 |
| 50 | 1710 | 490 | 71.4 |

### 3.2.2.1 First Reduction Step for Contact Model

The reduction method explained in Chapter 3.1.1.3 is applied in this step. The joint regions are selected by examining the normal load level along the nodes located at the mid-length of the contact surface which are specified in Figure 3.78. The normal

load value along this path is given in Figure 3.79. The 16 joint regions and the corresponding element numbers are in given in Figure 3.80.

The response obtained with linear system modes and 1 RDNM are given in Figure 3.81 and Figure 3.82. Although there is slight shift of resonance frequencies at lower excitation levels, the peak response values at higher excitation levels are captured with 16 joint region definition. The results of RDNM are coherent with the results of obtained with linear system modes. Examining the reduction of computational time given in Table 3.20, it is apparent that utilization of 1 RDNM is more feasible.

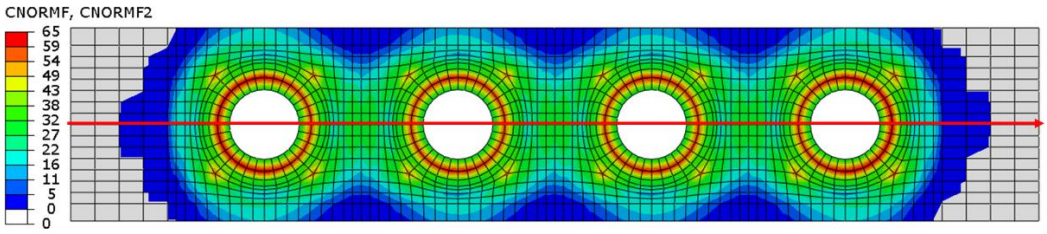


Figure 3.78. Middle Section of Contact Surface

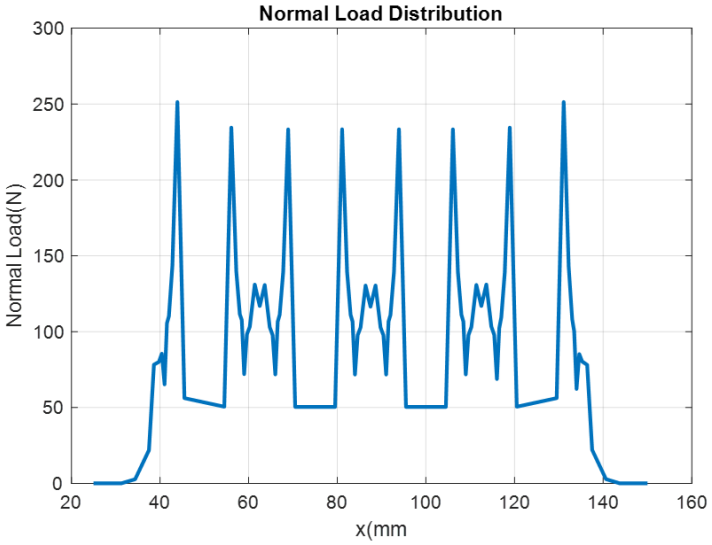


Figure 3.79. Normal Load Values Along the Middle Section Path

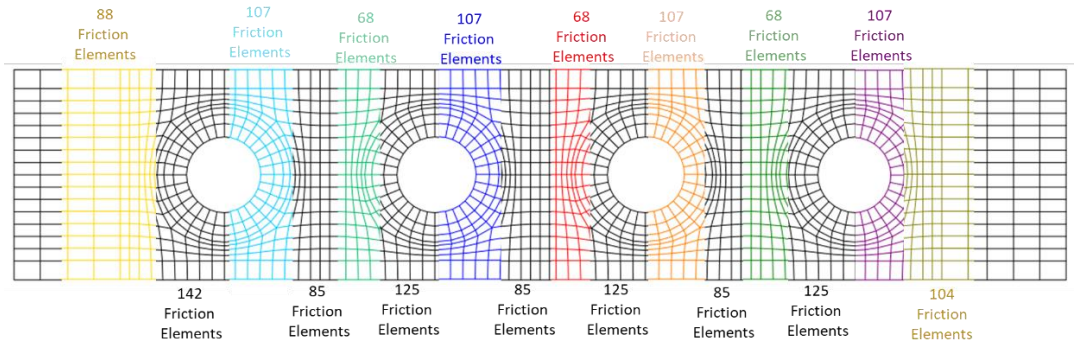


Figure 3.80. Location of 16 Joint Region on Contact Surface

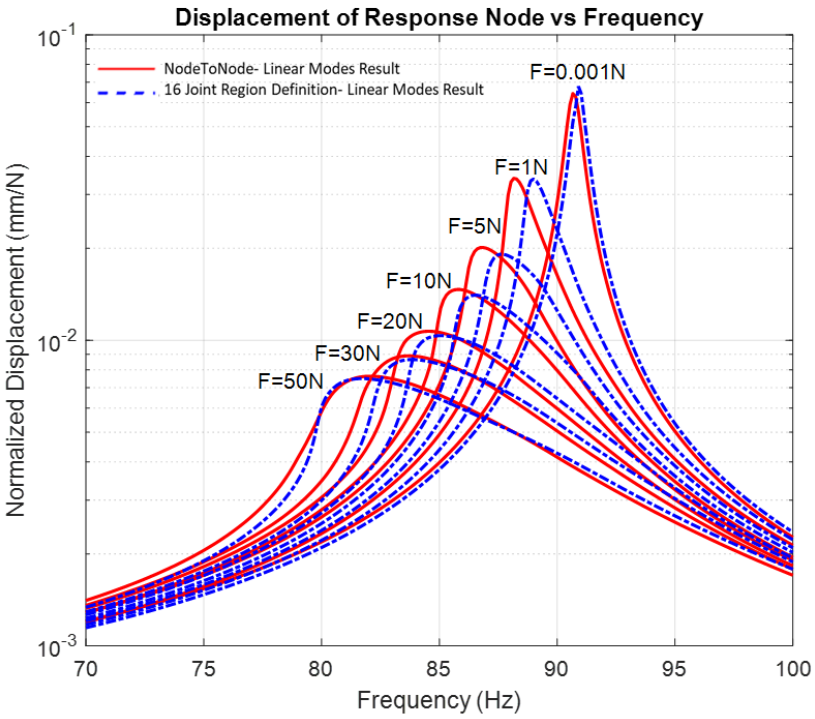


Figure 3.81. Normalized Response (mm/N) vs. Frequency (Hz) Graph for 16 Joint Region Utilizing 4 Linear System Modes

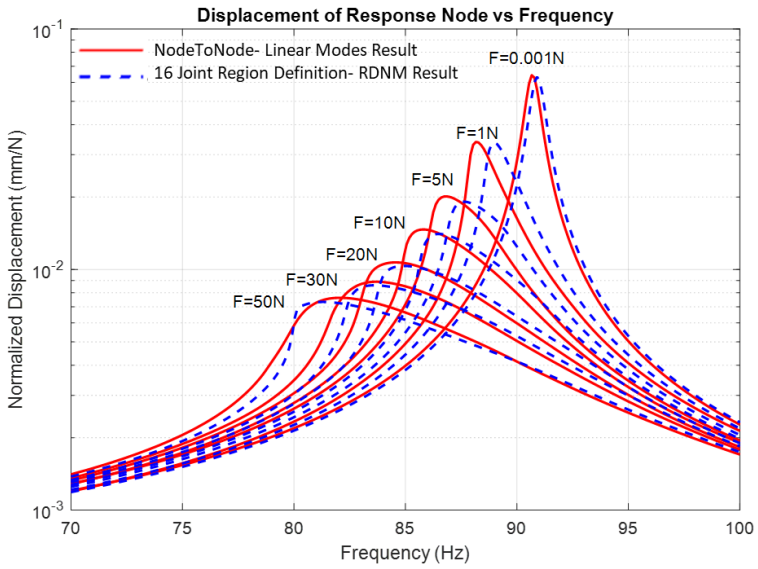


Figure 3.82. Normalized Response (mm/N) vs. Frequency (Hz) Graph for 16 Joint Region Utilizing 1 RDNM

Table 3.20.The Reduction in Computational Times of 16 Joint Region with Linear Modes and RDNM

| **Excitation Force Value (N)** | **Reduction Percentage in Time (%) of 16 Joint Region Utilizing 4 Linear Modes** | **Reduction Percentage in Time (%) of 16 Joint Region Utilizing 1 RDNM** |
|---|---|---|
| 0.001 | 41.6 | 81.7 |
| 1 | 34.9 | 80.0 |
| 5 | 32.1 | 79.2 |
| 10 | 32.4 | 79.4 |
| 20 | 28.9 | 78.9 |
| *30* | 32.8 | 78.5 |
| 50 | 35.4 | 77.8 |

### 3.2.2.2 Second Reduction Step for Contact Model

The optimization procedure explained in Chapter 3.2.1.2 is followed for the calculation process only considering the tangential stiffness ($k_u$) and normal load values ($\mu N$). The reduced joint regions are constructed with 4 macroslip elements. The optimized stiffness and normal load values are given in Table 3.21 and Table 3.22.

The results of reduced joint region definition are given in Figure 3.83 and Figure 3.84. The result at lowest excitation level is the same as the result of node-to-node model whereas for other excitation levels FRFs are shifted slightly.

Table 3.21.Optimized Stiffness Values of Reduced Joint Element with 4 Elements

| | $k_1(^{kN}/_{mn}$ | $k_2(^{kN}/_{mm})$ | $k_3(^{kN}/_{mm})$ | $k_4(^{kN}/_{mm})$ |
|---|---|---|---|---|
| 1st Joint | 1796.9 | 1433.5 | 1352.4 | 1436.9 |
| 2nd Joint | 1634.4 | 1765.0 | 1784.7 | 1764.1 |
| 3rd Joint | 1634.4 | 1765.0 | 1784.7 | 1764.1 |
| 4th Joint | 1634.4 | 1765.0 | 1784.7 | 1764.1 |
| 5th Joint | 3286.0 | 2882.9 | 2826.9 | 2833.6 |
| 6th Joint | 3614.2 | 3183.9 | 3197.5 | 3195.9 |
| 7th Joint | 3614.2 | 3183.9 | 3197.5 | 3195.9 |
| 8th Joint | 3614.2 | 3183.9 | 3197.5 | 3195.9 |
| 9th Joint | 2180.3 | 2174.4 | 2550.9 | 2442.9 |
| 10th Joint | 2795.4 | 2796.8 | 2705.2 | 2731.5 |
| 11th Joint | 2795.4 | 2796.8 | 2705.2 | 2731.5 |
| 12th Joint | 2795.4 | 2796.8 | 2705.2 | 2731.5 |
| 13th Joint | 1682.7 | 1727.6 | 1558.5 | 2202.2 |
| 14th Joint | 2232.8 | 1763.7 | 2263.1 | 2065.3 |
| 15th Joint | 2232.8 | 1763.7 | 2263.1 | 2065.3 |
| 16th Joint | 2232.8 | 1763.7 | 2263.1 | 2065.3 |

Table 3.22. Optimized Normal Load Values of Reduced Joint Element with 4 Elements

| | $\mu N_1(N)$ | $\mu N_2(N)$ | $\mu N_3(N)$ | $\mu N_4(N)$ |
|---|---|---|---|---|
| 1st Joint | 18.6 | 147.4 | 90.3 | 164.6 |
| 2nd Joint | 50.5 | 176.7 | 90.3 | 164.6 |
| 3rd Joint | 50.5 | 117.7 | 166.9 | 116.1 |
| 4th Joint | 42.4 | 54.5 | 146.7 | 56.6 |
| 5th Joint | 591.9 | 517.0 | 267.7 | 277.3 |
| 6th Joint | 591.9 | 517.0 | 267.7 | 277.3 |
| 7th Joint | 263.5 | 185.3 | 267.6 | 277.3 |
| 8th Joint | 222.4 | 227.8 | 643.5 | 650.5 |
| 9th Joint | 324.9 | 317.7 | 320.7 | 253.8 |
| 10th Joint | 324.9 | 317.7 | 242.1 | 253.8 |
| 11th Joint | 324.9 | 317.7 | 140.1 | 587.0 |
| 12th Joint | 324.9 | 317.7 | 568.4 | 253.8 |
| 13th Joint | 107.5 | 156.2 | 149.4 | 148.4 |
| 14th Joint | 107.5 | 156.2 | 149.4 | 75.0 |
| 15th Joint | 206.6 | 213.9 | 149.4 | 55.9 |
| 16th Joint | 180.9 | 66.2 | 149.4 | 23.8 |

The reduction percentage in computational times for reduced joint region definition is given Table 3.23. For linear system modes computational time is reduced to 3% from 65%. For 1 RDNM, the computational time is reduced to 1% from 22%. Since accuracy of responses is similar for linear system modes and 1 RDNM, implementation of RDNM is more advantageous.

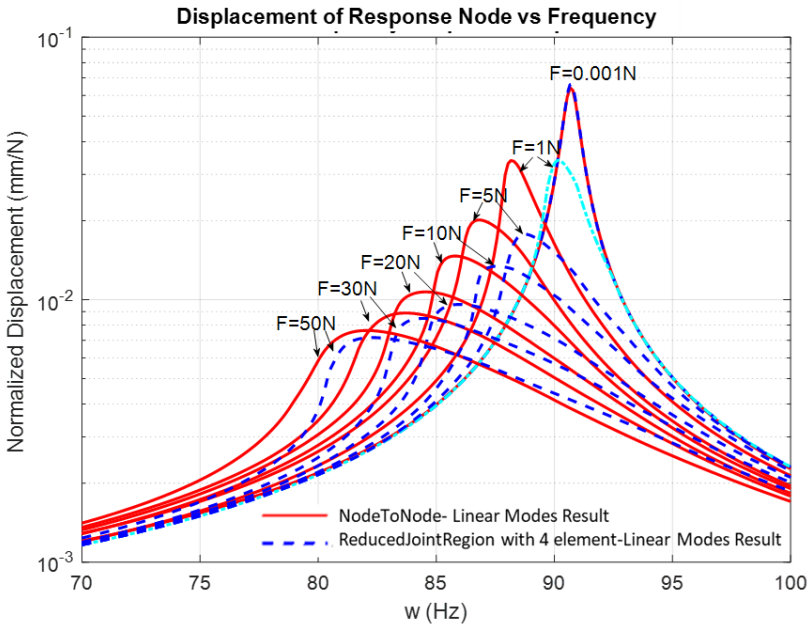


Figure 3.83. Normalized Response (mm/N) vs. Frequency (Hz) Graph of Reduced Joint of 4 Elements Utilizing Linear System Modes

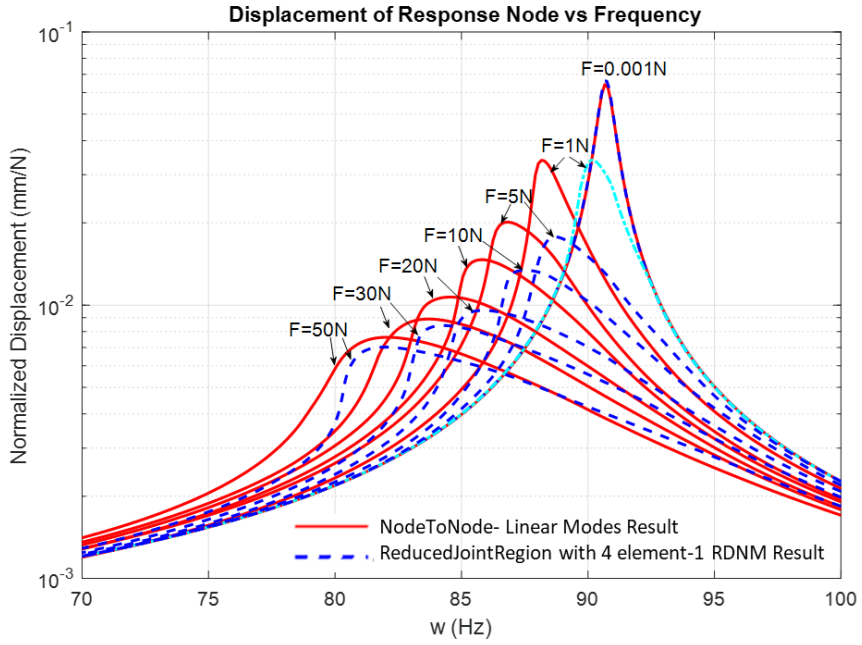


Figure 3.84. The Comparison of Normalized Response (mm/N) vs. Frequency (Hz) Graph for Reduced Joint Definition with 4 Elements Utilizing 1 RDNM

Table 3.23. The Reduction in Computational Times of Reduced Joint Region of 4 Elements with Linear Modes and RDNM

| **Excitation Force Value (N)** | **Reduction Percentage in Time (%) of Reduced Joint Region with 4 Elements Utilizing 4 Linear Modes** | **Reduction Percentage in Time (%) of Reduced Joint Region with 4 Elements Utilizing 1 RDNM** |
|---|---|---|
| 0.001 | 97.0 | 98.9 |
| 1 | 96.7 | 98.8 |
| 5 | 96.8 | 98.8 |
| 10 | 96.9 | 98.8 |
| 20 | 96.8 | 98.8 |
| *30* | 96.9 | 98.7 |
| 50 | 96.9 | 98.6 |

To summarize, the four bolted joint assembly at which 1693 nodes are in contact is examined by utilizing 1D dry friction element with variable normal load. Similar to previous case studies, the contact model is reduced in two steps. In the first reduction step, the contact area of interest is divided into joint regions considering the normal load variation across surface. In the second reduction step, the contribution of normal load variation to hysteresis loop is neglected while determining the optimized stiffness and normal load values. For all calculation steps, the accuracy of the response is preserved whereas the solution time is further reduced by implementing RDNM.

# CHAPTER 4

# CONCLUSION

To decrease the computational burden for obtaining accurate nonlinear dynamic response of bolted joints connections, a reduced order modeling method utilizing response dependent nonlinear modes is studied.

The response dependent nonlinear modes are calculated by adding the contribution of the nonlinear force to stiffness matrix. The corresponding nonlinearity matrix is constructed by taking the stiffness value of each macroslip element as the real part of the ratio of the nonlinear force value to displacement.

The contact model is reduced in two steps. In the first reduction step, the contact surface is divided into joint regions. The macroslip elements inside each joint region are connected in parallel such that the nonlinear characteristic of joint region is similar to microslip element. An artificial node is defined in-between contact surfaces. Another advantage of this reduction step is the reduction in the dimension of solved equation set. It was shown that the choice of joint regions can be made based on the normal load distribution along the contact surface.

In the second reduction step, the approximated microslip element is further reduced such that the hysteresis loops of the reduced joint element are the same as the joint element of interest. The results are compared with the response of node-to-node contact model. For both reduction steps, the results obtained with RDNM is coherent with the results of node-to-node contact model and the calculation time is much less while using RDNM. Another advantage of utilizing RDNM is the increased stability of the nonlinear solver which is especially important for analysis of the large systems.

The macroslip element with constant normal load assumption and variable normal load are included in models given in Chapter 3. The normal load values are taken

from the results of nonlinear static analysis conducted in commercial FEA software Abaqus. However, it should be kept in mind that normal load stays constant for specific design configurations. The motion in the direction of contact surface normal might introduce local separation of contact surfaces. The available reduced joint model only considers the tangential motion for the calculation of expected hysteresis loop. For further study, the formulae in the second reduction step can be extended to include the effect of normal load variation on hysteresis loop.

In the first reduction step, the location of artificial node is taken at the center of the joint region. For further study the location of the artificial node hence the defined mode shape's effect to results can also be examined.

## REFERENCES


[1] Cameron, T. M., and J. H. Griffin. “An Alternating Frequency/Time Domain Method for Calculating the Steady-State Response of Nonlinear Dynamic Systems.” Journal of Applied Mechanics, vol. 56, no. 1, 1989, pp. 149–154., doi:10.1115/1.3176036.

[2] Rezaiee-Pajand, M., et al. “A Novel Time Integration Formulation for Nonlinear Dynamic Analysis.” Aerospace Science and Technology, vol. 69, 2017, pp. 625–635., doi:10.1016/j.ast.2017.07.032.

[3] Liu, TianYun, et al. “An Efficient Time-Integration Method for Nonlinear Dynamic Analysis of Solids and Structures.” Science China Physics, Mechanics and Astronomy, vol. 56, no. 4, 2013, pp. 798–804., doi:10.1007/s11433-013-5021-9.

[4] Naess, A, and V Moe. “Efficient Path Integration Methods for Nonlinear Dynamic Systems.” Probabilistic Engineering Mechanics, vol. 15, no. 2, 2000, pp. 221–231., doi:10.1016/s0266-8920(99)00031-4.

[5] Poudou, Olivier, and Christophe Pierre. “Hybrid Frequency-Time Domain Methods for the Analysis of Complex Structural Systems with Dry Friction Damping.” 44th AIAA/ASME/ASCE/AHS/ASC Structures, Structural Dynamics, and Materials Conference, 2003, doi:10.2514/6.2003-1411.

[6] Guillen, J., and C. Pierre. “An Efficient, Hybrid, Frequency-Time Domain Method for The Dynamics of Large-Scale Dry-Friction Damped Structural Systems.” IUTAM Symposium on Unilateral Multibody Contacts, Jan. 1999, pp. 169–178., doi:10.1007/978-94-011-4275-5_17.

[7] Urabe, Minoru. “Galerkin's Procedure for Nonlinear Periodic Systems.” Archive for Rational Mechanics and Analysis, vol. 20, no. 2, 1965, pp. 120–152., doi:10.1007/bf00284614.

[8] Mickens, R.E. “Comments on the Method of Harmonic Balance.” Journal of Sound and Vibration, vol. 94, no. 3, 1984, pp. 456–460., doi:10.1016/s0022-460x(84)80025-5.

[9] Mickens, R.E. “A Generalization of the Method of Harmonic Balance.” Journal of Sound and Vibration, vol. 111, no. 3, 1986, pp. 515–518., doi:10.1016/s0022-460x(86)81410-9.

[10] Gourary, M M, et al. A New Computational Approach to Simulate Highly Nonlinear Systems by Harmonic Balance Method, 16AD. 16th IMACS World Congress Congress, document.

[11] Maple, Raymond C, et al. “Adaptive Harmonic Balance Method for Nonlinear Time-Periodic Flows.” Journal of Computational Physics, vol. 193, no. 2, 2004, pp. 620–641., doi:10.1016/j.jcp.2003.08.013.

[12] Lei Zhu, and C.E. Christoffersen. “Adaptive Harmonic Balance Analysis of-Oscillators Using Multiple Time Scales.” The 3rd International IEEE-NEWCAS Conference, 2005., doi:10.1109/newcas.2005.1496738.

[13] Laxalde, Denis. “Etude D'amortisseurs Non-linéaires appliqués Aux Roues aubagées Et Aux systèmes Multi-étages.” Thèse de doctorat: Mécanique: Ecully, Ecole centrale de Lyon, S.n., 2007.

[14] Yümer, Mehmet Ersin. “On the Non-Linear Vibration and Mistuning Identification of Bladed Disks.” Middle East Technical University, 2010.

[15] Sert, Onur, and Ender Cigeroglu. “A Novel Two-Step Pseudo-Response Based Adaptive Harmonic Balance Method for Dynamic Analysis of Nonlinear Structures.” Mechanical Systems and Signal Processing, vol. 130, May 2019, pp. 610–631., doi:10.1016/j.ymssp.2019.05.028.

[16] Menq, Chia-Hsiang, and J. H. Griffin. “A Comparison of Transient and Steady State Finite Element Analyses of the Forced Response of a Frictionally Damped Beam.” Journal of Vibration and Acoustics, vol. 107, no. 1, 1985, pp. 19–25., doi:10.1115/1.3274709.

[17] Menq, C.-H., et al. “The Influence of Microslip on Vibratory Response, Part I: A New Microslip Model.” Journal of Sound and Vibration, vol. 107, no. 2, 1986, pp. 279–293., doi:10.1016/0022-460x(86)90238-5.

[18] Menq, C.-H., et al. “The Influence of Microslip on Vibratory Response, Part II: A Comparison with Experimental Results.” Journal of Sound and Vibration, vol. 107, no. 2, 1986, pp. 295–307., doi:10.1016/0022-460x(86)90239-7.

[19] Budak, E., and OZGUVEN, H. N., “A dynamic analysis method for the harmonically excited nonlinear structures” Structural Vibration and Acoustics, ASME, DE 18-3,23-29, 1989

[20] Budak, E., and H. Nevzat Özgüven. “Iterative Receptance Method for Determining Harmonic Response of Structures with Symmetrical Non-Linearities.” Mechanical Systems and Signal Processing, vol. 7, no. 1, 1993, pp. 75–87., doi:10.1016/0888-3270(93)90006-i.

[21] Tanrikulu, Omer, et al. “Forced Harmonic Response Analysis of Nonlinear Structures Using Describing Functions.” AIAA Journal, vol. 31, no. 7, 1993, pp. 1313–1320., doi:10.2514/3.11769.

[22] Kuran, B., and H.N. Özgüven. “A MODAL SUPERPOSITION METHOD FOR NON-LINEAR STRUCTURES.” Journal of Sound and Vibration, vol. 189, no. 3, 1996, pp. 315–339., doi:10.1006/jsvi.1996.0022.

[23] Yang, B.D., et al. “Stick–Slip–Separation Analysis and Non-Linear Stiffness and Damping Characterization of Friction Contacts Having Variable Normal Load.” Journal of Sound and Vibration, vol. 210, no. 4, 1998, pp. 461–481., doi:10.1006/jsvi.1997.1305.

[24] Chen, J. J., and C. H. Menq. “Prediction of the Resonant Response of Frictionally Constrained Blade Systems Using Constrained Mode Shapes.” Volume 5: Manufacturing Materials and Metallurgy; Ceramics; Structures and Dynamics; Controls, Diagnostics and Instrumentation; Education, 2 June 1998, doi:10.1115/98-gt-548.

[25] Cigeroglu, Ender, et al. “A Microslip Friction Model with Normal Load Variation Induced by Normal Motion.” Nonlinear Dynamics, vol. 50, no. 3, 24 Jan. 2007, pp. 609–626., doi:10.1007/s11071-006-9171-4.

[26] Cigeroglu, Ender, et al. “Forced Response Prediction of Constrained and Unconstrained Structures Coupled Through Frictional Contacts.” Journal of

Engineering for Gas Turbines and Power, vol. 131, no. 2, 2008, doi:10.1115/1.2940356.

[27] Petrov, E. P. “A High-Accuracy Model Reduction for Analysis of Nonlinear Vibrations in Structures With Contact Interfaces.” Journal of Engineering for Gas Turbines and Power, vol. 133, no. 10, 2011, doi:10.1115/1.4002810.

[28] Krack, Malte, et al. “A Method for Nonlinear Modal Analysis and Synthesis: Application to Harmonically Forced and Self-Excited Mechanical Systems.” Journal of Sound and Vibration, vol. 332, no. 25, 2013, pp. 6798–6814., doi:10.1016/j.jsv.2013.08.009.

[29] Rosenberg, R. M. “Normal Modes of Nonlinear Dual-Mode Systems.” Journal of Applied Mechanics, vol. 27, no. 2, 1960, pp. 263–268., doi:10.1115/1.3643948.

[30] Krack, Malte. “Nonlinear Modal Analysis of Nonconservative Systems: Extension of the Periodic Motion Concept.” Computers & Structures, vol. 154, 2015, pp. 59–71., doi:10.1016/j.compstruc.2015.03.008.

[31] Touzé, Cyril. “Normal Form Theory and Nonlinear Normal Modes: Theoretical Settings and Applications.” Modal Analysis of Nonlinear Mechanical Systems, Springer, 2014, pp. 75–160.

[32] Karaağaçlı, Taylan, Cigeroglu, Ender, Özgüven H.N. “Numerical computation of nonlinear normal modes (NNMs) by using response dependent nonlinear mode (RDNM) concept”, Extended Abstract in: 38th International Modal Analysis Conference (IMAC), Houston, TX, USA (2020)

[33] Ferhatoğlu, Erhan, et al. “A Modal Superposition Method for the Analysis of Nonlinear Systems.” Special Topics in Structural Dynamics, Volume 6, Jan. 2016, pp. 269–278., doi:10.1007/978-3-319-29910-5_28.

[34] Ferhatoglu, Erhan, et al. “A New Modal Superposition Method for Nonlinear Vibration Analysis of Structures Using Hybrid Mode Shapes.” Mechanical Systems and Signal Processing, vol. 107, July 2018, pp. 317–342., doi:10.1016/j.ymssp.2018.01.036.

[35] Ferhatoğlu, Erhan. “A NEW MODAL SUPERPOSITION METHOD FOR NONLINEAR VIBRATION ANALYSIS OF STRUCTURES USING HYBRID MODE SHAPES.” Middle East Technical University, 2017.

[36] Segalman, Daniel J. “A Four-Parameter Iwan Model for Lap-Type Joints.” Journal of Applied Mechanics, vol. 72, no. 5, 2005, pp. 752–760., doi:10.1115/1.1989354.

[37] Brake, Matthew R. W., et al. “Reduced Order Modeling of Nonlinear Structures with Frictional Interfaces.” SpringerLink, Springer International Publishing, 1 Jan. 1970, link.springer.com/chapter/10.1007/978-3-319-56818-8_24.

[38] Brake, Matthew R., et al. “Variability and Repeatability of Jointed Structures with Frictional Interfaces.” SpringerLink, Springer International Publishing, 1 Jan. 2014, link.springer.com/chapter/10.1007/978-3-319-04501-6_23.

[39] Karapistik, Gokhan, and Ender Cigeroglu. “Reduced Order Modeling of Bolted Joints in Frequency Domain.” Nonlinear Structures and Systems, Volume 1, 2019, pp. 235–238., doi:10.1007/978-3-030-12391-8_33.

[40] Karapistik, Gokhan. “NONLINEAR REDUCED ORDER MODELING OF BOLTED JOINTS” Middle East Technical University, 2019.

[41] Ferhatoglu, Erhan, et al. “A Novel Modal Superposition Method with Response Dependent Nonlinear Modes for Periodic Vibration Analysis of Large MDOF Nonlinear Systems.” Mechanical Systems and Signal Processing, vol. 135, Jan. 2020, p. 106388., doi:10.1016/j.ymssp.2019.106388.

[42] Kizilay, Sefa. “A NEW JACOBIAN MATRIX CALCULATION METHOD TO DECREASE COMPUTATIONAL TIME IN PERIODIC FORCED RESPONSE ANALYSIS OF NONLINEAR STRUCTURES.” Middle East Technical University, 2019.

[43] “Abaqus Unified FEA.” SIMULIA™ by Dassault Systèmes®, www.3ds.com/products-services/simulia/products/abaqus/.

[44] “Matlab.” MathWorks, www.mathworks.com/products/matlab.html.